NUMERICAL SIMULATION OF DIRECT EXPANSION SOLAR-ASSISTED HEAT PUMP WATER HEATER USING CARBON DIOXIDE AS REFRIGERANT

A Thesis
Submitted to the Graduate Faculty
of the
North Dakota State University
of Agriculture and Applied Science

By

Mohammad Raisul Islam

In Partial Fulfillment
for the Degree of
MASTER OF SCIENCE

Major Department:
Mechanical Engineering

November 2013

Fargo, North Dakota

North Dakota State University
Graduate School

Title

Numerical Simulation of Direct Expansion Solar-Assisted Heat Pump Water Heater Using Carbon Dioxide as Refrigerant

By

Mohammad Raisul Islam

The Supervisory Committee certifies that this ***disquisition*** complies with North Dakota State University's regulations and meets the accepted standards for the degree of

MASTER OF SCIENCE

SUPERVISORY COMMITTEE:

Dr. Sumathy Krishnan
Chair

Dr. Yildirim Bora Suzen

Dr. Michael Stewart

Dr. Samee Ullah Khan

Approved:

12/4/2013
Date

Dr. Alan Kallmeyer
Department Chair

ABSTRACT

Compared to the conventional solar-assisted heat pump (SAHP) water heating system, a relatively more compact direct-expansion solar assisted heat pump (DX-SAHP) has been introduced, in which the solar collector acts as an evaporator. Details of the analytical studies of a CO_2 transcritical cycle on SAHP water heating system are presented in this study. A numerical model has been developed to optimize the system design and operating parameters. The simulation model can predict the performance of the system COP, collector efficiency and heat capacity. An experimental prototype using the evacuated tube U-pipe solar collector utilized to verify the simulation results. The results show that both the solar radiation and ambient temperature have a significant impact on the DX-SAHP system's thermal performance. Year round performance showed that, theoretically, the system could achieve on an average, COP of 2 – 3.2, collector efficiency of 40 – 62% and water temperature to be about 43° – 56°C.

ACKNOWLEDGEMENTS

First and foremost, I am truly grateful to my supervisor – Dr. Sumathy Krishnan, for her invaluable guidance, unwavering support, encouragement and patience throughout my studies. Her encouragement helped me discover the true attitude of learning and working. Needless to say, I would not have enjoyed this research without her careful attention and direction, as well as the freedom I received from her.

I am also indebted and thankful to Dr. Suzen, Dr. Stewart and Dr. Khan for being a part of my committee. I would like to thank Mechanical Engineering Department at North Dakota State University for giving me the opportunity to accomplish this master's program.

I like to take this opportunity to express deep sense of gratitude to my parents, who gave everything they could to make me what I am today. Their touching care and love provided me the necessary strength to withstand the pressure of my research program. Their contributions to this work, though invisible, are invaluable to me.

This research was in part supported by a grant from the Pakistan-US Science and Technology Cooperation Program, US Department of State (jointly administered by the National Academics and Higher Education Commission of Pakistan).

TABLE OF CONTENTS

ABSTRACT iii

ACKNOWLEDGEMENTS iv

LIST OF TABLES viii

LIST OF FIGURES ix

NOMENCLATURE xii

CHAPTER 1. INTRODUCTION 1

1.1. General Introduction 1

1.2. System Description 4

1.3. Outline of Thesis 5

CHAPTER 2. LITERATURE REVIEW 7

2.1. Available Solar Radiation in North Dakota 7

2.2. A Brief History of SWH Systems 8

2.3. Categorized Studies Conducted on SWH Systems 10

2.3.1. Passive SWH Systems 11

2.3.2. Active SWH Systems 13

2.4. Comparison Between SAHP System and DX-SAHP System 18

2.5. Transcritical Heat Pump Cycle 25

2.5.1. Thermophysical Properties of CO_2 27

2.5.2. Fundamentals of CO_2 Transcritical Cycle and Performance 31

2.6. Influence of Key Variables on SWH System Design 34

CHAPTER 3. SCOPE AND OBJECTIVES OF THIS STUDY 37

CHAPTER 4. THERMODYNAMIC ANALYSIS 39

4.1. Evaporator / Solar Collector Model 40
4.1.1. Two-phase Flow in the Solar Collector 44
4.1.2. Governing Equations for Evacuated Tube U-pipe Solar Collector 45
4.2. Compressor Model 51
4.3. Condenser / Hot Water Storage Tank Model 52
4.4. Expansion Device 55
4.5. Available Solar Energy from the Solar Collector 55
CHAPTER 5. SYSTEM MODELING AND SIMULATION PROCEDURE.....58
5.1. Solution Procedure 58
5.2. Cycle Performance Measurement 63
5.3. Error Analysis.....64
CHAPTER 6. MODEL VALIDATION AND PARAMETRIC STUDIES 65
6.1. Model Validation.....65
6.2. Baseline Simulation and Parametric Studies.....69
6.2.1. Effect of Compressor Speed and Collector Area.....70
6.2.2. Effect of Solar Radiation Intensity 73
6.2.3. Effect of Ambient Temperature and Wind Speed 76
6.2.4. Effect of Condensing and Evaporating Temperature 79
6.2.5. Combined Effect of Solar Collector Area and Storage Volume 80
6.2.6. Effect of Collector Area and Condenser Coil Length 82
6.2.7. Seasonal Performance Variation 83
CHAPTER 7. CONCLUSIONS AND FUTURE RESEARCH.....86
7.1. Future Research 88
REFERENCES 90

APPENDIX. PROGRAM CODE 100
A.1. MATLAB Functions 100
A.1.1. Heat Pump Model 100
A.1.2. Solar Collector Model 103
A.1.3. Compressor Model 109
A.1.4. Condenser Model: Part 1 110
A.1.5. Condenser Model: Part 2 111
A.1.6. Condenser Model: Part 3 114
LIST OF PUBLICATIONS 117

LIST OF TABLES

Table Page

1. Existing capacity of SWH from the year 2007 to 2010 [2 – 3] 1
2. A brief comparison of CO_2 with other conventional refrigerants [49] 28
3. A comparison of saturation temperature drop of CO_2 with other conventional refrigerants [49, 55] 31
4. Geographical data of Fargo, North Dakota [89] 57
5. Main parameters used in the performance evaluation of DX-SAHP water heating system 59
6. Design parameters used for the experimental set-up 66

LIST OF FIGURES

Figure Page

1. Average annual growth rates of renewable energy capacity, 2005 to 2010 [3] 2
2. Schematic diagram of a direct-expansion solar assisted heat pump water heating system 5
3. P-h diagram of transcritical CO2 heat pump cycle 5
4. (a) Average temperature range [8] and (b) average percentage of possible sunshine by months [7] in Fargo, North 8
5. Schematic diagram of thermosyphon SWH system [19] 12
6. Schematic diagram of ICS solar water heating system [20] 13
7. Schematic diagram a direct circulation SWH system [21] 14
8. Schematic diagram of indirect water heating presented by Kuang et al. [22] 15
9. Schematic diagram of standard air system configuration [23] 16
10. Conventional domestic SWH system in adverse weather regions [24] 18
11. Schematic of Heat Pump system 19
12. Pressure-enthalpy (P-h) diagram of HP cycle 20
13. Conventional solar-assisted heat pump system 21
14. Direct Expansion Solar-assisted Heat Pump (DX-SAHP) system 22
15. Pressure-enthalpy (P-h) diagram of a transcritical HP cycle 26
16. (a) a comparison of vapor pressure of CO_2 with other refrigerants; (b) specific heat variation of CO_2 for different pressures [49, 52] 30
17. Variation of transport properties of CO_2: (a) thermal conductivity; (b) viscosity [53] 31

18. CO_2 transcritical P-h diagram describing the effect of condenser pressure on heating capacity and COP [49] 32

19. Temperature profile for (a) latent condensation process; (b) CO_2 supercritical gas cooling process [56] 33

20. Input and output parameters for modeling the potential approximation of solar water heating system [68] 35

21. A comparison between flat-plate and evacuated tube solar collector with respect to their design benefit 42

22. Schematic of the evacuated tube U-pipe solar collector and its components: (a) CO_2 flow direction; (b) construction of the unit glass tube; (c) cross-sectional view of the collector tube; and (d) differential control volume used in the present analysis 43

23. Hot water storage tank with immersed single coil condenser: (a) schematic of the storage tank; (b) heat transfer between CO_2 flow to the surrounding water; (c) top view of storage tank; and (d) thermal network between the CO_2 flow to the ambient 53

24. Flow chart of the simulation model 60

25. Boundary conditions at solar collector inlet and outlet points 62

26. Evacuated tube U-pipe solar collector used for experimental set-up 66

27. Comparison of solar collector efficiency variation profile between simulation and experimental results 68

28. A comparison between theoretical and experimental results of CO_2 outlet temperature over the test time of the day 68

29. Comparison between theoretical and experimental results of solar collector efficiency over the test time of the day 69

30. Effect of compressor speed on system COP and heat rejection at the condenser 71

31. Effect of compressor speed for different collector area 72

32. Variation of collector tube temperature and solar collector efficiency with compressor speed 73

33. Effect of solar radiation for different collector area on COP values 75

34. Variation of differences of mean fluid temperature over ambient temperature as a function of I_T and T_a 75

35. Variation of CO_2 mass flow rate as a function of T_a 76

36. Effect of ambient temperature (T_a) on the system performance in terms of COP and solar collector efficiency..... 77

37. Effect of wind speed (V) on the system performance in terms of COP and solar collector efficiency..... 78

38. Effect of condensing temperature on system COP and collector efficiency 78

39. Effect of evaporating temperature on system COP at different condensing temperatures 79

40. Combined effect of solar collector area and storage volume on the system performance as COP values..... 81

41. Combined effect of solar collector area and storage volume on the system performance in terms of collector efficiencies 82

42. Effect of condenser coil length on the system performance..... 83

43. Variation of monthly averaged COP and solar collector efficiency..... 84

44. Variation of monthly averaged temperature profile for T_{wo}, T_{con}, and T_{at} 85

NOMENCLATURE

A……area, (m^2)

$A_{c,i}$…….inner circular area of the condenser coil, (m^2)

$A_{c,o}$……outer circular area of the condenser coil, (m^2)

C_b……..bond conductance, (W/m K)

C_p……..specific heat capacity, (Kj/kg K)

C_{pv}…….avg. sp. heat capacity at const. pr. and volume, (kJ/kg K)

C_f……...frictional pressure drop coefficient

COP……..coefficient of performance

D……outer diameter, (m)

d…….inner diameter of U-tube, (m)

F……....fin efficiency

F'……...collector efficiency factor

f……..friction factor

G……mass velocity, (kg/m^2 s)

Gr……..Grashof number

g…….gravitational acceleration, (m/s^2)

$h_{g,conv}$……..convective heat transfer coefficient, (W/m^2 K)

$h_{g,cond}$……..conduction heat transfer coefficient, (W?m^2 K)

$h_{g,r}$……..radiation heat transfer coefficient, (W/m^2 K)

h_{fg}……enthalpy of vaporization, (kJ/kg)

h…….enthalpy, (kJ kg-1) / heat transfer coefficient, (W/m^2 K)

h'……heat transfer coefficient, (W/m^2 K)

I_T……global solar radiation intensity, (W/m^2)

I_d ……diffuse solar intensity, (W/m^2)

I_b……beam solar intensity, (W/m^2)

K……thermal conductivity, (W/m K)

L……length, (m)

M……...mass, (kg)

$\dot{m}$ ……..mass flow rate, (kg/s)

N……compressor speed, (rpm)

Nu……...Nusselt number

P…….pressure, (Pa) / electrical power inlet, (W)

Pr……Prandtl number

$\dot{Q}$…….net heat energy, (W)

Q_u……useful heat, (W)

Q_{load}……heat energy supplied to the load, (W)

Re……Reynolds number

Ra……Rayleigh number

r……radius, (m)

S…….....absorbed solar radiation, (W/m^2) / stroke length of comp, (m)

T……..temperature, (°C)

T_1…….temperature at the outlet of solar collector, (°C)

T_1'…….temp of CO_2 in the collector at single-phase vapor region, (°C)

$\dot{W}$…….net work, (W)

Greek Letters

α……..solar absorbtance

β……..tilt angle / coefficient of thermal expansion, (K^{-1})

δ……..thickness, (m) / angle of deflection

Δ……..difference in quantity

θ……..time difference of the day

λ……..thermal conductivity, (W/m K)

ε……...thermal emissivity

τ……...solar transmittance

ρ……...density, (kg/m^3)

μ……...dynamic viscosity, (N s/m^2)

ν……kinematic viscosity, (N s/m^2)

η……efficiency

σ……Stefan Boltzmann constant (5.67 x 10-8 W/K^4 m^2)

Subscripts

a…….ambience

at……absorber tube

b…….bore

c…….selective coating / CO_2

con…….condenser

coll…….collector

coil…….condenser coil

dis……..discharge

e…….evaporator / exit

f……..fluid

g…….glass / vapor

i……..inlet

isen…….isentropic

m……metal / mechanical

o…….outer

suc……..suction

t……..tank

v……..vapor / volumetric

w…….water

1. INTRODUCTION

1.1. General Introduction

Rapid economic growth around the world is largely dependent on the excessive utilization of the fossil fuels (e.g. crude oil, coal etc.). In this process, large quantities of pollutants are being pumped into the atmosphere causing serious damage to the natural balance of the eco-systems. In addition, continual decrease of fuel deposition compels intensive research in further developing the alternative energy resources. In particular, renewable energy sources have the capacity to play a significant role in replacing conventional fuels in four distinct zones, such as electric power production, hot water production, transportation of fuels, and countryside (off-grid) power services. Figure 1 represents the average annual growth in various renewable energy sectors, and by 2010 over 100 countries had initiated policy targets or promotion incentives related to renewable energy. Since 1980 the use of solar technology has increased at a rate of about 30% yearly [1]. In 2010, Renewable Energy Policy Network has reported that about 70 million houses are now using solar water heating (SWH) systems worldwide [2]. The total installed capacity of SWH systems and space heating systems increased by an estimated 16%, reaching only about 185 GW of thermal energy globally (Table 1).

Table 1: Existing capacity of SWH from the year 2007 to 2010 [2, 3]

Selected indicators	**2007**	**2008**	**2009**	**2010**
Renewable power capacity (including hydro) (GW)	1,085	1,150	1,230	1,320
Solar hot water capacity (existing) (GW_{th})	125	130	160	185

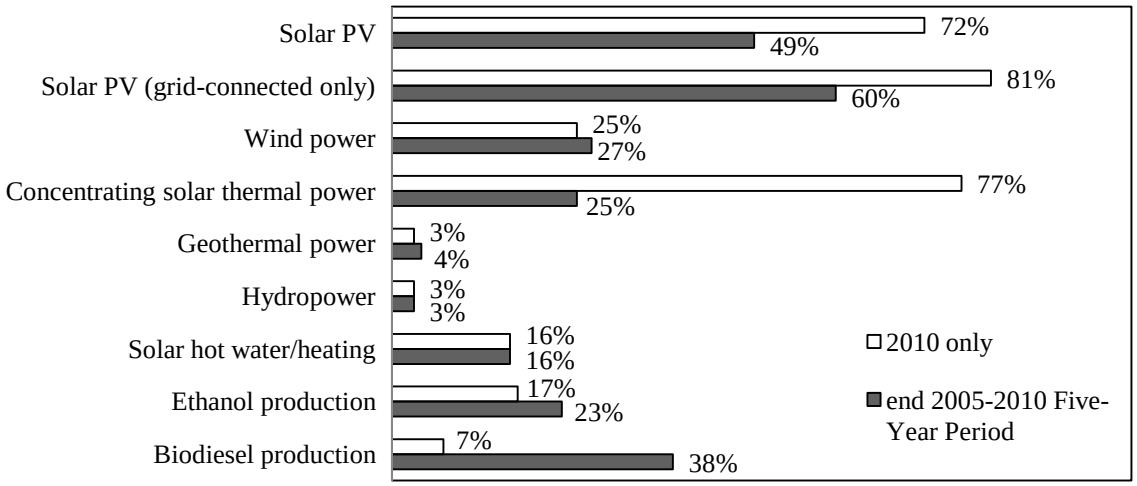

Figure 1: Average annual growth rates of renewable energy capacity, 2005 to 2010 [3]

Considering environmental pollution and energy issues as a background, there exists a need to further research in exploiting renewable energy sources for various applications. Since the signing of Kyoto protocol in 1997 [4], to reduce greenhouse gas emissions by about 5%, the technologically developed countries have had a motivation to switch-over to the ecologically safe chlorine-free refrigerants. The use of hydro-fluorocarbon (HFC) fluids was once thought to be the most acceptable replacement of hydro-chlorofluorocarbon (HCFC) fluids. However, both the categories are in the list of scheduled phase-out because of their influence on the global warming potential (GWP) being far more high, typically above 150 GWP compared to the natural refrigerants. This fact has renewed the interest in utilizing environmentally benign natural fluids, such as: water, air, ammonia, silicon oil, propane and CO_2.

The present study is focused in utilizing solar energy as the heating source; to meet the hot water demand in solar-adverse regions. Very low ambient temperature and wind chill temperatures that prevail in these regions have posed a hurdle (freezing issues) in

utilizing conventional solar collectors. To overcome this issue, the CO_2 is used as an alternative refrigerant in this study. As such, it is non-toxic, non-flammable, has low freezing point, low GWP and has shown to have neutral effect on depleting ozone layer. Moreover, its' inert gaseous behavior, ready availability overcomes the issues pertaining to the corrosion problems and production ability/distribution logistics.

Research on CO_2 based system started since 1990 when Lorentzen [5] utilized a transcritical refrigeration cycle. A wide variety of heat pump and air conditioning systems have used CO_2 as refrigerant. Recently, CO_2 heat pump investigated water heaters are commercially available in the market [6]. One of the systems that could utilize the benefit of using CO_2 is the direct expansion solar-assisted heat pump (DX-SAHP) water heating system. In a DX-SAHP system, refrigerant passes directly through the solar collector where evaporation process takes place. This system is different from the conventional SAHP system, in which, generally a secondary circulation loop is used to transfer thermal energy. By the removal of any secondary circuit in the system (DX-SAHP) requires less refrigerant fluid compared to the conventional one (SAHP). Also, the use of CO_2 is benign, since it is naturally safe and poses no threat on environment in case of leakage.

In the present study, a detailed numerical model has been developed for a SWH system using transcritical direct-expansion heat pump cycle and CO_2 as refrigerant. Model accuracy has been verified for the evaporator section (solar collector) using the experimental data obtained at Fargo, ND, USA, weather conditions. The developed model has been further verified by comparing with the experimental results reported by other researchers. The current study aims at using evacuated tube U-pipe solar collector as an evaporator and examines the influence of various parameters on the system performance.

Operating parameters, such as: solar radiation, collector area, compressor speed and storage volume are varied to obtain the optimal performances of the system in terms of COP, collector efficiency and heating capacity. These simulated results will be useful for to optimally design heat pump integrated SWH system, using CO_2 as the working fluid.

1.2. System Description

Figure 2 shows the schematic of a direct-expansion solar assisted heat pump (DX-SAHP) water heating system consists of an evacuated tube U-pipe solar collector as an evaporator, a compressor, an immersed heat exchanger in a hot water storage tank which acts as a condenser and an expansion device. Initially, liquid CO_2 is allowed to flow directly through the heat removal U-pipe that is inserted into the evacuated tube solar collector. With gain in solar radiation, liquid CO_2 gets heated and eventually gets vaporized. The evaporated refrigerant is then compressed in the subsequent compression process [1 – 2] to a supercritical vapor pressure state. Energy released by the supercritical CO_2 vapor through the coil condenser immersed in the storage tank, used to heat water. Finally, the high pressure but low temperature CO_2 is throttled [3 – 4] to the evaporator pressure. All the events described above are shown in the idealized pressure-enthalpy diagram (Fig. 3).

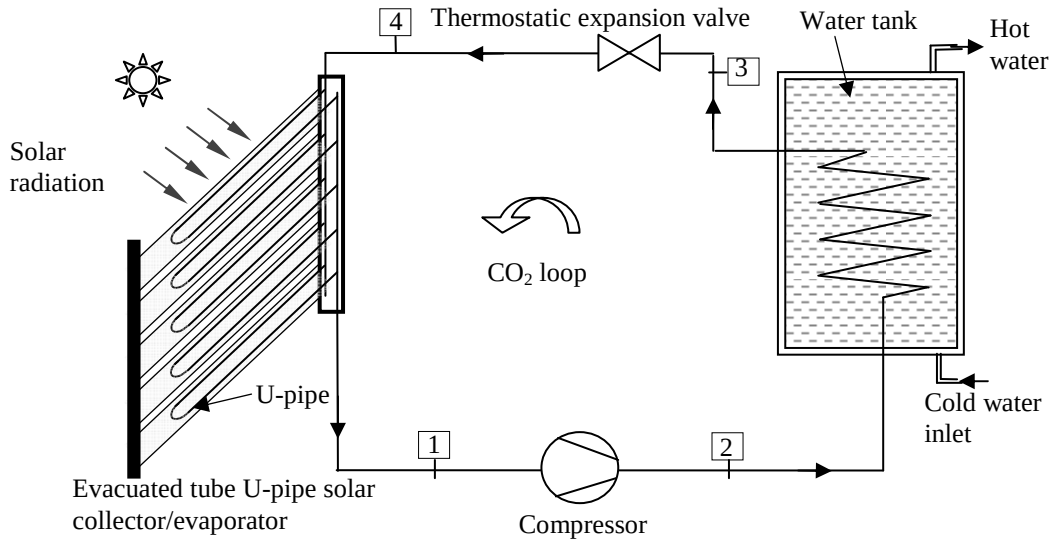

Figure 2: Schematic diagram of a direct-expansion solar assisted heat pump water heating system

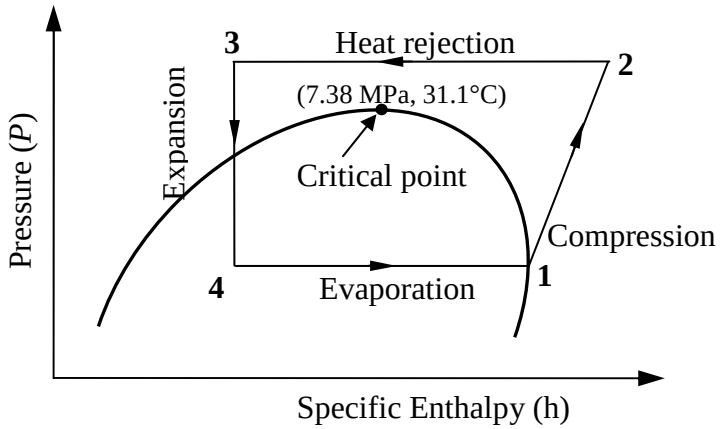

Figure 3: P-h diagram of transcritical CO_2 heat pump cycle

1.3. Outline of Thesis

The present study is detailed in seven chapters. Literature review pertaining to SWH systems including the performance, recent trends, and various economic aspects of SWH systems are presented in chapter 2. An overview of the scope and objectives of the

present study is given in chapter 3. Chapter 4 provides an in-depth thermodynamic analysis of different components considered into the system. Chapter 5 describes the model development and the simulation procedure. Chapter 6 includes the model validation and design optimization of such system. Based on the optimum results, the seasonal performance variation is also shown. Final chapter summarizes the important merits of the system and also suggests future research direction in the said field of work.

2. LITERATURE REVIEW

The present study's focus is about the SWH system being operated in a direct expansion heat pump mode, using carbon dioxide as a refrigerant in a transcritical cycle. This review attempts an in-depth analysis of different technologies used in SWH systems for the purpose to determine important features that influence the SWH performance.

2.1. Available Solar Radiation in North Dakota

North Dakota receives higher percentage of available sunshine hours yearly. On an average, this state receives 58 – 62% of total possible sunshine hours annually [7]. The percentage of sunshine hours is the measure of time between sunrise and sunset. About three-fourths of the possible yearly sunshine is registered for the month of July and hence the most sunny and November receives minimum sunshine hours compared to other months. Annually, an average of 2,600 to 2,800 sunshine hours are recorded in North Dakota with an average of daily 14,644 – 15,480.8 MJ/m^2 of solar insolation. Even though the sunshine hours between January to June varies considerably in North Dakota, the percentage of available sunshine hours remains uniform, +/- 55% for any given month (Fig 4).

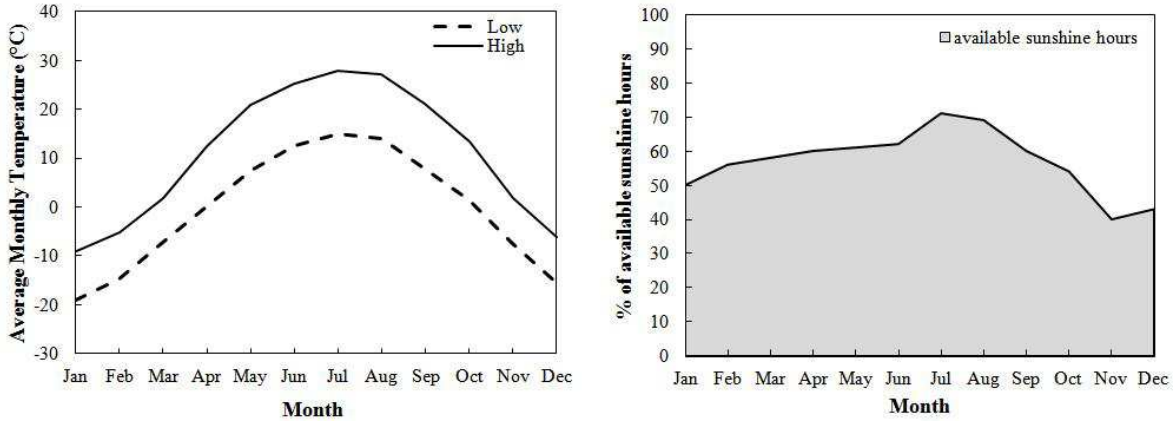

(a) (b)

Figure 4: (a) Average temperature range [8] and (b) average percentage of possible sunshine by months [7] in Fargo, North

2.2. A Brief History of SWH Systems

SWH advanced from hypothesis to a prototype in the year 1767 by Swiss naturalist De Saussure, who built an insulated box painted black at its bottom with two panes of glass covering at the top [9]. It was called as "Hot Box", hence the invention was capable of aiding in cooking, heating, and producing hot water. But the first commercial SWH, named Climax, was patented in the US by Clarence M. Kemp in 1891 [10]. His idea was further implemented as an integral collector storage solar water heater. Kemp placed a metal tank within a wooden box covered by a glass cover at the top part. His system produced hot water (38.8^0C) on sunny days. As an alternate to burning wood or expensive fuel for heating water, the SWH became popular in California and many other states very quickly. A third of all of the homes in Pasadena, California had SWH systems by 1897 [11]. In early 1900s, several researchers focused their attention in improving the design of the SWH system to make it durable and efficient. In 1909, William Bailey tailored the Kemp's SWH

system, by segregating it into two major parts; the solar thermal collector for collecting solar radiation along with storage tank for storing the produced hot water. Further, to prevent heat losses the storage tank was insulated. For the first time in the SWH field, William Bailey introduced the thermosyphon principle to aid the circulation of water in the collector and storage tank [12]. In 1950, Japan's first commercial SWH was designed by Yamamoto by getting an inspiration from a view of a large bath tub, filled with water that was kept outside in the sunshine for a longer period of time. Later, SWH units based on the closed-pipe system were introduced.

Solar heated water was utilized for several applications. Until 1930, hot water for domestic purposes and for space heating were mainly engaged by the coal fired boilers [13]. SWH become a commercial product in the early 1960s. Typical thermosyphon-based SWH uses an absorber area of 3–4 m^2 flat-plate type solar collectors to energize a capacity of 150–180 liters storage tank. Yet another popular types of SWH, is the forced circulation water heating system. Except for solar collectors, other accessory items such as the storage tank incorporated with piping, pump, and differential thermostat are usually kept indoors.

Solar assisted systems not only rely on the conventional mode of utilizing energy but also other systems, such as heat pump (HP) and photovoltaic thermal (PV/T). In 1927, HP technology was first patented by an English inventor Haldane [14]. However, before the 1960s, due to a record poor reliability of the HP units, the commercial distribution was very limited. Since then, research focus was directed on, and by the year 1970, the HP technology has been improved in quality and reliability. Moreover, the researchers had been motivated to find new alternative energy sources for energy production since the big oil crisis in 1973. This further aided the application of HP technology and it became

widespread for both heating and cooling purposes. Although solar HP technology has shown higher efficiencies (400–600%) in respective functions, its capital cost is high, and hence it may not be suitable in places where cost of the system becomes a constraint [15, 16].

Production of the SWH is now in packaged form and developed into a considerable business in the 21st Century. In countries such as China, Australia, Germany, Greece, Israel, and USA, the manufacturing of SWHs has become a part of the industrial sector. Self-motivation is a factor that worked behind the rapid expansion of SWH manufacturing industries in most parts of Europe. Currently, commercially available SWHs employ the following types as the packaged form: a system being operated by passive mode with an anti-freeze working fluid, solar-assisted heat pump system, a variety of evacuated solar collectors of both flat-plate and tubular in shape and an active circulation system driven by pumps facilitating a wide range of flow rates.

2.3. Categorized Studies Conducted on SWH Systems

Depending on the nature of heat transfer through the working fluid, SWH systems can be broadly classified into: direct systems and indirect systems. In the direct system, water is heated directly in the collector. In the indirect system, a heat transfer fluid is heated in the collector which is then passed through a condenser or a heat exchanging device to heat water. Similarly, depending on the circulation of working fluids, SWH systems can also be grouped into either: passive circulation system or active circulation system. Passive circulation systems refer to thermosyphonic method in which the density difference induces the circulation of the fluid, naturally. On the other hand, active circulation employs a pump to effect forced circulation of the working fluid.

Kalogirou [17] classified solar energy systems used for water heating application into five different categories: (a) thermosyphon systems, (b) integrated collector storage (ICS) systems, (c) direct circulation systems, (d) indirect water heating systems, and (e) air systems. The first two category falls under passive circulation mode while the rest three into active circulation mode. To overcome the freezing of the working fluid, during adverse weather conditions, different techniques have been employed such as recirculation or drain-down technique and drain-back technique for direct and indirect SWH systems, respectively. Usually differential thermostats are used to control the system in accordance to the hot water demand with an exception to thermosyphon and integrated collector storage systems. In the following sections, a variety of SWH systems are reviewed and classified in terms of circulation methods and applications.

2.3.1. Passive SWH Systems

The passive system (Figure 5) works on the principle of density difference to transport heat energy. Potable heat transfer fluid (i.e. water) is heated by a solar collector and the natural convection drives the water from the solar collector unit to the hot water storage tank. Water becomes less dense due to solar heating and expands according to the temperature rise. Hot water is circulated to the storage tank, and the relatively cooler water from the bottom of the tank is circulated to the solar collector device. This flow is dependent on the duration of sunshine, since it aids density variation which in turn affects the flow of water. To reduce pipe friction, a larger pipe diameter is recommended rather than the normal size (2–3 inch diameter). Usually, connecting lines are kept at an angle to prevent the development of larger air bubbles that would resist the flow of water. Also, the solar collector-inlet is connected to the bottom of the storage tank to avoid reverse flow. In

situations, where the collector working pressure is less than the direct supply of city water, suitable pressure reduction valves are used. Usually an auxiliary heater is included to augment the heating process of a SWH, in particularly when used in solar adverse regions [18].

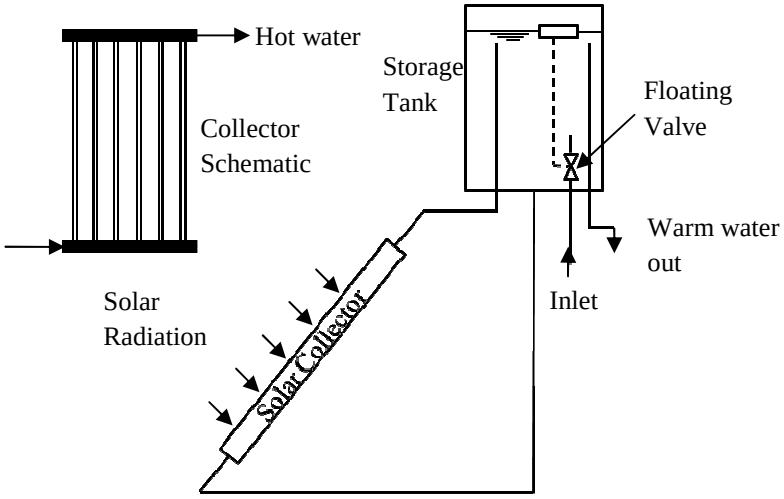

Figure 5: Schematic diagram of thermosyphon SWH system [19]

Unlike the conventional SWH system in which a collector acts as an absorber of sunlight, the ICS system utilizes both the collector as well as the storage tank as an absorber to collect solar radiation (Fig. 6). In most cases, the entire exterior part of the reservoir acts as an absorber. However, these systems are subjected to heavy heat losses, especially during non-sunshine hours. Several measures, such as selective absorber surface coatings, insulating materials, and a single or double glazing glass covers have been used to reduce the heat losses. A few other techniques were also attempted to culminate the heat loses: movable protection cover, insulated baffle plate, and utilizing phase change material (PCM) inside the storage tank. Researchers have also attempted to use transparent insulating materials for the appropriate exposed parts. Further, to reduce the heat losses, the

storage tank was operated on thermal stratification modes, by drawing the hot water from the top of the storage tank and cold water inlet to the bottom of the tank.

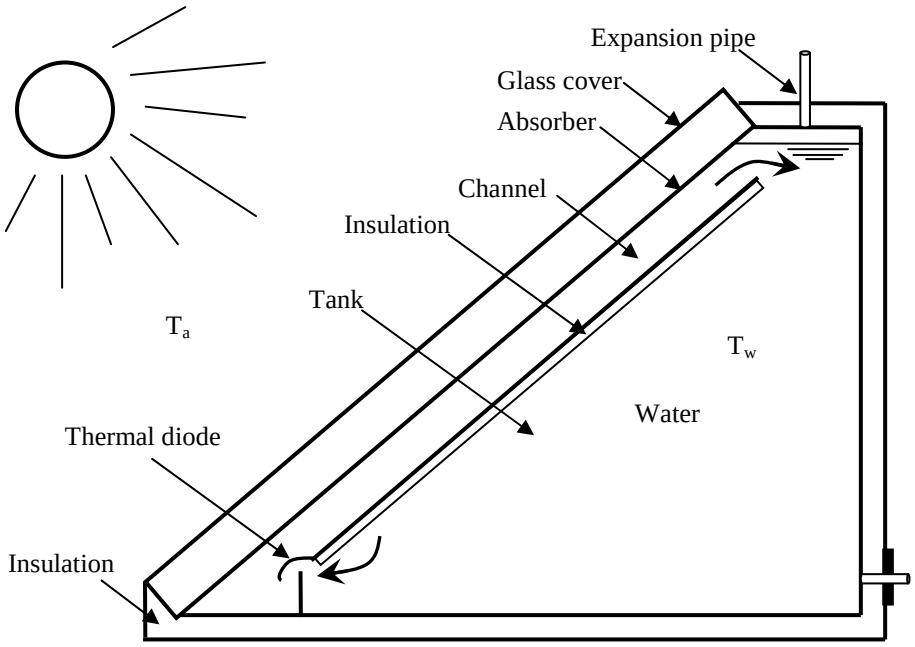

Figure 6: Schematic diagram of ICS solar water heating system [20]

2.3.2. Active SWH Systems

Unlike passive systems, active circulation systems require a pump to circulate water from storage tank to the collector to get heated. The hot water flows back to the storage system and is ready for the end-user (Fig. 7). The pump is usually controlled by a differential thermostat that regulates water at the top header by a sufficient margin to the bottom of the tank. A check valve prevents the reverse circulation to avoid nighttime thermal losses from the collector. The collectors can be positioned either above or below the storage tank as pump is used to activate circulation. Direct circulation system is generally used only under situations when freezing is not a concern. Sometimes, water

from the cold storage tank or city water supply can be used directly into the system. Care should be taken when quality of water is hard or acidic, in a direct circulation system since it would result in scale deposition which in turn may cause clogging or corrosion of the collector tubes. Direct circulation systems more commonly employ a single storage tank which is with an auxiliary heater. However, in few case-studies, two-tank storage systems have been used as well.

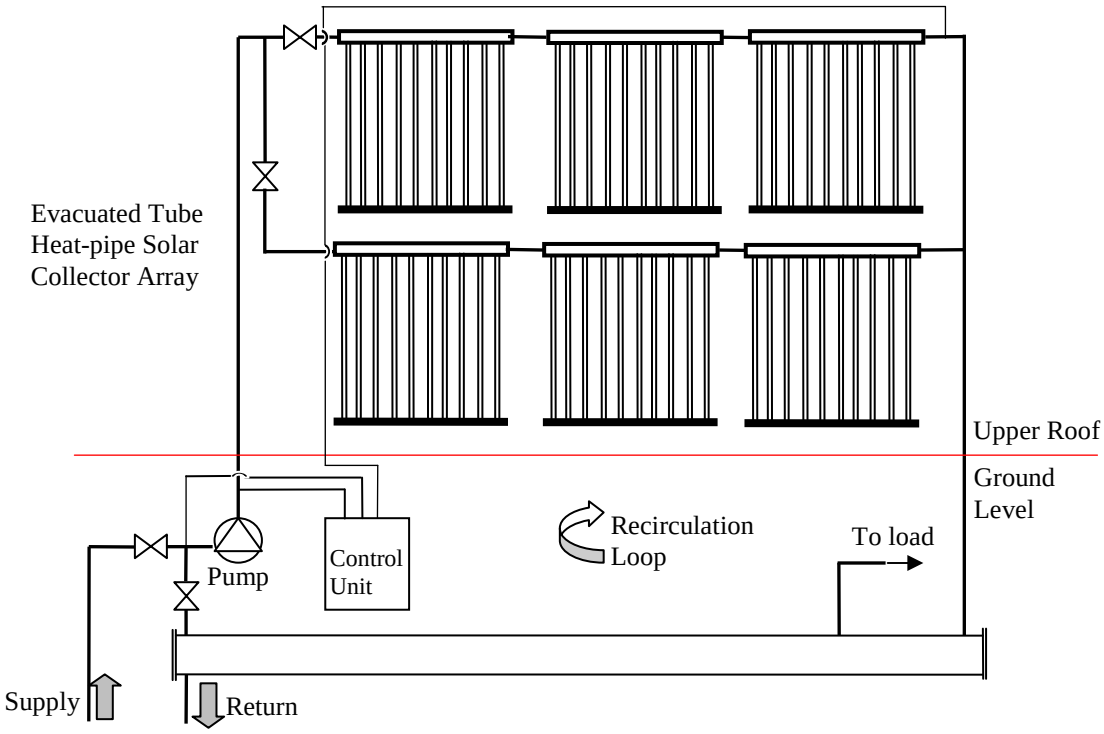

Figure 7: Schematic diagram a direct circulation SWH system [21]

Indirect systems of SWH utilize two circulation loops to effect heating: (a) the closed-collector loop and (b) the open storage tank loop. Usually, the heat transfer fluid is circulated within the closed-collector loop, to gain the heat and is then passed through a heat exchanger where heat is transported to the potable water that flows in an open loop to

the storage tank. There are several different types of working fluids used in the closed loop, such as water, refrigerants, and anti-freeze mixtures. The heat exchanger can either be an internal system (Fig. 8) (placed inside the water storage tank or outside of the storage tank) or as an external system. An expansion tank integrated with a pressure relief valve is used in the closed circulation loop system. In the pressurized system, the tank is provided (an additional expansion tank) to have a control on temperature and pressure of the working fluid. However, for the unpressurized system, the tank is provided to release the pressure when required to vent.

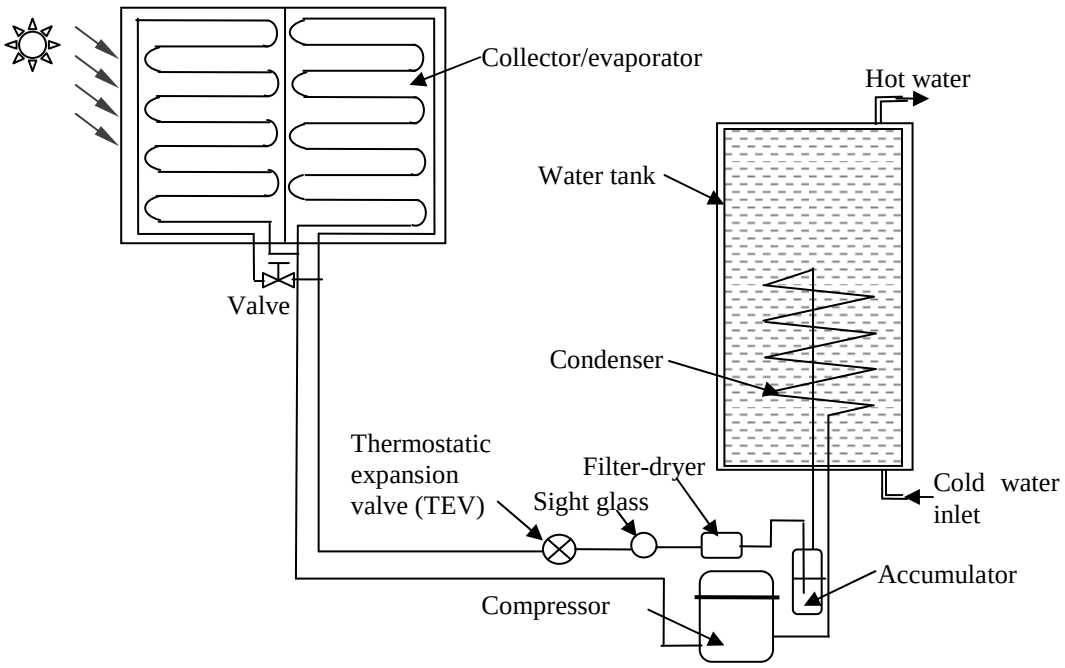

Figure 8: Schematic diagram of indirect water heating presented by Kuang et al. [22]

Unlike water or other refrigerants, air has also been used as working fluid, for its unique advantages. Compared to the conventional SWH system, air can be used as a working fluid even during freezing weather conditions, is non-corrosive, and requires only

low maintenance requirements. However, the system is generally large and requires considerably large space for air handling unit. A typical arrangement of a solar air heating system incorporated with a pebble bed storage unit is illustrated in Fig. 9. Fans and dampers are incorporated to aid the system operation. The heat gained by the air in the collector duct is released through a heat exchanger to aid domestic hot water supply of up to $80^{o}C$.

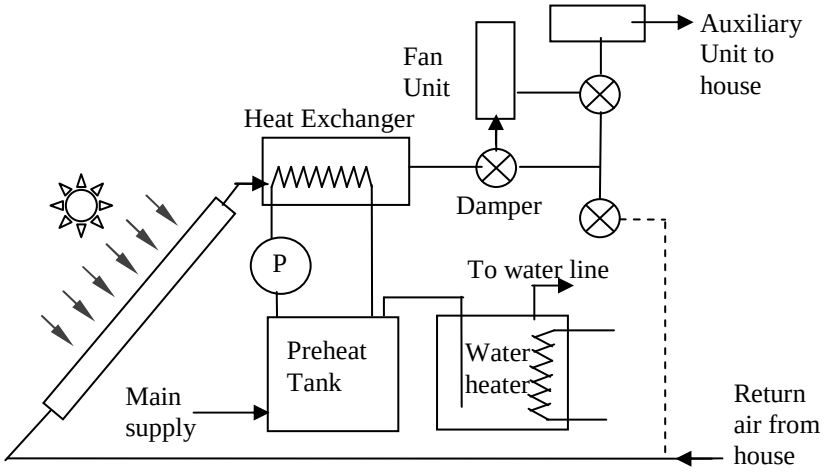

Figure 9: Schematic diagram of standard air system configuration [23]

A major drawback of the air systems is that air has low heating capacity and its performance deteriorates further when the ambient temperature is very low. During the inevitable situations, when the SWH system has to be employed, to operate in adverse weather conditions (where ambient temperature can go below 0°C) certain modifications are introduced in the design of SWH system to overcome the freezing issues. One such modification is to operate the direct circulation system in drain-back mode. Generally, a differential controller integrated pump is used to circulate water from the storage tank to

the solar collectors. A drain-down valve provides the freeze protection function. While turned on by the controller, the valve isolates the solar collector inlet from the storage tank outlet. At the same time, the differential controller opens a valve that permits water to drain away from the collector. In order to drain water out from the bottom of collectors, a vacuum breaker is installed at the top of each collector to allow the air circulation. For well-known reasons, such as, low cost and superior anti-freeze performance, all-glass vacuum tube collectors are commonly used in domestic SWH system. In the past few decades, majority of vacuum tube collectors were used for domestic water heating purposes. As expected, the performance of vacuum collectors is higher than flat-plate collector due to low convection heat loss from the absorber. The heat transfer model evaluates the performance of all-glass vacuum tube collectors incorporated in a direct circulation system was developed by Li et al. [24]. This simplified model takes into account of natural circulation in single glass tube as well as forced flow circulation in the manifold header. The flow equations were obtained by analyzing the friction losses and buoyancy forces inside the tube. A positive agreement was observed between the predicted and computed collector outlet temperatures, and the deviation was within 5%. The system schematic is shown in Fig. 10. Walker et al. [25] designed and installed a direct circulation SWH system at the Social Security Administration's Mid-Atlantic Center in Philadelphia. Evacuated-tube heat-pipe solar collector of 36 m^2 net absorber area was employed to energize the storage tank. The simplicity in design and low erection cost made the system attractive to be implemented in commercial buildings. Unlike conventional systems, in this system the incoming water was preheated in the recirculation loop.

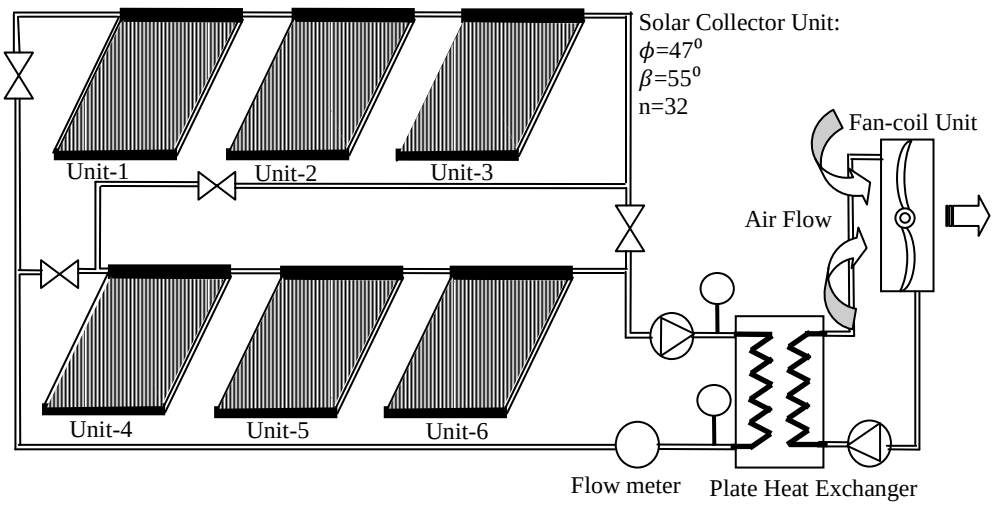

Figure 10: Conventional domestic SWH system in adverse weather regions [24]

Due to the fact that evacuated tube collector generate high temperatures beyond 100°C, it might be a point of concern when operating in regions where the ambient temperature and solar radiation availability is high during summer. To prevent thermal losses from the evacuated tube, a high temperature switch can be employed. This control switch can overcome the abovementioned issue. To overcome the two temperature extremes, such as overheating in summer and freezing in winter, air can be used as the working fluid in the circulation tubes rather than using water directly. A fan is used to mobilize the air through the flow distribution tubes and the concentric air-to-water heat exchanger delivers the heated water to the horizontal storage tank.

2.4. Comparison Between SAHP System and DX-SAHP System

Heat pump systems transfer heat energy from low temperature heat source to a high temperature heat sink against a temperature gradient. The delivered heat is generally used

to heat air or water. The heat usually absorbed from ambient air, solar, geothermal, or any reusable waste energy source. The energy transport in the heat pump system is carried out by a refrigerant fluid which follows four thermodynamic stages in a complete cycle. Figure 11 shows the basic processes of the heat pump cycle. During evaporation, the abounded heat energy is being absorbed by the working fluid and goes through the phase-change phenomena from liquid to vapor. The saturated vapor is then pumped by a compressor to rise up to the condensation pressure. The raised pressure eventually increases the temperature of the working fluid. At this condensation pressure and temperature, the heated fluid rejects heat energy and throttles to a lower evaporator pressure to complete a full thermodynamic cycle. The basic thermodynamic processes are also shown in the pressure-enthalpy diagram of Fig. 12.

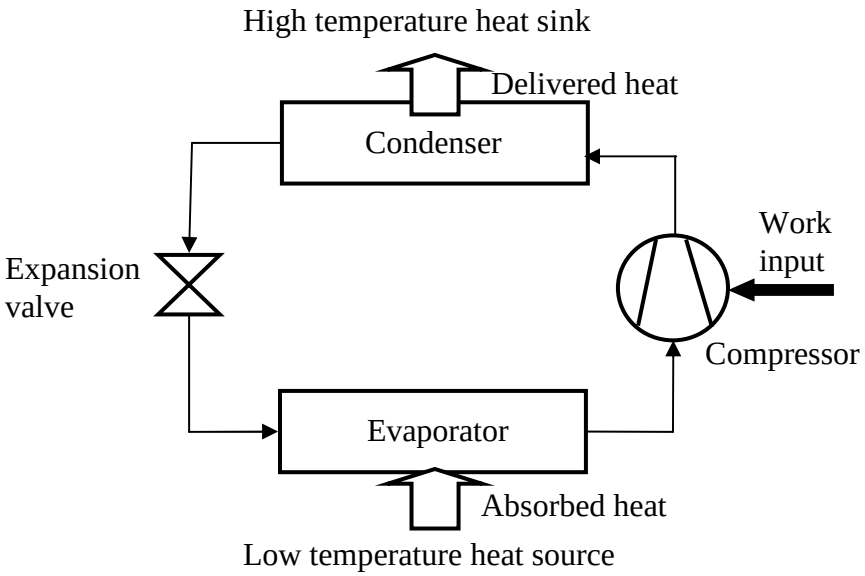

Figure 11: Schematic of Heat Pump system

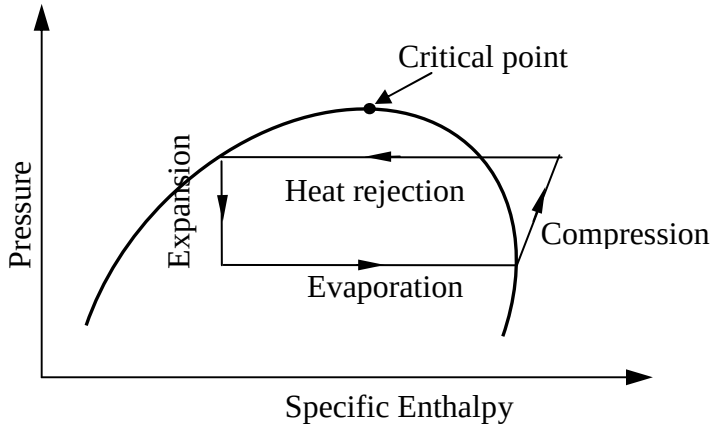

Figure 12: Pressure-enthalpy (P-h) diagram of HP cycle

The thermodynamic cycle explained above shears the subcritical zone since its pressure and temperature remains below the critical point for its complete cycle. Critical point is the peak point on the saturated dome at which both saturated liquid and vapor states are similar and beyond this point the fluid phase is called as supercritical state [26]. Most of the heat pump systems are designed to use the working fluid having higher critical point and hence always work in the subcritical mode. The performance of the HP systems is measure by the coefficient of performance as COP. It is the ratio of heat delivery to the work energy input into the system. The COP of the HP system can be more than unity because of the delivered heat energy very often reaches multiple times higher than the compressor work input.

$$COP = \frac{Heating\ Capacity}{Work\ Input} \quad (1)$$

Conventional solar-assisted heat pump (SAHP) systems utilize the solar collector and heat pump as separate units and used an intermediate heat exchanger to complete the heat transfer circuit. The use of SAHP increased as the commercial solar collectors entered

into the market. Several researchers have developed and tested various SAHP models [27 – 30]. However, recently developed direct-expansion solar assisted heat pump (DX-SAHP) systems integrate the solar collector and heat pump evaporator unit into a single unit [31-36]. The above mentioned types have used flat-plate solar collector as evaporator and halocarbons as refrigerant. A DX-SAHP system employs solar collector as an evaporator. The refrigerant that passes through the solar collector expands directly by the useful heat gain from the solar radiation and undergoes a phase transition phenomena from liquid to the vapor state. The differences between the SAHP and DX-SAHP system configurations can be understood by observing Fig. 13 and Fig. 14.

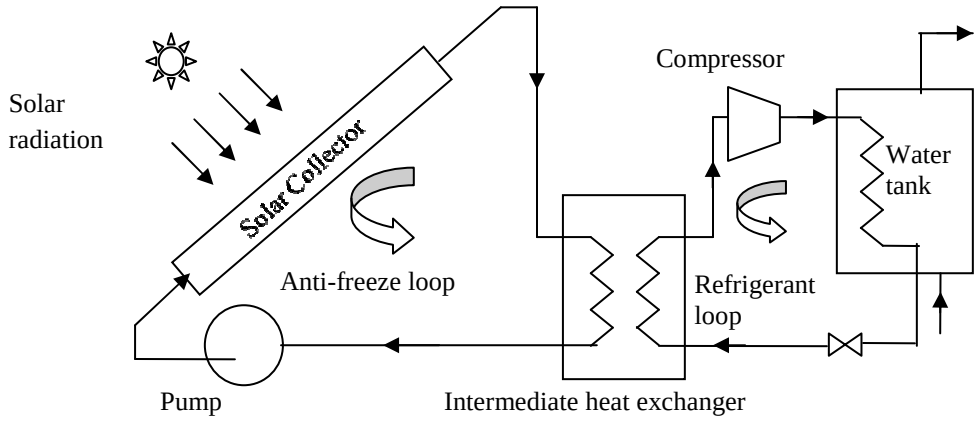

Figure 13: Conventional solar-assisted heat pump system

The performance of a DX-SAHP system directly influenced by the incident solar radiation due to the elimination of an extra heat transfer loop as it is needed in the conventional SAHP system. This useful heat gain by the refrigerant can be improved by maintaining the evaporator temperature slightly higher than the ambient conditions. Higher the temperature difference between the evaporator and the surroundings result in higher

heat losses reflecting in lower efficiency of the system. Hence, it is preferable to maintain the evaporator (collector) temperature at low or closer to ambient temperature in order to minimize heat losses from the collector. However, it is preferred to operate the evaporator in the temperature range of 0° – 10°C higher than the surroundings, because of the fact that, higher temperature effects higher useful heat gain [37]. One of the critical designs pertaining to the solar-assisted heat pump system is the proper sizing of solar collector. Sizing of the solar collector is necessary because of the heat absorbing capacity which needs to be matched with the evaporative capacity of the compressor. A proper matching between solar collector and compressor minimizes heat losses and impacts the system performance as a whole. By adding a compressor capacity modulator, an off-design condition such as, seasonal variation can be optimized.

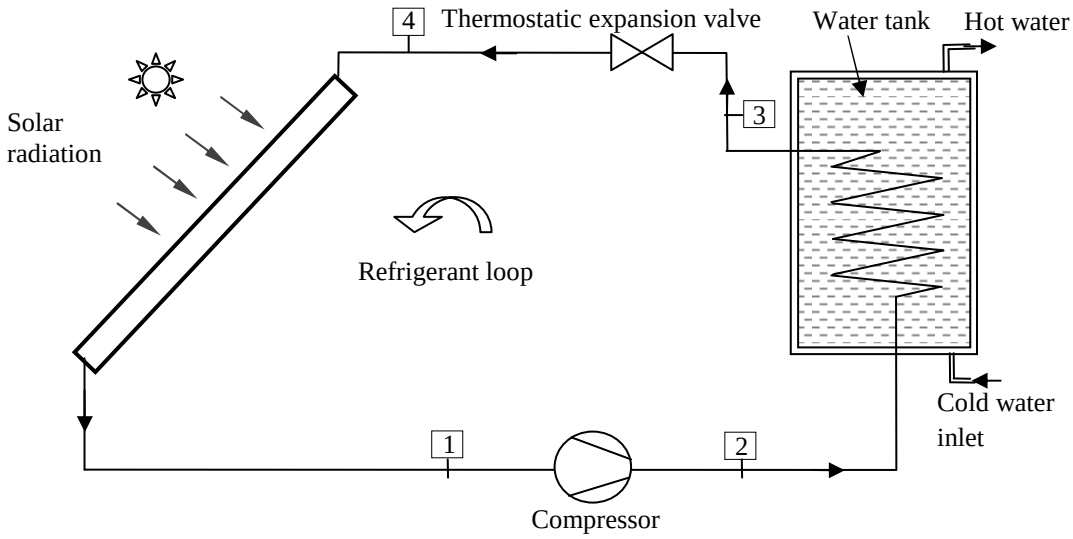

Figure 14: Direct Expansion Solar-assisted Heat Pump (DX-SAHP) system

There are many potential benefits of using a DX-SAHP system over a conventional SAHP. Due to the use of many synthetic refrigerants, corrosion problem can be minimized

into the DX-SAHP system. Therefore, long term uses can be assured of the solar collector used in DX-SAHP system in comparison with a water-based solar collector where corrosion is a big problem. In a water-based system, freezing is an issue for solar-adverse region. However, a DX-SAHP system easily overcomes this problem since most of the refrigerants have a very low freezing point. Since DX-SAHP system does not require an extra intermediate heat exchanger, it improves thermal performances of the system and reduces the initial system cost.

There exists numerous works [38 – 45] related to the heat pump mode of SWH systems and some significant investigations are discussed in this section. A variable capacity direct expansion solar-assisted HP system for the DWH purpose was tested by Chaturvedi et al. [38]. The system used a bare solar collector acting as an evaporator for the heat pump system. The system was tested for the widely varying ambient conditions, and accordingly the compressor speed was varied through a variable frequency drive. The observational results showed that the coefficient of performance (COP) of the system can be enhanced extensively by reducing the speed of the compressor when the ambient temperatures are higher. Hence, such systems perform better in summer compared to winter.

Hawlader et al. [39] designed, fabricated, and tested a combined solar-assisted HP dryer and water heater that had been examined under the ambient conditions of Singapore. The system consisted of a variable-speed reciprocating compressor, solar collector as evaporator, water storage tank and, an air-cooled condenser. To assess the influence of different variables and the performance of the system, a Formula Translation (FORTRAN)-aided simulation program was developed. The system performance with and without an

auxiliary water heater, was compared in terms of the performance parameters, such as SF and COP. The COP values of the predicted and experimental studies were reported to be 7.0 and 5.0, respectively. Similarly, the SF was 0.65 and 0.61, respectively.

The performance of an integral-type solar assisted heat pump (ISAHP) water heater was carried out by Chyng et al. [40]. Simulations were performed based on the assumption that, except the storage tank, all other components are at steady-state. The model agreed well with the experimental data and the predicted results were within 10% of the measured data. Analytical and experimental studies on a direct-expansion solar-assisted heat pump (DX-SAHP) water heating system were conducted by Kuang et al. [41]. The system comprised of a 2 m^2 bare flat-plate collector was used as an evaporator as a part of the refrigerant cycle. The long-term thermal performance of the system was predicted by a simulation model. The results have shown that monthly average COP ranged from 4 to 6, while the solar collector efficiency varied from 40–60%. A similar work was carried out by Li et al. [42]. The DX-SAHP system comprised of 4.2 m^2 area of solar collector as evaporator, a 0.75 kW hermetic compressor of rotary type, 150 liters water storage tank with a copper coil of 60 m length submerged into the tank, a thermostatic expansion valve, and R-22 refrigerant was used as the working fluid. The system was shown to heat 150 liters of water a day to a temperature of 51°C, when the maximum solar radiation received at noon was about 955 W/m^2. The exergy analysis on each of the element of the DX-SAHP water heating system, identified that most heat losses occurred in the compressor, followed by the collector, and the condenser. To further enhance the thermal performance (for the SWH system as well as all the other components), additional methods were also suggested. Hepbasli [43] also carried out exergy analysis to evaluate the performance of a

solar-assisted domestic hot water tank coupled with ground-source heat pump (GSHP). Along with the GSHP system components, a solar collector of 12 m^2 surface area and a water storage tank was integrated to it. Results proved that, it is possible to attain 14.5% efficiency for residential SWH system and 44.06% when the entire system is taken into account.

Heat pipes were also introduced in heat pump application for water heating purposes. Huang et al. [44] worked on heat pipe solar-assisted conventional heat pump (HPSAHP) water heating system. The performance of the combined solar heat pipe collector and conventional HP were examined to calculate the overall COP of the system. When solar radiation was low, the system operated in HP mode. However, during the clear sunny days, the heat-pipe mode operated independent of electrical energy input, to higher thermal efficiency. The results showed that the COP of the hybrid-mode of operation could attain as high as 3.32, and as such its performance was higher by about 29% compared to the HP mode of operation. Guoying et al. [45] carried out a numerical study to evaluate the operational performance of a solar air-source heat pump (SASHP) water heater. This system was specially designed which utilizes a flat-plate solar collector being provided with spiral-finned tubes to collect energy both from solar radiation, as well as from the surrounding air. For the given meteorological conditions of Nanjing, China, the theoretical results showed that the designed SASHP water heater of 150 liters capacity could efficiently heat water up to 55°C.

2.5. Transcritical Heat Pump Cycle

Unlike conventional HP cycle, the transcritical HP rejects thermal energy at above critical point. The evaporated refrigerant is being compressed by a compressor and raised

to a pressure and temperature higher than P_{crit} and T_{crit}. As there is no condensation process beyond critical point, the cooling of the heated fluid is called gas cooling process. In the supercritical phase, there exists only single phase and hence the heat rejection takes place as sensible cooling. The rest of the thermodynamic stages in transcritical HP cycle remain the same as the conventional one and the difference can be seen by comparing the P-h diagram of Fig. 12 with that of the Fig. 15.

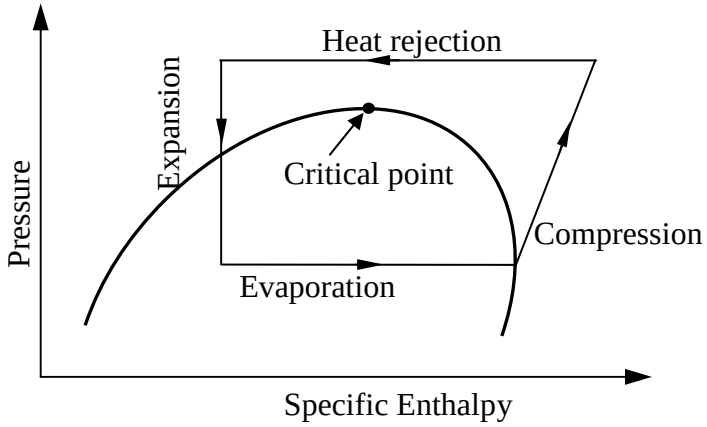

Figure 15: Pressure-enthalpy (P-h) diagram of a transcritical HP cycle

As it can be observed from the saturation dome on P-h diagram of CO_2, the advantage of using transcritical cycle can be realized in terms of heat of vaporization. The heat of vaporization of CO_2 decreases significantly as the condensing temperature approaches near to critical point (31.1°C, 7.38 MPa). Similarly, heat absorption by the liquid-vapor phase change minimizes if the evaporating temperature nears the critical temperature. Therefore, the CO_2 system which operates in subcritical manner rejects small amount of heat and correspondingly the outlet temperature of the condenser remains low. For air-cooled CO_2 refrigeration system which operates in subcritical mode, offers lower

performance when surrounding air temperature reaches the critical temperature. Hence, for better system performance, condensing temperature should remain higher than ambient. Therefore, in a CO_2 transcritical cycle, higher heat rejection temperature can be achieved which improve the heat pump system applications.

2.5.1. Thermophysical Properties of CO_2

Refrigerants are primarily developed for vapor compression refrigeration systems for cooling rather than heating. The utilization of CO_2 as refrigerant for the vapor compression cycle was introduced in 1866 by Thaddeus Lowe. Pearson [46] studied a detail historical development of CO_2 in the refrigeration systems. However, CO_2 has a limitation since it needs robust components for its high pressure system. At the early 1900, the invention of HFC and HCFC fluids took the interest from CO_2 for its expensive and robust design. Although HFC and HCFC fluids have higher thermodynamic efficiency, they also have many detrimental effects on the environment. Therefore, interest on using natural refrigerants into the refrigeration, air conditioning and heat pump systems renewed for environmental safety issues and its protection.

There are many natural substances, such as, water, air, ammonia, sulfur dioxide, silicon oil, propane and CO_2 which have the potentiality for using as refrigerant. Among these fluids, water has freezing issues, when exposed to the weather conditions below 0°C. Similarly, the thermodynamic cycle dealing with air as working fluid has relatively low cycle efficiency. Ammonia and sulfur dioxide also have their own drawback of being slightly toxic. The use of silicon oil is restricted to its use due to the high viscosity. Although purified propane as refrigerant is gaining favor, but when mixed with air it is highly flammable. CO_2 is the natural refrigerant which imposes negligible impact on the

environment. In 1990, Gustav Lorentzen first patented CO_2 transcritical cycle for the automotive air conditioning system application [5]. The patented automotive air conditioning system using CO_2 transcritical cycle was further tested by Lorentzen and Pettersen [47] and compared the performances with a similar R12 system. The test results showed a positive encouragement for further development of such system [48].

Design of heat pump system and its performance is dependent on the selection of refrigerant, since the thermophysical properties of a refrigerant are important for heat transfer process. Table 2 is showing some of the physical natures of CO_2 which are different from many other conventional refrigerants. In this section, a detail of CO_2 properties will be discussed in order to get a better idea about the use of CO_2 in transcritical heat pump systems.

Table 2: A brief comparison of CO_2 with other conventional refrigerants [49]

Refrigerants	**R-12**	**R-22**	**R-134a**	**R-410A**	**Ammonia**	**CO_2**
ODP/GWP	1/8500	0.05/1700	0/1300	0/1900	0/0	0/1
Flammability/toxicity	N/N	N/N	N/N	N/N	Y/Y	N/N
Normal boiling point (°C)	-29.8	-40.8	-26.2	-52.6	-33.3	-78.4
Critical pressure (MPa)	4.11	4.97	4.07	4.79	11.42	7.38
Critical temperature (°C)	112	96	101.1	70.2	133.0	31.1
Refrigeration capacity (kJ/m^3)	2734	4356	2868	6763	4382	22545

As it can be seen from the table 2, the critical temperature of CO_2 is very low compare to other working fluids. Due to the high critical point of any HFC and HCFC fluids, the conventional vapor compression cycle rejects heat in the condensing temperature below the critical point. But in the system pertaining with CO_2 as refrigerant, this heat rejection temperature very often exceeds the critical point and hence does not share the liquid-vapor mixture phase region. The heat rejection in this process is called the gas

cooling process and rejects heat only in the sensible cooling. Therefore, heat rejection process of the gas cooler undergoes in the transcritical cycle. However, the critical pressure of CO_2 is relatively very high (7.38 MPa). This makes the CO_2 heat pump cycle experiences with high working pressure. Although in the CO_2 HP cycle, evaporator pressure ranges between 2 – 5 MPa, the gas cooler pressure can reach up to 15 MPa [50]. This pressure range is quite low in the case of R134a where at 50°C the condenser pressure is only 0.13 MPa [51]. Due to high working pressure, the CO_2 systems face many design challenges. One of such is the design of compressor capacity. However, current technological development on the manufacturing of high pressure compressors make the transcritical CO_2 heat pump cycle feasible for the commercial uses [49]. In fact, it could be beneficial in terms of heat transfer properties of using such high pressure CO_2 system. This leads to higher vapor density (shown in Fig. 16(a)) resulting higher volumetric refrigeration or heating capacity of the HP system. The profit can be drawn compared to other refrigerants in terms of smaller volumetric mass flow rate for the same magnitude of energy gain. Thus the system design is compact in nature [49 – 50].

The heat transport properties of CO_2 are favorable especially near to its critical point compared to other conventionally used working fluids. Supercritical properties of CO_2 need to be understood in order to realize the refrigerant behavior in transcritical HP cycle. There occurs a sudden supercritical property variation near the pseudo-critical temperature point (T_{pc}) of CO_2. It is the temperature at which specific heat (C_p) reaches to its maximum value for a given pressure, as it is seen from Fig. 16 (b). Besides, C_p value decreases with the increase of working pressure and pseudo-critical temperature. C_p value attains much higher only near the critical pressure. CO_2 transport properties (thermal

conductivity and viscosity) also vary abruptly near the T_{pc}. These heat transport properties affect the performance of the transcritical HP cycle on the gas cooler heat rejection process. Oh and Son [53] predicted the heat transport properties of the supercritical CO_2 in order to evaluate heat transfer coefficient in horizontal tubes for the gas cooling process and found a significant variation near the pseudo-critical region.

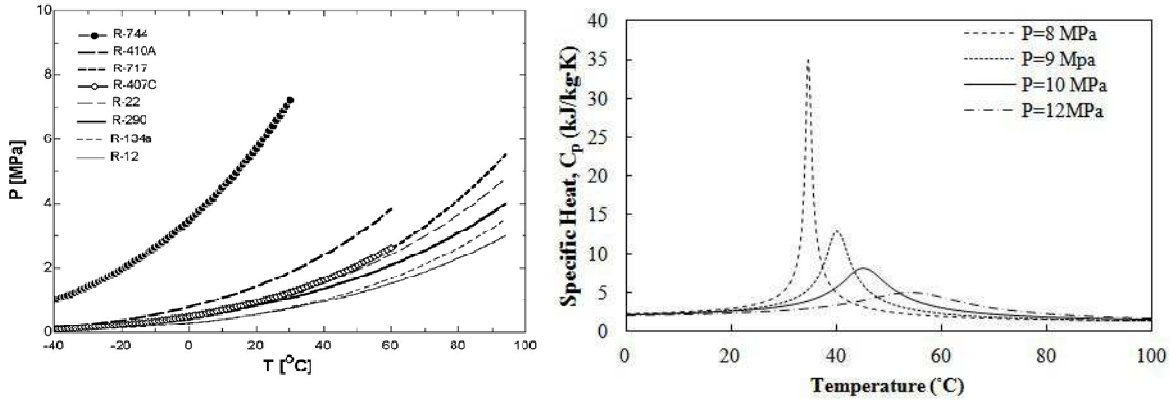

(a) Vapor pressure (b) Specific heat

Figure 16: (a) a comparison of vapor pressure of CO_2 with other refrigerants; (b) specific heat variation of CO_2 for different pressures [49, 52]

Figure 17 illustrates these variations of CO_2 transport properties as thermal conductivity and viscosity. Thermal conductivity of CO_2 is 20% higher for saturated liquid and 60% higher for saturated vapor conditions comparing to R134a at 0°C temperature. In contrast, liquid viscosity of CO_2 is 40% lower than R134a [54]. A unique property of CO_2 over other refrigerants is that it experiences only a very small change in saturation temperature with a given change in saturation pressure (Table 3). Decrease in evaporator pressure creates a saturation temperature drop which impacts the cycle efficiency by

lowering down the evaporator outlet temperature. Therefore, saturation temperature drop for a given pressure drop is an important parameter for the evaporation process. Thus the efficiency of CO_2 direct expansion heat pump system does not affect much with the large change in pressure.

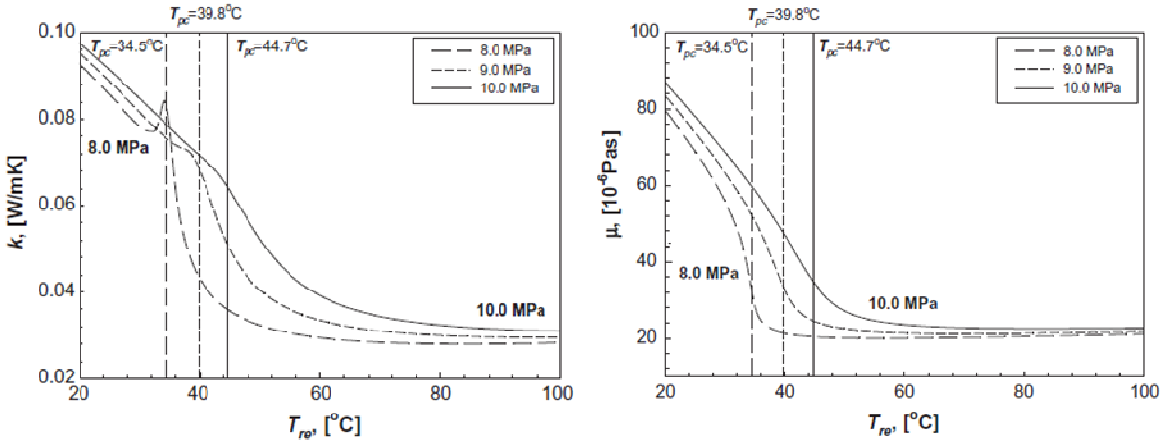

(a) Thermal Conductivity (b) Viscosity

Figure 17: Variation of transport properties of CO_2: (a) thermal conductivity; (b) viscosity [53]

Table 3: A comparison of saturation temperature drop of CO_2 with other conventional refrigerants [49, 55]

	R-134a	**R-410A**	**CO_2**
(dT_{sat}/dP_{sat}), (°C/1 kPa)	0.1	0.04	0.01

2.5.2. Fundamentals of CO_2 Transcritical Cycle and Performance

Since CO_2 has a low critical point compared to other refrigerants, CO_2 systems undergo the transcritical cycle operation when the ambient temperature is relatively higher. As the heat rejection process occurs in the supercritical stage at higher pressure, the low

pressure heat addition remains subcritical. The heat rejection pressure is an important operating parameter for the transcritical heat pump cycle operation. For a given condenser outlet temperature, there exists an optimum condenser pressure. Kim et al. [49] explained this optimum pressure which depends on the particular S-shaped isotherms near the pseudo-critical or in the supercritical zone. For a constant condenser temperature, the rejected heat amount changes by the change of condenser outlet pressure (shown in Fig. 18). Consequently, the compressor work also changes linearly. The effect can be realized in COP value. Since the heat rejection increases at lower pressure and slows down at higher pressure, it increases the COP value up to a certain pressure limit and decreases beyond that.

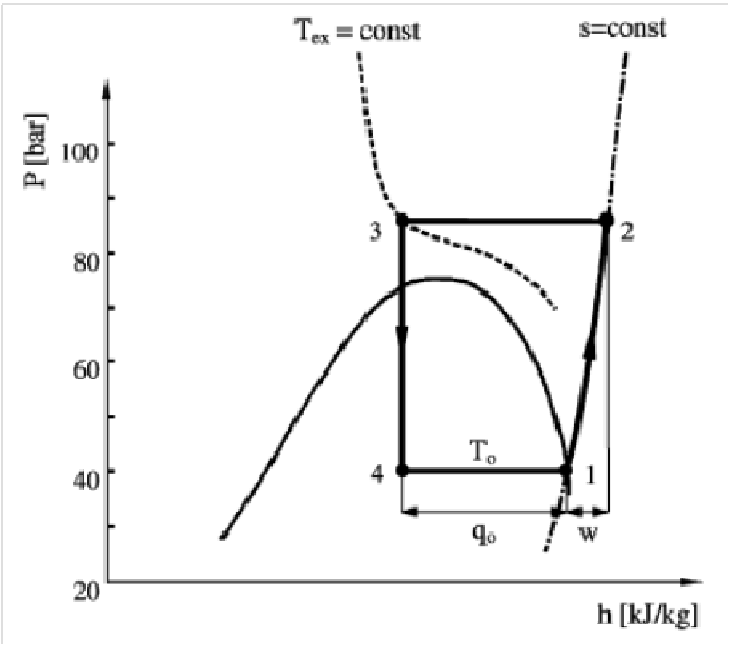

Figure 18: CO_2 transcritical P-h diagram describing the effect of condenser pressure on heating capacity and COP [49]

Air and water heating are two major applications employing heat pumps. However, the gas cooling process of the CO_2 transcritical heat pump is particularly suitable for water heating purpose. Gas cooling occurs at the supercritical stage and there exists no saturation condition at supercritical pressure. Therefore, heat transfer process in the gas cooler takes place in the sensible cooling process. A continuous temperature gliding profile occurs across the CO_2 transcritical gas cooling process which is different from other condensation process following by the latent heat rejection. Most of the commonly used refrigerants have higher critical point compared to CO_2. Therefore, these refrigerants share the two-phase mixtures at the condenser during the latent heat rejection process. Figure 19 is illustrating this distinction between continuous glide profile and the latent heat rejection. It is beneficial for water heating since both the water and CO_2 temperature profile matches closely and hence recovers heat exchanger effectiveness and decreases entropy generation.

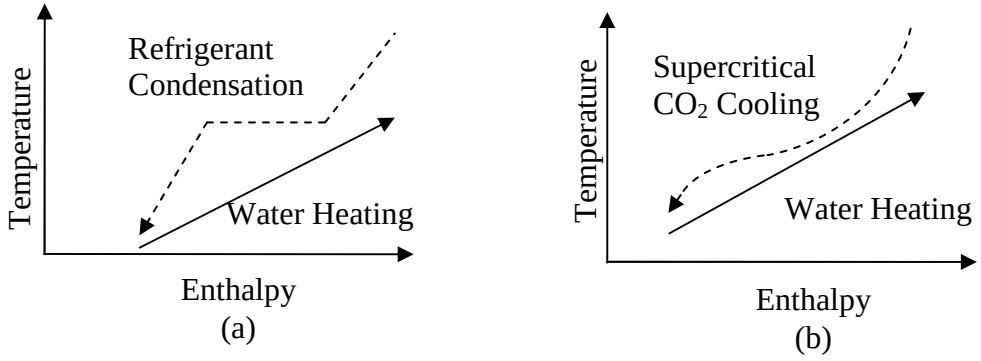

Figure 19: Temperature profile for (a) latent condensation process; (b) CO_2 supercritical gas cooling process [56]

In this study, the use of CO_2 in a transcritical cycle has primarily been focused in which heat rejection occurs in the supercritical stage where only sensible cooling or heating takes place. Several researchers have conducted studies on transcritical CO_2 heat pump

cycle for automotive cooling and heating applications [57 – 58]. Transcritical CO_2 cycle can also be applicable for water heating purposes where large temperature increments are generally required. Literature shows that there exist several studies on transcritical CO_2 heat pump water heaters [49, 59 – 63]. A detailed comparative study [62] between heat pump water heater using CO_2 and R134a has been presented by Cecchinato et al. and concluded that CO_2 could be a potential alternative for synthetic refrigerants. Richter et al. [64] reported that when a heat output is subjected to low outdoor temperatures CO_2-based heat pump water heating system showed higher heating capacity than a similar system using R410a.

2.6. Influence of Key Variables on SWH System Design

The potential of any renewable technology is dependent on the proper assessment of planning and promoting the system among the end-users. A method to evaluate the market potential for DWH has been presented by Voinvontas et al. [65]. The method has been based on a Geographical Information System (GIS). The model took into consideration the parameters associated with geographical variability that influenced solar radiation and power requirements for the specified area. The size of the population and the number of families greatly influenced the energy demand in residential energy uses. The above discussed model provides some special insight into the energy savings and profits that could be obtained from a large-scale deployment of DWH systems. This model is helpful to analyze the variation in energy demand with the time discrepancies of solar radiation. However, it was restricted only to the domestic sector and did not account for the variation in load. A typical domestic hot water load pattern has been analyzed by Mutch [66]. Minor variations of time discrepancies on load patterns do not have any major impact

on the performance of DWH systems. The techno-economic evaluations play an important role in establishing a strong market strategy for SWH systems and also persuade necessary information for energy policy decisions. Chandrasekar and Kandpal [67] have developed a comprehensive nomograph to determine the potential factors influence for the performance of SWH systems. Using some of these potential inputs, Pillai and Banerjee [68] developed a methodology to estimate the potential for SWH systems, by taking into account of both micro and macro level inputs as shown in Fig. 20.

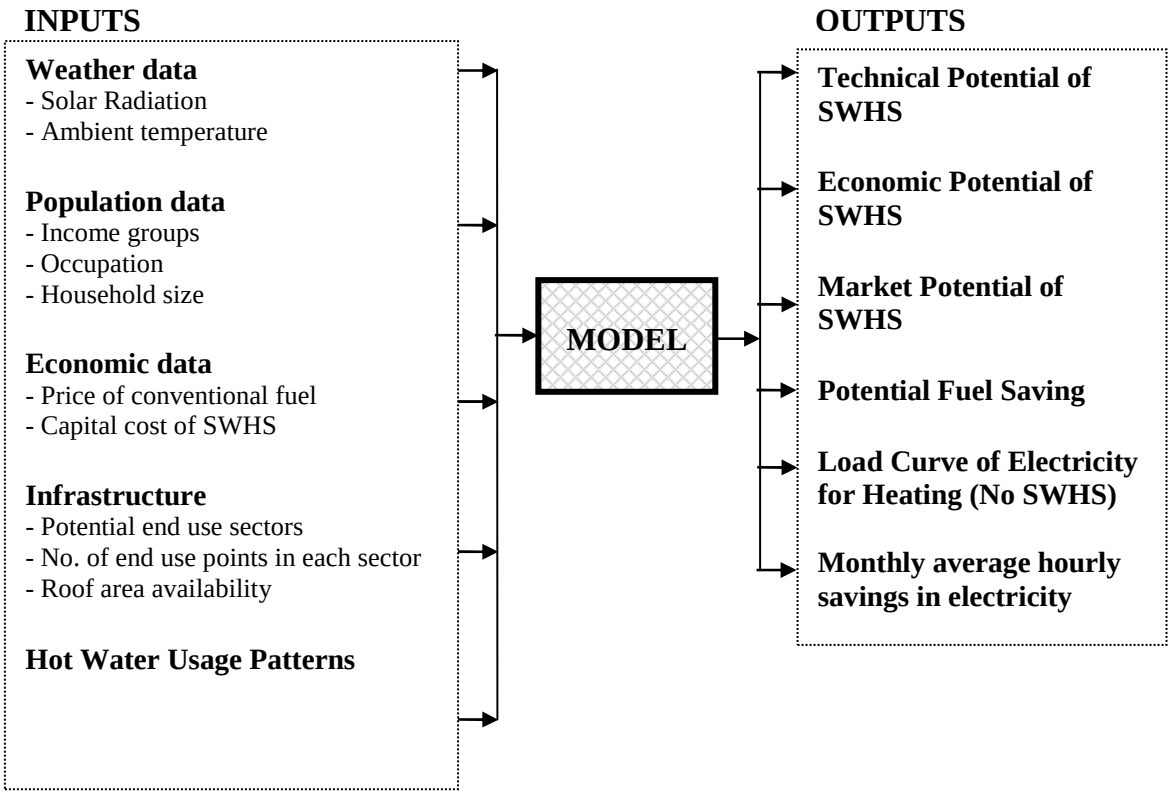

Figure 20: Input and output parameters for modeling the potential approximation of solar water heating system [68]

Another simple method to evaluate the effectiveness of SWH systems is to assess the energy savings by the product of the solar fraction (SF) and the numbers of SWH integrated buildings. To implement the cost-benefit analysis more effectively, Pan et al. [69] proposed the concept of number of effective solar days and effective solar radiation (ESR) instead of using the total annual solar radiation parameter which may overestimate the amount of energy benefits. ESR calculation was based on the tap water temperature and the solar insolation for each region to figure out the applicability of SWH system. Their model was based on Taiwan and estimated the ratios of ESR to total annual solar radiation in the range of 82 – 89%. The popular f-chart method [70] and the demographic data for a target region can also be used to assess the estimated power savings due to the installation of domestic SWH systems.

Optimization of solar collector area to the storage tank capacity for a hybrid SWH was studied by Misra [71]. It was reported that the use of auxiliary heater inside the storage tank causes large amount of heat loss due to the fact that the hot water storage tank needs to maintain a large volume of water at constant delivery temperature. Reducing the auxiliary energy consumption could improve the economics of the system. Therefore, it was recommended to provide auxiliary heater at the load point.

3. SCOPE AND OBJECTIVES OF THIS STUDY

Based on the overall understanding of the literature, the performance of solar heat pump systems, particularly the direct expansion type solar-assisted heat pumps has a scope to utilize for a broad range of end-users. Most of the experimental works summarized in the literature were carried out widely varying conditions, using HFC and HCFC refrigerants. However, due to the environmental concerns, many of the conventionally used HFC and HCFC working fluids have lead to scheduled phase-out. Hence, researchers have renewed their research focus on natural working fluid like CO_2, which has proven to have less detrimental impact on environment. Yet another aspect at SWH is uses of water solar thermal collectors are limited in the solar-adverse regions due to freezing issues. However, the state of art in turns of technological development has shown that direct expansion solar-assisted CO_2 transcritical HP systems can also show competitive performance like conventional SAHP systems using traditional refrigerants.

An attempt has been made in this study to investigate theoretically a SWH integrated system direct expansion solar-assisted heat pump, using CO_2 as refrigerant. For the evaporator component of the heat pump, an evacuated tube collector with a heat removal U-pipe is considered as the heat source. It is expected that the combination of heat pump technique with evacuated tube U-pipe solar collector, using CO_2 as working fluid would meet the heating load requirement, even when exposed to solar adverse conditions (low ambient temperatures and wind chill temperatures).

This thesis intends to accomplish the following tasks: (i) to perform a thorough thermodynamic analysis of the said system, (ii) to develop a numerical model of a direct expansion solar-assisted heat pump (DX-SAHP) water heating system using CO_2 in a

transcritical cycle under a quasi-steady state operation, (iii) to simulate the numerical model of DX-SAHP system in order to identify the dominant operating parameters of the system under study, (iv) to investigate the design and operating parameters on the system performance and to understand the relative significance of these operating parameters, (v) to optimize the system component based on the numerical results, especially to bind an optimal match between compressor capacity and area of solar collector, to ensure successful system operation.

4. THERMODYNAMIC ANALYSIS

The schematic of the direct expansion solar-assisted heat pump (DX-SAHP) system using CO_2 transcritical cycle is shown in Fig. 2 of Chapter 1. A quasi-steady state process has been considered to determine the performance of each component as well as the overall system. Model development of the system entails a detail thermodynamic analysis for each of the component pertaining to the system. The four main stages of the cycle such as – evaporation, compression, heat rejection and expansion are shown in Fig. 3 in p-h diagram. Based on the 1st law of thermodynamics, the generalized energy equation for the chosen control volume (component of the system) is given below:

$$\dot{Q} + \dot{m}_i \left(h_i + \frac{1}{2} u_i^2 + g Z_i \right) = \dot{W} + \dot{m}_e \left(h_e + \frac{1}{2} u_e^2 + g Z_e \right) \qquad (2)$$

Considering the following assumptions, the above energy equation can be expressed as

(i) A quasi-steady state system operation

(ii) Kinetic and potential energy differences are insignificant

$$\dot{Q} = \dot{W} + \dot{m}(h_i - h_e) \qquad (3)$$

Depending on the operating conditions in the evaporator, the atmospheric air acts like an additional heat source or sink beside solar energy. The thermodynamic process 4–1 represents the evaporation process in which CO_2 undergoes phase change from liquid to vapor (Fig. 2 in Chapter 1). The evaporated refrigerant is then compressed in the subsequent compression process 1–2 to a supercritical vapor pressure stage. The supercritical CO_2 at a high pressure and temperature goes through the process 2–3 in the condenser, where the working fluid gets condensed. The energy released by the

supercritical CO_2 vapor (in coil condenser) is then utilized to heat the water by sensible cooling process through a heat exchanger, which has been immersed into the hot water storage tank. Finally, the high pressure but low temperature CO_2 is throttled to the evaporator pressure by the throttling process shown as process 3–4, where pressurized CO_2 flashes through the thermostatic expansion valve to attain its initial pressure conditions (evaporator pressure). This completes one full cycle. Subsequent cycles follow the same sets of events, by which water in the storage tank eventually gets heated up. The process continues as long as solar radiation is available on the solar collector. The events described above are shown in the idealized pressure-enthalpy diagram (Fig. 3 in Chapter 1). As shown, the transcritical cycle shares a low-pressure sub-critical zone and a supercritical high pressure side in any given cycle of operation. In the studied transcritical cycle, it is ensured that CO_2 is compressed close to its critical point. This is because, one of the distinct characteristics of supercritical CO_2 is that, near the critical point it shows a rapid change in thermodynamic and transport properties even with a small change in temperature. This particular region is called the 'pseudo-critical' zone where the specific heat coefficient reaches its maximum for a given pressure and temperature [49].

4.1. Evaporator/Solar Collector Model

A number of studies have been performed to improve the existing solar collectors design as well as its efficiency [17, 72 – 75]. The improvement methods used include structural changes, introduction of new materials and coatings, and various working fluids. Recently, one of the new collectors, namely, evacuated tube U-pipe solar collector has been studied for electric power and heat generation using CO_2 as the working fluid [76 – 79]. Zhang and Yamaguchi [80] have studied the convective heat transfer characteristics of

supercritical CO_2 in a horizontal circular tube in forced convection mode and identified several heat enhancement mechanisms which are superior to a water-based collector system. In order to investigate the influence of CO_2 as a working fluid in a U-tube inserted glass evacuated solar collector, Zhang et al. [81] made a detailed study on the collector characteristics with CO_2 as the working fluid and found that the annually-averaged efficiency could attain above 60% which is much higher than the water-based collectors where annual maximum efficiency could reach only up to 50%.

Moreover, proper selection of the solar collector can minimize the heat losses. Selective surface coatings along with the vacuum insulation between the two concentric tubes are two main distinct design aspects of the evacuated tube solar collector, compared to the flat plate solar collector. Thus, evacuated tube collector enhances higher useful heat gain along with minimal heat losses [74]. Due to absence of air or any other heat transfer medium between the two concentric tubes, the heat losses pertaining to convection is very much minimized. Figure 21 illustrates a comparative design benefit of using evacuated tube solar collector over flat-plate solar collector.

Therefore, evacuated tube collectors are currently widely used in the solar adverse regions, especially for residential solar thermal applications. However, glass evacuated tubes cannot sustain high pressure condition. As an alternative, U-pipe inserted evacuated tubes are commonly used solar collector to deal with a high pressure thermodynamic cycle in the solar heat pump systems.

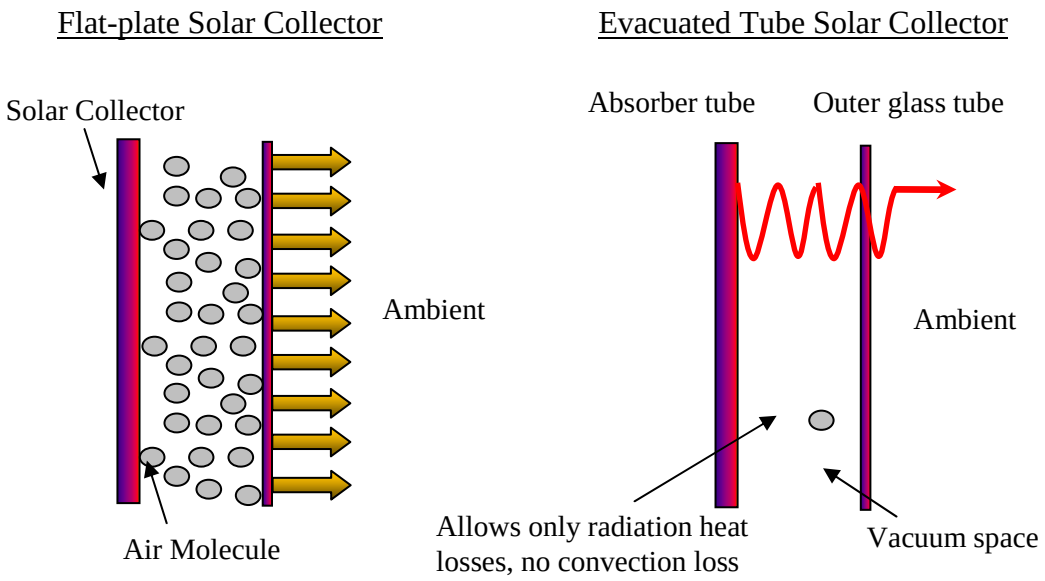

Figure 21: A comparison between flat-plate and evacuated tube solar collector with respect to their design benefit

The evaporator component (U-pipe inserted glass evacuated tube solar collector) of the heat pump system used in this study is shown in Fig. 22. Important features of this system are: (a) the outer and inner glass tubes placed concentrically to provide the vacuum space in between them, (b) selective absorber coating painted inside the inner tube and (c) copper U-pipe placed inside the inner glass tube with a fin connected together. The characteristic features of glass evacuated tube solar collectors are its collective effect of vacuum insulation between the concentric tubes and the selective surface coatings that results in enhanced heat extraction efficiency [74]. As the solar radiation passes through the glass tubes, it is absorbed by the surface coating placed inside the inner tube. The absorbed heat is then transferred to the U-tube by conduction and in turn to the working fluid inside the U-tube by convection heat transfer method affecting an increase in the temperature and pressure of the working fluid.

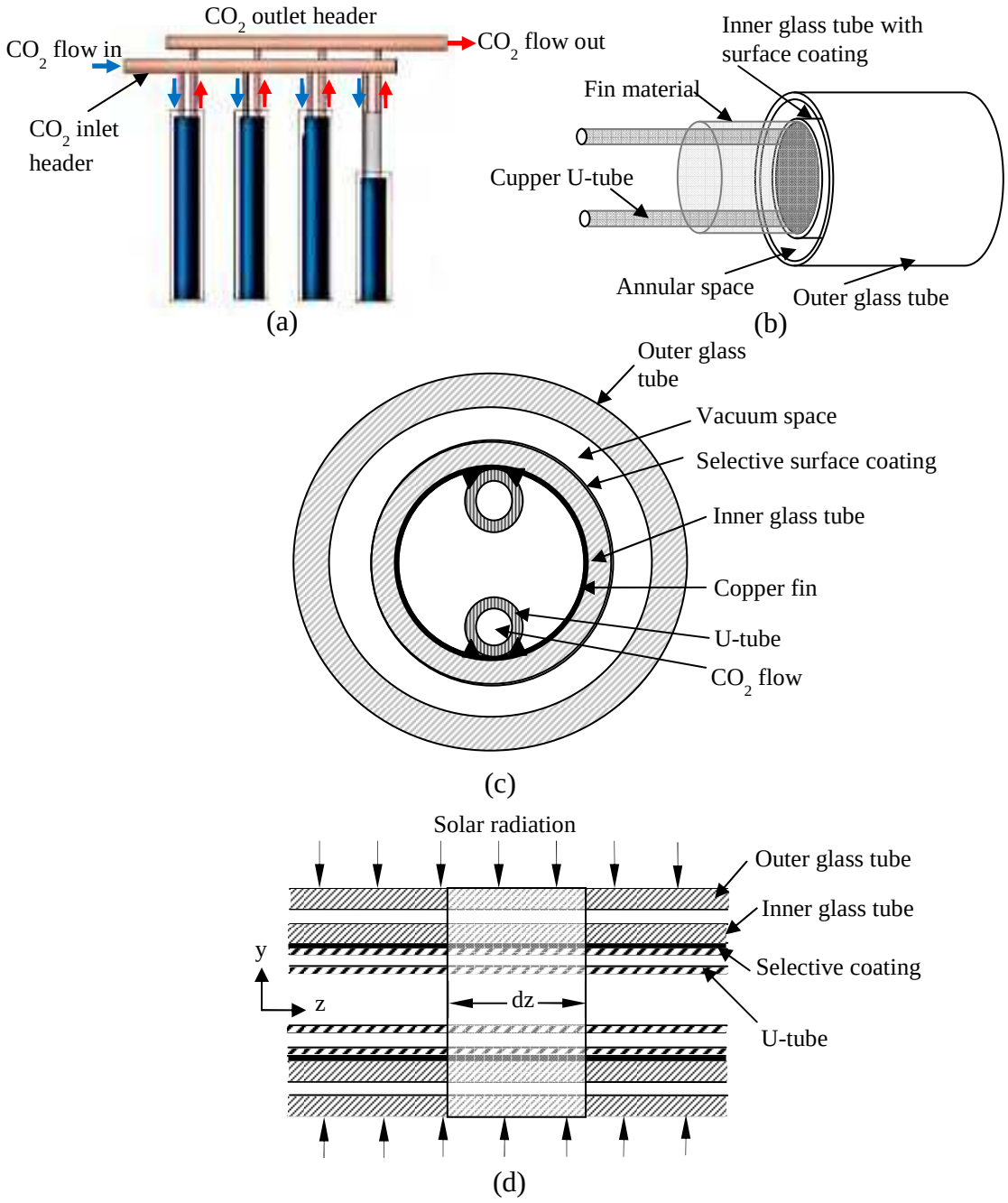

Figure 22: Schematic of the evacuated tube U-pipe solar collector and its components: (a) CO_2 flow direction; (b) construction of the unit glass tube; (c) cross-sectional view of the collector tube; and (d) differential control volume used in the present analysis

4.1.1. Two-phase Flow in the Solar Collector

The two-phase flow condition in the solar collector tubes is assumed to be at thermodynamic equilibrium. It is also assumed that the change in enthalpy solely effect the change in the vapor quality (dryness fraction), by the solar radiation input. In addition, the pressure drop across the solar collector tube is insignificant since it is assumed to have a negligible effect on the vapor quality change due to the second-order effect. Depending on the mass flow rate of the fluid, different flow regions develop in the liquid and vapor phases ranging from mist flow (small droplets in vapor) to bubbly flow (small-sized bubbles in liquid). Hence, determining the exact flow region is essential, for the analysis of the two-phase flow since it varies depending on the type of flow region. Baker [82] has illustrated a map-based two-phase flow region for different vapor and liquid mass flow rates. In the context of the present study, though the said two-phase flow regions develop, but it is extremely quick and reaches saturated vapor/superheated conditions. Hence, incorporating the flow field in the analysis is difficult, since there involves uncertainties regarding the determination of proper boundary conditions for each flow field. In the available literature, pressure drop across the evaporation process is predicted either by Martinelli Nelson's method or Owen's homogeneous method [83]. The Martinelli Model calculates the pressure drop for two-phase separated flow region and the Owen's Model deals with that of misty or bubbly flow regions. However, none of these models properly match the predicted pressure drop to that of the experimentally obtained data, especially during the evaporation process in the solar collector. Therefore, a simple Homogeneous Equilibrium model could effectively predict the pressure drop characteristics to the acceptable accuracy levels in the two-phase flow regions. The model assumes that both the

vapor and liquid phases undergo the same velocity and can be replaced as a single phase pseudo-fluid. Though the property of this single phase fluid is different compared to vapor or liquid phases, its value represents an average value of the two distinct phases. Thus Homogeneous Equilibrium model employs a simple form of using single phase flow and includes the vapor and liquid mixture flow effects. Chaturvedi et al. [84] investigated the flow effects on two-phase flow regions and noticed that dispersed flow region could be achieved in solar collector evaporation process. Homogeneous Equilibrium model incorporates the dispersed flow region in the analysis to predict the pressure drop in the solar collector and hence this model has employed in the present study.

4.1.2. Governing Equations for Evacuated Tube U-pipe Solar Collector

Following assumptions are made to simplify the one-dimensional heat transfer analysis of the evacuated tube U-pipe solar collector used in the present study:

i. Heat absorption by the outer glass tube of the solar collector is considered insignificant.
ii. Thermal resistances of the outer glass tube, surface coating, metal tube and fin are neglected.
iii. Radial temperature gradients among surface coating, metal U-tube and fin are assumed to be negligible.
iv. Averaged heat flux in the circumferential direction is used as the boundary condition [75].

For one-dimensional, steady, two-phase flow, the useful heat gain (Q_u) of the solar collector is defined from Wallis [85] equation as

$$Q_u = A_{coll}F'\left[I_T\left(\tau_g\alpha_g\right) - U_L\left(T_f - T_a\right)\right] \tag{4}$$

In Eq.(4), overall heat loss coefficient (U_L) is defined as the sum of top loss coefficient (U_t) and edge loss coefficient (U_e).

$$U_L = U_t + U_e \tag{5}$$

Edge loss coefficient is neglected due to the assumption of proper heat insulation at the edges of the solar collector. Top loss coefficient (U_t) can be defined as:

$$U_t = \left(\frac{1}{h_{g,conv}} + \frac{1}{h_{g,r}} + \frac{1}{h_{g,cond}}\right)^{-1} \tag{6}$$

where $h_{g,conv}$ is the heat transfer coefficient between the outer glass tube and the ambient due to convection (W/m^2 K), $h_{g,r}$ is the radiation heat transfer coefficient from the inner glass tube to the outer glass tube (W/m^2 K) and $h_{g,cond}$ represents conduction heat transfer coefficient between the inner glass tube and the fin (W/m^2 K). The heat transfer coefficient $h_{g,conv}$ and $h_{g,r}$ can be written as:

$$h_{g,conv} = 5.7 + 3.8V \tag{7}$$

$$h_{g,r} = \frac{\sigma\varepsilon_{at}}{1 + \frac{\varepsilon_{at}D_{at}}{\varepsilon_{at}D_{at}}\left(1 - \varepsilon_{at}\right)}\left(T_{at}^2 + T_g^2\right)\left(T_{at} + T_g\right) \tag{8}$$

The conduction heat transfer coefficient expressed in Eq.(6) and the edge loss coefficient can be obtained from the theoretical [75] and experimental results [86] which were

calculated as 0.2796 (W/m^2 K) and 0.1687 (W/m^2 K) respectively. From the Fig. 22(c), the heat loss of the evacuated tube can be written as:

$$U_t(T_{at} - T_a) = h_{g,r}\left(T_{at} - T_g\right) + h_{g,cond}\left(T_{at} - T_g\right) \tag{9}$$

In the above Eqs.(6)-(9), the unknown parameters are U_t, $h_{g,r}$, V, T_{at}, T_g and T_a. Using the known parameters V, T_{at} and T_a rest of the unknown parameters have been calculated by iterative numerical procedure (secant method). The calculated values are then used to compute the overall heat loss coefficient of the solar collector which is one of the important parameters to estimate the performance of the solar collector.

The collector efficiency factor (F') is determined by the following formula as given by Hottel-Whilliar Bliss model [23]

$$F' = \frac{1/U_L}{W\left[\frac{1 + U_L/C_b}{U_L[d + (W-d)F]} + \frac{1}{C_b} + \frac{1}{h_f' \pi d}\right]} \tag{10}$$

The standard fin efficiency (F) is given as:

$$F = \frac{\tanh[m(W-d)/2]}{m(W-d)/2} \tag{11}$$

and the constant value, m is defined as:

$$m = \left[\frac{U_L}{\lambda\delta(1 + U_L/C_b)}\right]^{1/2} \tag{12}$$

For the evaluation of inner tube temperature (T_{at}), copper tube connected between the inlet and outlet of metal U-tubes is treated as fin and a second-order temperature equation is derived by considering a small element on the fin [75].

$$\frac{d^2T_{at}}{dy^2} = \frac{-S + U_L(T_{at} - T_a)}{\lambda\delta(1 + U_L/C_b)} \tag{13}$$

Temperature of the working fluid inside the U-tube is determined by dividing the evaporation process into differential control volumes of length *dz* shown in Fig. 22(d). Such discretization is employed to improve the accuracy of the calculation and the thermo-physical property variations near the critical region of the CO_2. Thermodynamic properties are assumed to be constant in each of the differential control volume segments. The calculated outlet properties of each element then become the inlet state of the successive element. Applying the first law of thermodynamics to each segment of the differential elements, the following thermal expressions are obtained.

Outer glass tube:

$$\alpha_g r_g I_T + r_{at} h_{at}\left(T_{at} - T_g\right) + \frac{r_{at}\sigma\left(T_{at}^4 - T_g^4\right)}{1/\varepsilon_g + \left(r_{at}/r_g\right)\left(1/\varepsilon_g - 1\right)} = r_g h_a\left(T_g - T_a\right) + r_g \sigma \varepsilon_g \left(T_g^4 - T_a^4\right) \tag{14}$$

Inner glass tube:

$$\tau_g \alpha_g r_{at} I_T + \frac{K_g (T_c - T_{at})}{\ln\left[1 + \left(\frac{\delta_{at}}{2r_{at}}\right)\right]} = r_{at} h_{at}\left(T_{at} - T_g\right) + \frac{r_{at}\sigma\left(T_{at}^4 - T_g^4\right)}{1/\varepsilon_g + \left(r_{at}/r_g\right)\left(1/\varepsilon_g - 1\right)} \tag{15}$$

Surface coating and U- tube:

$$\tau_g^2 \alpha_c r_{at} I_T = \frac{K_g (T_c - T_{at})}{\ln\left[1 + \left(\frac{\delta_{at}}{2r_{at}}\right)\right]} + 2 r_m h_c \left(T_c - T_f\right) \tag{16}$$

Working fluid (CO_2):

$$\dot{m}_f C_P \frac{dT_f}{dZ} = r_m h_c \left(T_c - T_f\right) \tag{17}$$

The Eq.14 through Eq.17 are simplified to formulate a single expression in first order differential equation for calculating the temperature of the working fluid as

$$\frac{dT_f}{dZ} = \frac{\tau_g^2 \alpha_c r_{at} I_T + \tau_g \alpha_g r_{at} I_T + \alpha_g r_g I_T - r_g \sigma \varepsilon_g \left(T_g^4 - T_a^4\right) - r_g h_a \left(T_g - T_a\right)}{2\dot{m}_f C_P} \quad (18)$$

The heat transfer coefficient (h'_f) of the working fluid for the two-phase flow region in the horizontal tubes is defined by the following relationship [84].

$$h_f^{'} = \frac{0.0082 K_f}{d_i} \left(Re_{d_i}^2 J \Delta x h_{fg} / L\right)^{0.4} \quad (19)$$

where J is the dimensional constant with a fixed value of 778 and Δx is the change in quality of the CO_2 between inlet and exit state [84]. Quality change in the above equation is assumed due to the enthalpy change only, neglecting the pressure effects on the quality. Reynolds number is based on internal diameter (d_i) and liquid viscosity of the two-phase CO_2. In the superheated region, the h'_f is obtained using the following Dittus-Boelter relationship.

$$h_f^{'} = 0.023 Re_{d_i}^{0.8} Pr_{d_i}^{0.4} \frac{K_f}{d_i} \quad (20)$$

Pressure drop of CO_2 inside the U-tube is obtained by considering the homogeneous two-phase mixture flow and by using mass, momentum, and energy balance relationship explained by Chaturvedi et al. [84]. The simplified correlations are listed below.

$$\frac{dP}{dz} = -\frac{\frac{2C_f G^2}{d_i}\left(v_f + x v_{fg}\right) + G^2 v_{fg} \frac{dx}{dz}}{\left(1 + G^2 \left(x \frac{dv_g}{dP} + (1-x)\frac{dv_f}{dP}\right)\right)} \quad (21)$$

$$\dot{m}_f \frac{dx}{dz} = \frac{WF^{'}}{h_{fg}} \left[I_T(\tau\alpha) - U_L\left(T_f - T_a\right)\right] \quad (22)$$

The frictional pressure drop coefficient (C_f) depends on the laminar and turbulent nature of the fluid flow inside the U-tube which is the function of Reynolds number and it is defined using the following:

$$C_f = \frac{16}{Re_{d_i}}, \quad Re < 2300 \tag{23}$$

$$C_f = \frac{0.079}{Re_{d_i}^{0.25}}, \quad Re \geq 2300 \tag{24}$$

In Eq. (21), the saturated fluid properties are calculated by choosing a polynomial fit curve for v_f, v_g and v_{fg} as a function of pressure. A fourth-degree polynomial fit is chosen to find the above properties of CO_2 which is valid in the pressure range of 2 – 7.3 MPa. The error involved by this polynomial fit remains within 1% range and is mainly useful for numerical solution method. The degree of superheating in each iterative process is evaluated using the following expression.

$$\Delta T = T_1 - T_1^{'} \tag{25}$$

The superheated single-phase region starts at the length of U-tube denoted as z_0 and can be written as

$$z_0 = -\frac{C_{pv} \log_e \left[\frac{T_1 - T_a - S/U_L}{T_1^{'} - T_a - S/U_L}\right] \dot{m}_f}{F^{'} U_L W} \tag{26}$$

The instantaneous efficiency of the solar collector is calculated by the following expression:

$$\eta_{coll} = \frac{Q_u}{A_{coll} I_T} \tag{27}$$

The useful energy received by the solar collector can also be obtained as a function of the change in enthalpy of the inlet and outlet (exit) state of the collector.

$$Q_e = \dot{m}_f \Delta h \tag{28}$$

4.2. Compressor Model

In a positive-displacement reciprocating compressor, piston-cylinder arrangement is used to deliver working fluid at a higher pressure and hence, compressor runs the heat pump cycle. The performance of the heat pump cycle can be controlled by regulating the mass flow rate of the working fluid delivered by a compressor. The mass flow rate of the carbon dioxide through the compression process is obtained by the following expression as:

$$\dot{m}_f = \rho_{suc} \eta_v V_s \frac{N}{60} \tag{29}$$

where N is denoted as compressor speed in rpm. The swept volume (V_s) using the following formula.

$$V_s = i \frac{\pi D_b^2 S}{4} \tag{30}$$

The volumetric (η_v), mechanical (η_m) and isentropic (η_{isen}) efficiency formulas of the compressor is used from the correlations developed by Oritz et al. [57]. All the efficiency expressions are obtained as the function of suction to discharge pressure ratios.

$$\eta_v = \frac{\dot{m}_f}{\rho_{suc} V_s N/60} = 0.9207 - 0.0756 \left(\frac{P_{dis}}{P_{suc}}\right) + 0.0018 \left(\frac{P_{dis}}{P_{suc}}\right)^2 \tag{31}$$

$$\eta_m = \frac{W_{com}}{P_{in}} = 0.9083 - 0.0884 \left(\frac{P_{dis}}{P_{suc}}\right) + 0.0051 \left(\frac{P_{dis}}{P_{suc}}\right)^2 \tag{32}$$

$$\eta_{isen} = \frac{h_{2,isen} - h_1}{h_2 - h_1}$$

$$= -0.26 + 0.8952\left(\frac{P_{dis}}{P_{suc}}\right) - 0.2803\left(\frac{P_{dis}}{P_{suc}}\right)^2 + 0.0414\left(\frac{P_{dis}}{P_{suc}}\right)^3 - 0.0022\left(\frac{P_{dis}}{P_{suc}}\right)^4 \quad (33)$$

The internal compression work (W_{com}) is the function of power consumption which depends on the mass flow rate, isentropic efficiency and the isentropic enthalpy change of the refrigerant.

$$W_{com} = \dot{m}_f \frac{\left(h_{2,isen} - h_1\right)}{\eta_{isen}} \quad (34)$$

Compressor work can also be expressed in terms of enthalpy change of refrigerant between the inlet and outlet state.

$$W_{com} = \dot{m}_f \Delta h \quad (35)$$

4.3. Condenser/Hot Water Storage Tank Model

For the water storage tank model, water temperature within the tank is assumed to be uniform at any instance of time. The schematic and the modes of heat transfer between CO_2 and water in the storage tank is shown in detail in Fig. 23. The hot water demand is supplied to the load directly from this tank. Therefore, for non-stratified or a mix tank model with the immersed condenser, the following expression could be used to evaluate the increment rise in water temperature.

$$M_w C_{pw} \frac{dT_w}{dt} = Q_{con} - (UA)_t (T_w - T_a) - Q_{load} \quad (36)$$

Heat rejected in the condenser to the water in the storage tank takes into account of the heat absorbed by the evaporator model and the work done by the compressor.

$$Q_{con} = Q_{con} + W_{com} \tag{37}$$

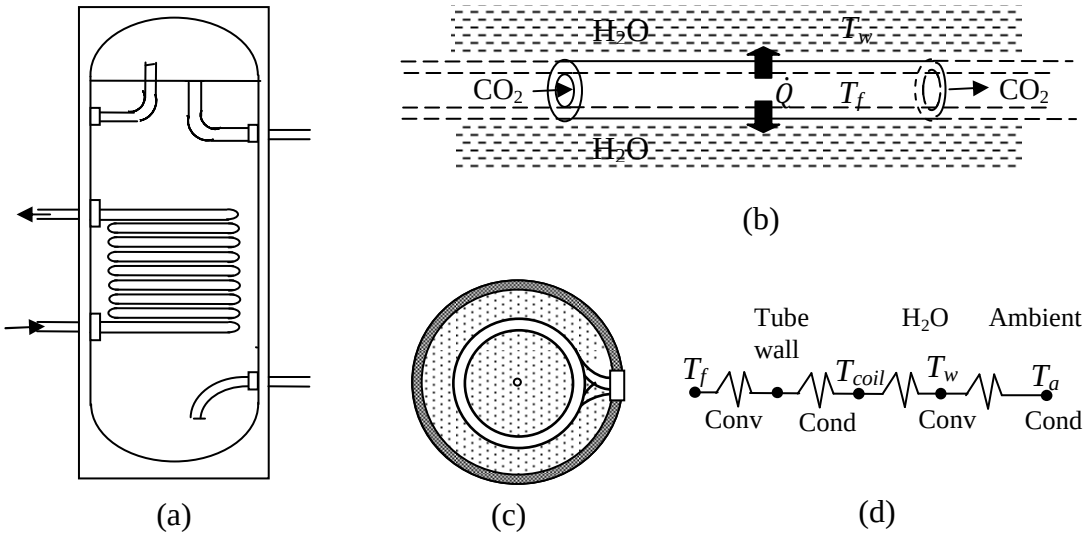

Figure 23: Hot water storage tank with immersed single coil condenser: (a) schematic of the storage tank; (b) heat transfer between CO_2 flow to the surrounding water; (c) top view of storage tank; and (d) thermal network between the CO_2 flow to the ambient

Similarly, the total heat dissipation from the condenser is also obtained by the following expression.

$$Q_{con} = (UA)_{coil}(T_{con} - T_w) \tag{38}$$

In the above expression (Eq. 38), $(UA)_{coil}$ is the overall heat transfer coefficient of the condenser coil. It is the sum of the thermal resistive values, including the convective

resistance offered by CO_2, conductive resistance of the cooling coil and convective resistance of the water.

$$(UA)_{coil} = \left(\frac{1}{h_c^{'} A_{c,i}} + \frac{\delta_{coil}}{K_{coil} A_{c,o}} + \frac{1}{h_w^{'} A_{coil}}\right)^{-1} \tag{39}$$

The condensation process will be in the supercritical region for any steady-state cycle and hence it follows the single-phase sensible cooling process. The heat transfer coefficient of CO_2 within cooling coil to the inner tube wall of the cooling coil is evaluated using the following Nusselt correlation.

$$h_c^{'} = \frac{K_c Nu_i}{d_i} \tag{40}$$

The overall Nusselt number (Nu_i) within the cooling coil includes the temperature drop across and is evaluated based on the Petukhov-Popov correlation [87].

$$Nu_i = \frac{(f/8)}{K_1 + K_2 (f/8)^{1/2} (Pr^{2/3} - 1)} \tag{41}$$

where the friction factor f and the constants K_1 and K_2 are defined as:

$$f = (1.82 \ln(Re) - 1.64)^{-2}; \quad 3000 \leq Re \leq 5 \times 10^6 \tag{42}$$

$$K_1 = 1 + 3.4f \tag{43}$$

$$K_2 = 11.7 + 1.8/(Pr)^{1/3} \tag{44}$$

Similarly, the outside film coefficient between the outer tube walls to the water in the storage tank is evaluated using immersed heat exchanger tested by Farrington and Bingham [88].

$$h_0 = \frac{K_{wall} Nu}{d_o} \tag{45}$$

$$Nu = CRa_{d_o}^m \tag{46}$$

The convection coefficient *C* and the constant *m* of the above equation are taken from a similar immersed heat exchanger tested by Farrington and Bingham [88] of 0.9 and 0.25, respectively. The Rayleigh number in Eq. (43) can be written as

$$Ra_{d_0} = Gr_{d_0} Pr = \frac{g\beta d_o^3 (T_{wall} - T_w)}{\nu^2} \frac{\mu C_P}{K_w} \tag{47}$$

Pressure drop of CO_2 through the immersed condenser is calculated using the Darcy friction factor, using the Blasius correlation for the flow in a smooth tube.

$$\Delta P = f \frac{\Delta L}{2\rho_c} \left(\frac{G_c^2}{d_i} \right) \tag{48}$$

4.4. Expansion Device

The CO_2 pressure drop from condenser pressure to the evaporator pressure is affected through a thermostatic expansion valve. Ideally, the throttling process is assumed to be isenthalpic, and considered to be a steady state device. Therefore, enthalpy across the expansion valve can be written as:

$$h_3 = h_4 \tag{49}$$

4.5. Available Solar Energy from the Solar Collector

The total radiation intensity received on a horizontal plane at any given instance is assumed to vary sinusoidally from sunrise to sunshine according to

$$I_T = I_{max} \sin\left(\frac{\pi\theta}{l}\right) \tag{50}$$

where I_{max} is the maximum intensity of solar radiation occurring at solar noon (12:00 hours), l is the length of the day in hours and θ is the difference between time of the day (at any given instance) and the sunrise time in hours. The diffuse solar intensity (I_d) on a horizontal plane is assumed to be 15% of I_{max}.

The daily total solar radiation intensity (I_β) on an inclined surface includes: beam, diffuse and ground reflected radiation. This formula is obtained as

$$I_\beta = I_b R_b + I_d\left(\frac{1+\cos\beta}{2}\right) + (I_b + I_d)\rho_g\left(\frac{1-\cos\beta}{2}\right) \tag{51}$$

where beam radiation factor (R_b) is defined as

$$R_b = \frac{\cos\theta}{\cos\theta_z} = \frac{\cos(\phi-\beta)\cos\delta\cos\omega + \sin(\phi-\beta)\sin\delta}{\cos\phi\cos\delta\cos\omega + \sin\phi\sin\delta} \tag{52}$$

Beam and diffuse radiation are usually measured by some of meteorological stations; but, North Dakota Climate Office [89] only measures global solar intensity. It needs to consider both beam and diffuse radiation to calculate the total solar incident on a tilted surface. An hourly average diffuse radiation is usually measured by correlating the ratio of diffuse to global radiation considering hourly clearness index, k_T.

$$\frac{I_d}{I_T} = \begin{cases} 1.0 - 0.249k_T; & for\ k_T < 0.35 \\ 1.557 - 1.84k_T; & for\ 0.35 < k_T < 0.75 \\ 0.177; & for\ 0.75 < k_T \end{cases} \tag{53}$$

where k_T is the ratio of total solar radiation intensity (I_T) to that of extraterrestrial radiation (I_o) on a horizontal surface.

Using the meteorological parameters of Fargo, North Dakota as tabulated in Table 4 can be used to estimate I_o on a given day of the year by the following formula:

$$I_o = G_{sc}\left[1 + 0.033\cos\left(\frac{360n}{365}\right)\right](\sin\phi\sin\delta + \cos\phi\cos\delta\cos\omega) \quad (54)$$

in which angle of deflection denoted as δ is defined as

$$\delta = 23.45\sin\left[\frac{360}{365}(284 + n)\right] \quad (55)$$

Table 4: Geographical data of Fargo, North Dakota [89]

Parameters	**Values**
Latitude (Φ)	+46.90°
Longitude	-96.82°
Tilt angle (β)	46.90°

5. SYSTEM MODELING AND SIMULATION PROCEDURE

The mathematical modeling of the proposed DX-SAHP system to predict the thermodynamic performance is simplified based on the following general assumptions:

(i) Quasi-steady state conditions are approximated within the chosen time interval.

(ii) The refrigerant is uniformly distributed among all the heat removal pipes in the evacuated tube solar collector and is considered to be saturated at the exit of the collector.

(iii) Pressure drop and heat loss in the connecting pipes are neglected.

(iv) Frictional losses in the evaporator and the condenser are negligible.

(v) A good thermal insulation over the CO_2 loop is assumed, i.e. thermal loss to the surroundings is neglected.

(vi) A non-stratified hot water storage tank is considered for the simulation.

(vii) Kinetic and potential energy changes are assumed to be insignificant.

5.1. Solution Procedure

A numerical computational model in MATLAB has been developed to analyze the characteristics of the components mentioned in Chapter 4, which holistically dictates the thermal performance of the DX-SAHP system. Input parameters (Table 5) for the simulation cycle include: collector properties (Table 5), meteorological data [89], initial storage water temperature and the compressor speed. The thermodynamic properties of the CO_2 used in analyzing each component of the system were generated using REFPROP 8.0 software.

Table 5: Main parameters used in the performance evaluation of DX-SAHP water heating system

Components	Parameters	Value
Evacuated tube U-pipe solar collector Properties of absorber coating	Absorbtance	0.927
	Transmittance	0.08
	Reflectance	0.033
Properties of glass tubes	Thermal conductivity	1.25 (W/m K)
	Transmittance	0.90
	Absorbtance	0.05
	Reflectance	0.05
	Emittance	0.83
	Outer tube outer diameter	47 mm
	Thickness	1.2 mm
	Inner tube outer diameter	37 mm
	Length of the tube	1.7 m
Properties of U-tube	Outer diameter	8 mm
	Conductivity	400 (W/m K)
	Bond conductance	30 (W/m K)
Compressor (Reciprocating-type, hermetic)	Swept volume per stroke	0.00001972 m^3
Condenser/Storage tank	Thermal conductivity of insulation	0.0346 (W/m K)
	Thickness of insulation	5 mm
	Outer diameter of the condenser coil	8 mm
	Thickness	1 mm
Simulation parameters (standard)	Initial water temperature	7°C (winter) 15°C (fall and spring)
	Wind speed	3.0 (m/s) (all seasons)

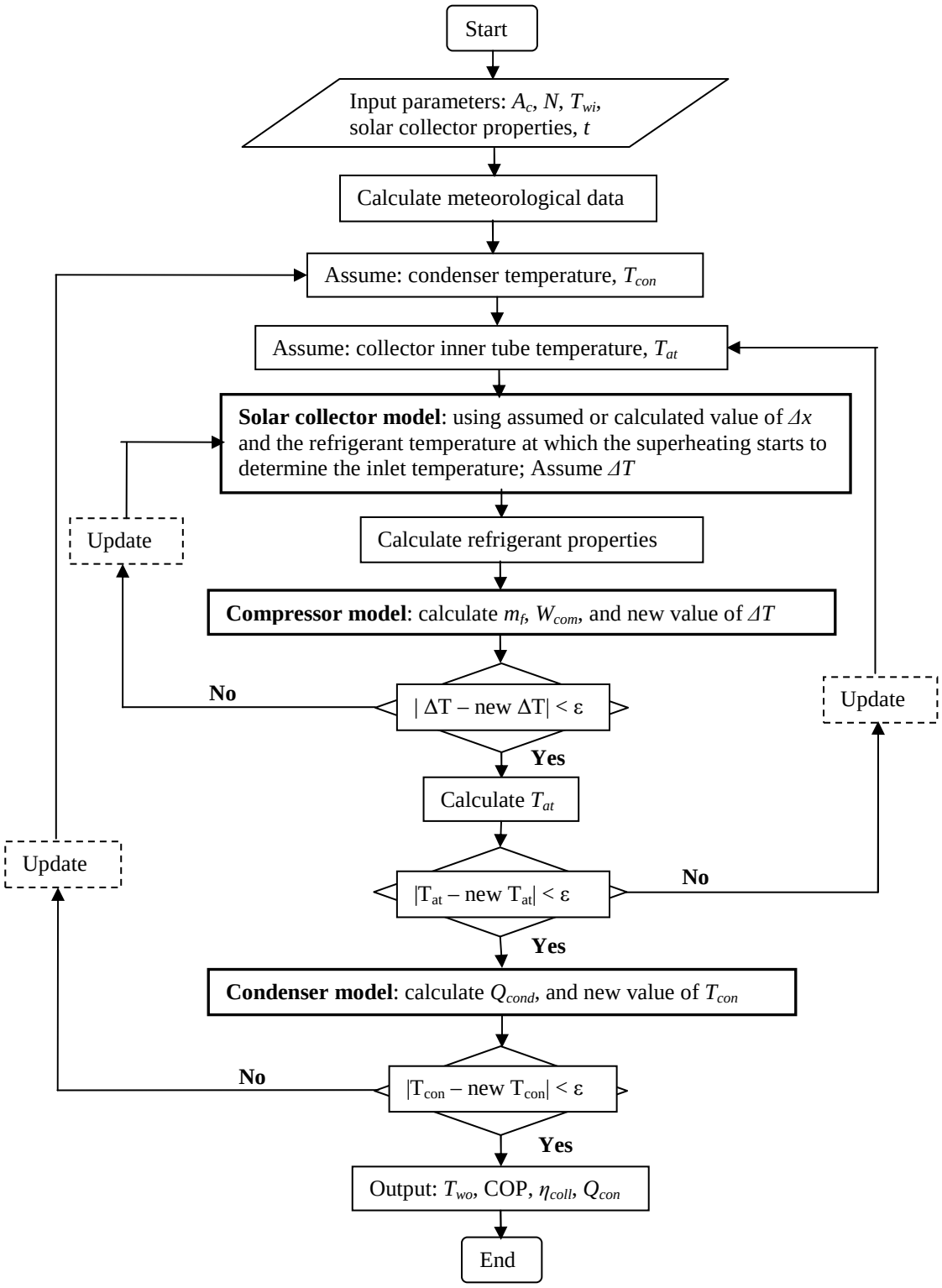

Figure 24: Flow chart of the simulation model

Figure 24 describes the flow chart of the simulation procedure. To start a simulation cycle, the operating parameters are set as input, along with the assumed solar collector and condenser temperature at the outlet state. The collector temperature (T_{at}) is determined by adjusting the initial guessed degree of superheat value. The compressor and solar collector model are called upon to determine the inlet and outlet state of each process. Once the solar collector temperature has come under the specified tolerance limit, the program proceeds to evaluate the outlet state of the condenser. Finally, the condenser temperature is adjusted with the value less than the tolerance limit and the current operating condition is considered as steady-state. The program evaluates all the inlet and outlet states of each components of the system, heat gain of the collector, heating capacity, compressor power, and COP.

In real situation, when the working fluid exits from the solar collector with a specific degree of superheat, there remains a mixture of both superheated and two-phase flow in the collector tubes. Except for the energy equation, all the other equations explained in Chapter 4 are suitable for two-phase analysis. Therefore, it is necessary to determine the length of the collector tube over which superheating state takes place. For developing the solution procedure, it requires to determine the case when the refrigerant exits the solar collector in the saturated vapor state.

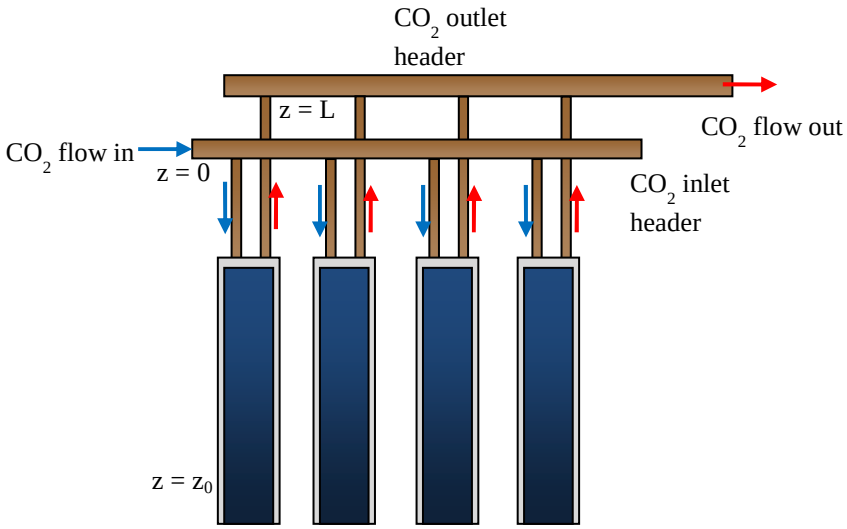

Figure 25: Boundary conditions at solar collector inlet and outlet points

Forth-order Runge-Kutta method [90] is used for solving the differential equations described in Section 4.1.2 (Eq. 21 and 22). Boundary condition of vapor quality (x) is specified at the beginning of the U-pipe ($z=0$) which has a value of 0.0 (Fig. 25). Boundary conditions determining the pressure is unknown at both the ends of the U-pipe ($z=0$ and $z=L$). However, at $z=0$, the enthalpy at the exit of expansion valve is equal to the enthalpy at the inlet of solar collector. Therefore, the boundary condition can be expressed as:

$$h_4 = h_3 = h_f(P_4) + x_4 h_{fg}(P_4) \tag{56}$$

As h_3 is known, Eq. (56) offers a compatibility condition for pressure in terms of vapor quality. Therefore, determination of P_4 and x_4 should satisfy the above condition. For the starting point of any numerical simulation, it is needed in Runge-Kutta method to specify the value of pressure and vapor quality at $z=0$. To start a cycle analysis, pressure at the exit of solar collector (P_1) is assumed. A good starting guess is to assume the exit saturation temperature of solar collector is to equal the ambient temperature. For saturation condition,

there exists a saturation pressure for each saturation temperature. This saturation condition is the second boundary condition which is assumed at $z=L$. Now, as the specific volume at the solar collector exit can be obtained, the compressor mass flow rate (described in Section 4.2) is determined. With all these values, differential equations described in Eq. 21 and 22 can be solved by Runge-Kutta method in terms of pressure and vapor quality. This in turn useful to predict solar collector inlet ($z=0$) state. Therefore, enthalpy at the inlet of collector (h_4) can be determined from P_4 and x_4. The computed enthalpy is then compared with h_3 and if it satisfies Eq. (56), the initial guess value is correct. It is unlikely to converge the solution only in one iteration and therefore a new assumption of P_1 is needed. This solution procedure repeats unless boundary condition described in Eq. (56) is achieved. Once the solution process determines P_1 within tolerable limit, the thermodynamic cycle analysis is carried out to calculate the performance parameter as COP.

5.2. Cycle Performance Measurement

The performance of the entire DX-SAHP system is predicted by evaluating the heating capacity and the coefficient of performance (COP). Heating capacity is the amount of heat rejected by the condenser (Eq.38) and the COP reflects the ratio of the heat rejection by the condenser (Q_{con}) to the electrical power required to operate the compressor (W_{com}).

$$COP = \frac{Q_{con}}{W_{com}} \tag{57}$$

5.3. Error Analysis

To compare the simulation results of the present DX-SAHP water heating system to the experimental work, a method of error calculation need to be defined such as root mean square percent deviation. The root mean square deviation is expressed as the following formula:

$$e = \sqrt{\frac{\sum(e_i)^2}{n}} \tag{58}$$

where, $$e_i = \frac{X_i - Z_i}{X_i} * 10 \tag{59}$$

In the above expression, X_i is the i^{th} data point of the theoretical value, Z_i is the experimental value and n is the total data points. The root mean square deviation is used to predict as to how well the simulation results of the proposed DX-SAHP design correlates to the experimental studies.

6. MODEL VALIDATION AND PARAMETRIC STUDIES

6.1. Model Validation

A model validation is essential to ensure that the simulation results are reliable; additionally, the model can be used to identify the optimal design and operating values which are essential in erecting experimental prototypes and in turn pave a way for commercialization.

However, to the best of the authors' knowledge, no experimental or theoretical results have been published on this particular type DX-SAHP solar water heater, using evacuated fin-integrated U-tube collector with CO_2 as the working fluid operating in a transcritical cycle. Hence, model validation had been conducted by separately investigating the evaporation model in isolation from the system, which is the most critical to overall simulation accuracy. To examine the accuracy of the evaporation model adopted in this study, a simple thermosyphon based experimental set-up was designed and fabricated. The predicted results were then compared with the solar collector under stagnation conditions. The experimental design and operating parameters of the collector were then used in the theoretical model to generate the simulation results. The design details of the experimental set-up (Figure 26) are listed in Table 6.

Figure 26: Evacuated tube U-pipe solar collector used for experimental set-up

Table 6: Design parameters used for the experimental set-up

Components	Material	Parameters	Value
Solar Collector Properties	Absorbing coating	Absorptivity	0.92
		Emissivity	0.193
	Outer glass tube	Outer diameter	0.047625 m
		Inner diameter	0.0381 m
		Thickness	0.0015875 m
	Air layer	Conductivity	1.2 W/m K
		Thickness	0.001 m
		Conductivity	0.03 W/m K
	Copper fin	Thickness	0.0006 m
		Conductivity	307 W/m K
	U-tube	Outer diameter	0.00635 m
		inner diameter	0.003175 m
		Thickness	0.015875 m
	Length of tubular collector		3.6576 m
	Bond conductance		30 W/m K
	Collector area		1.15 m^2

The validity of the analytical approach adopted in this study was verified with the experimental results, in terms of collector efficiency and the temperature of the working fluid. Experimental results pertaining to 23rd May, 2013 were used for comparison. Figure 27 shows the efficiency profile of the evacuated tube U-pipe solar collector. The maximum global solar radiation intensity recorded by the pyranometer on the day of experiment was 600 W/m^2. As seen in the Figure 27, experimental data points are clearly scattered about the straight line which confirms that the collector efficiency agrees well with the predicted results. Figure 27 also shows that efficiency reduces linearly with an increase in the parameter $(T_f - T_a)/I_T$. The slope of the profile is negative and is a function of U_L. This is due to the fact that, as the difference between the working fluid and ambient temperature rises, the radiation and convection losses from the collector also increase. In general, as per the law of conservation of energy, the collector performance can be further improved by increasing energy transmission through the collector to the working fluid (useful energy) and minimizing the collector heat losses, with improved insulation techniques.

The theoretical model was further verified by comparing the predicted CO_2 temperature with the measured data of the collector outlet. As shown in Fig. 28, the simulated results are in well accordance with the experimental results until noon. However, beyond noon, there exists an inconsistency between the measured and predicted values, which is caused by the sudden overcast of clouds, during the test day. The experimental collector efficiency during the test day was also compared with the simulation results, as shown in Fig. 29. Simulation results follow a similar trend to that of experimental values and found a mean absolute deviation of 15%.

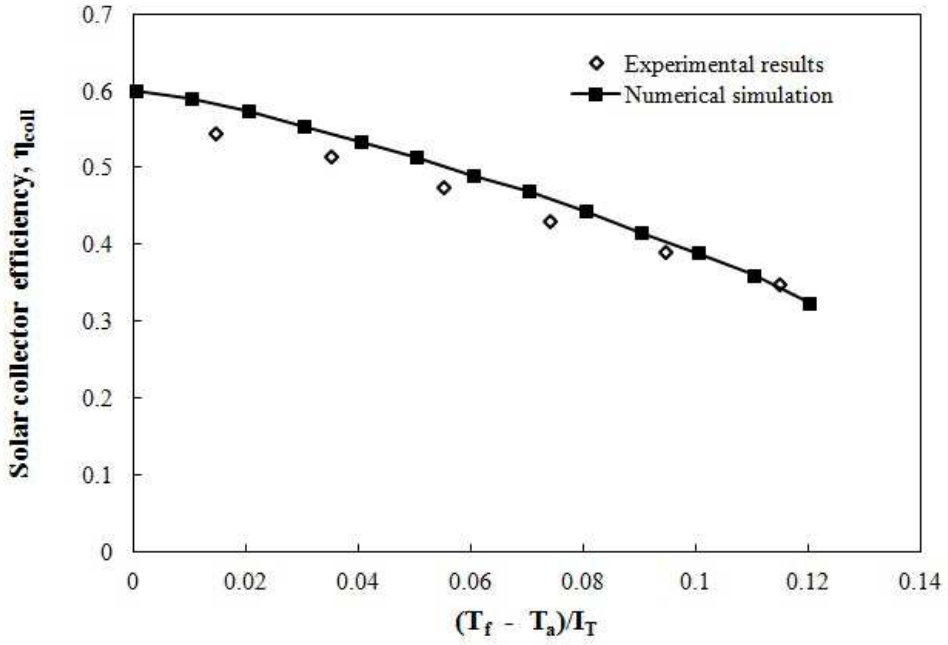

Figure 27: Comparison of solar collector efficiency variation profile between simulation and experimental results

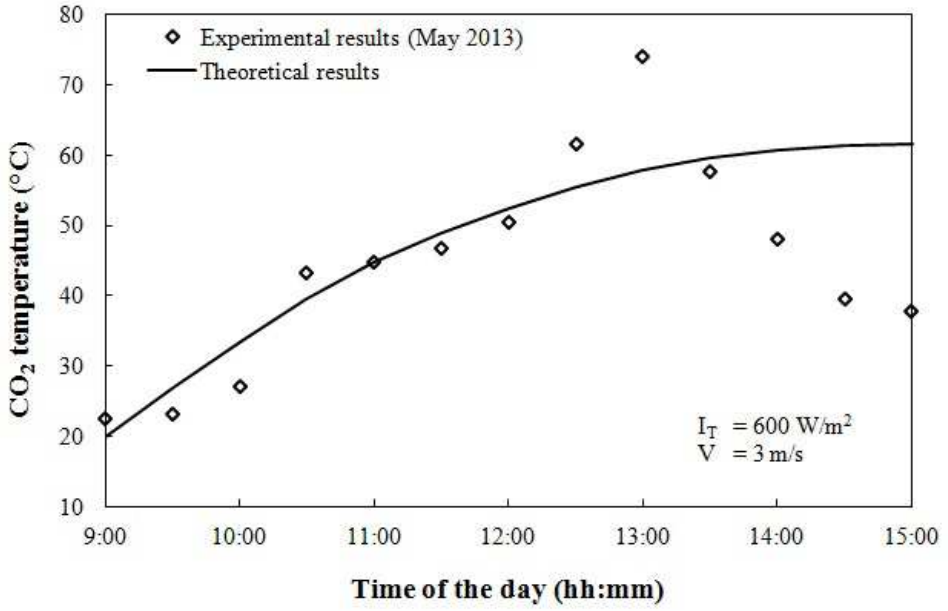

Figure 28: A comparison between theoretical and experimental results of CO_2 outlet temperature over the test time of the day

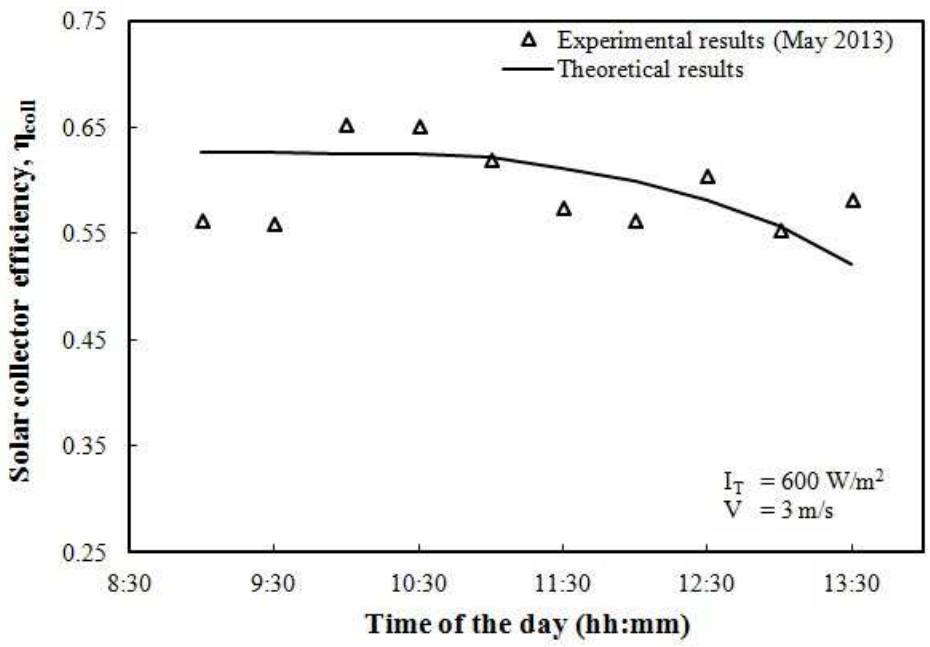

Figure 29: Comparison between theoretical and experimental results of solar collector efficiency over the test time of the day

Based on the validation results shown in Fig. 27 – 29, it can be said that the accuracy of the theoretical model is adequate to investigate the year-round performance of the proposed DX-SAHP water heating system.

6.2. Baseline Simulation and Parametric Studies

Theoretical analysis performed in Chapter 4 is used here to show the thermal performance of the proposed DX-SAHP water heating system in terms of COP, solar collector efficiency and heating capacity. A number of operating parameters such as: solar radiation, collector area, compressor speed, ambient temperature and storage volume, strongly influence the overall performance of the system, and are used to investigate the system under study. The simulation model identifies the important variables and therefore enables to perform the parametric study. A standard case is defined to evaluate the effects

of various parameters and is listed in the Table 5 of Section 5.1. To evaluate the effect of each parameter, all other variables remain constant at their standard values. The inlet water temperature to the storage tank is taken as an average of circulating tap water temperature.

6.2.1. Effect of Compressor Speed and Collector Area

To avoid the two-phase properties at the inlet of the compressor, it is assumed to deal with only the vapor phase discharged from the solar collector as either saturated vapor or at supercritical state. Therefore, though a part of the solar collector will go through the two-phase region, it is ensured that it is in the vapor region before entering into the compressor inlet. Throughout the steady state cycle shown in Fig. 30, it is observed from the simulated results that a transcritical operating condition is achieved. A heat sink of relatively low temperature (-5° – 10°C) plays a key role to ensure efficient transcritical operation.

The compressor effect on the overall performance of the system has been assessed by varying the speed of the compressor. Figure 30 shows the effect of compressor speed within a range of 900 to 1500 rpm on COP and heat output at the condenser, for different solar intensity levels. The collector area and the ambient temperature were set to the base values of 1.91 m^2 and 10°C, respectively. At any given speed of the compressor, COP increases with an increase in the solar intensity. It is due to the fact that solar intensity has a positive influence on the evaporation temperature, in turn requiring only low compressor speeds to accomplish the task of raising the fluid's temperature to the desired value. It could also be noted from the Fig. 30 that, as the compressor's speed increases, the COP value reduces. It is due to the fact that the discharge temperature increases along with an increase in speed of the compressor. At lower compressor speeds (around 1000 to 1100

rpm), the DX-SAHP system could reach a COP value of 2 – 2.5 with a heat capacity rate of about 2.4 – 3.0 kW. However, as the speed of the compressor further increases, the COP value decreases, although the heat extraction rate is much higher. This is due to the fact that, increase in the compressor speed is aided only with the work input which reflects in lower COP values.

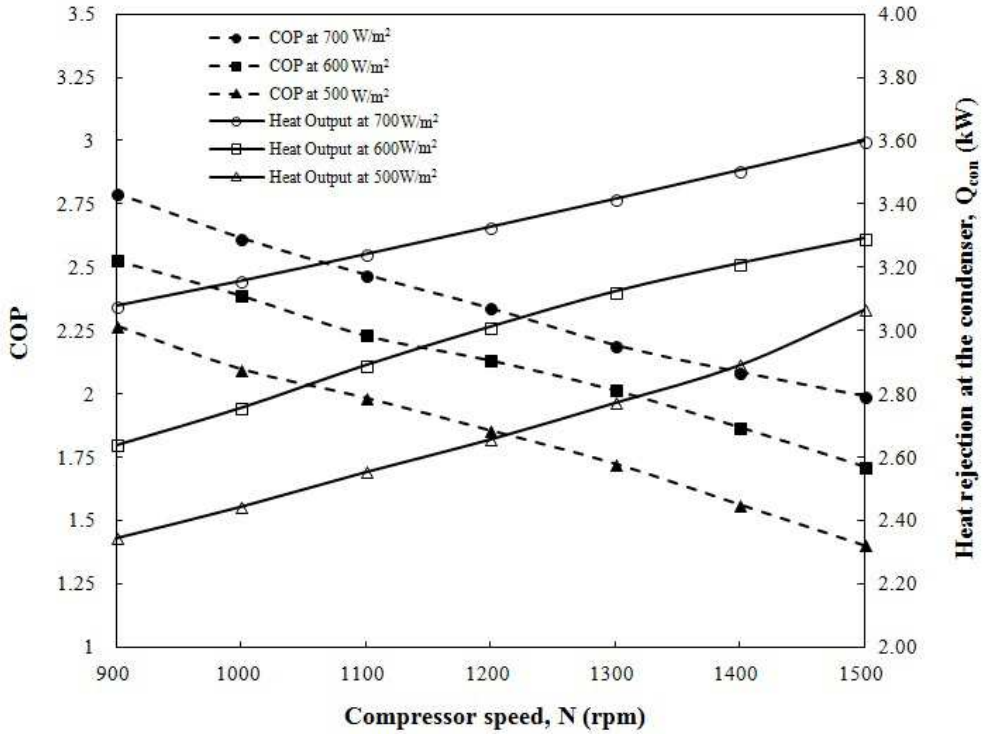

Figure 30: Effect of compressor speed on system COP and heat rejection at the condenser

Figure 31 illustrates the variation of COP as a function of compressor speed considering solar collector area as a parameter. For a fixed compressor speed, the COP rises with the increase in collector area. If the solar collector area is more, the working fluid evaporates in the evaporator comparatively at a higher temperature which results in decrease in the compressor work and thus leading to a higher COP.

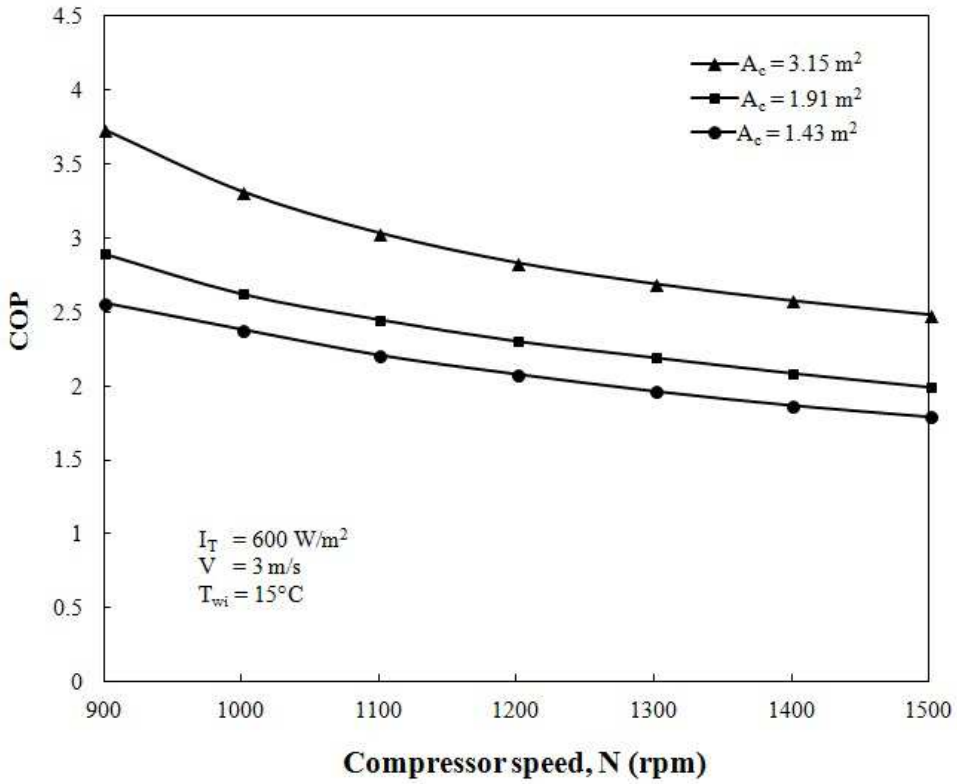

Figure 31: Effect of compressor speed for different collector area

Effects of the compressor speed on solar collector efficiency and evaporation temperature are shown in Figure 32. The results have been predicted for the solar radiation of 600 W/m^2 and collector area of 1.91 m^2. An increase in the compressor speed facilitates higher refrigerant mass flow rate through the solar collector which lowers working fluid temperature. This phenomena leads to a lower heat loss from the solar collector and increase the solar collector efficiency. However, for any given compressor speed, as the collector area increases, it effects higher working fluid temperature, eventually leading to a decrease in the collector efficiency. This performance disparity between the system COP and the solar collector efficiency, for the given collector size and ambient conditions, shows that, there is room to identify an optimum compressor speed, which will help in

attaining a reasonable value in the COP and solar collector efficiency. Based on the results it could be discerned that, the predicted optimal compressor speed matches the existing collector design. In the situation of mismatches, it can be easily overcome by integrating a variable speed compressor to the DX-SAHP system, which would ensure an increase in the seasonal thermal performance.

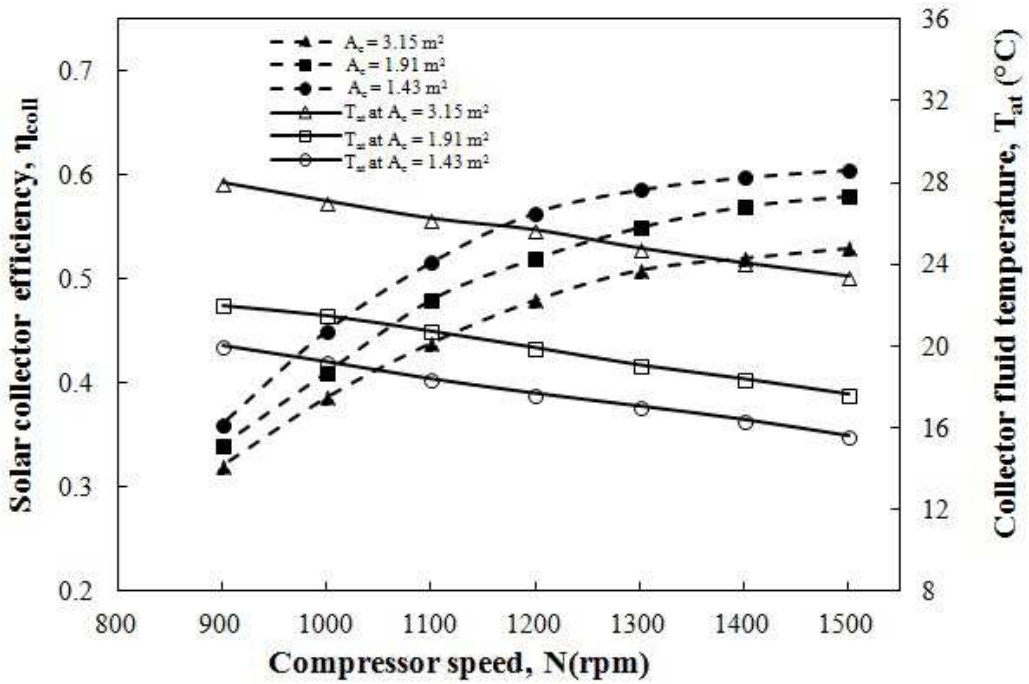

Figure 32: Variation of collector tube temperature and solar collector efficiency with compressor speed

6.2.2. Effect of Solar Radiation Intensity

The results discussed in Figures 27 and 28, pertain to a given intensity of solar radiation. As the radiation can vary over a wide range in a year, it would be interesting and informative to study its effect on the performance of DX-SAHP water heating system. Accordingly, the analysis was carried out for various intensities, the noon values of which

are varied in steps of 100 W/m^2, from 200 – 700 W/m^2. The results obtained for three different commercially available [91] evacuated tube collector areas, are shown in Figure 33. This figure shows that, the system COP increases with increase in the intensity of solar radiation, for any given collector area. This is because of two reasons: (i) the higher solar radiation intensity heats the CO_2 to a higher temperature; consequently, the heat recovery in the storage tank is higher, (ii) rise in collector temperature also aids natural convection currents and the cumulative effect of the natural and forced convection, results in higher mass flow rate, which in turn lowers the evaporator (collector) temperature. Lower the evaporator temperature, lower would be the heat losses and higher the collector efficiency as well as the system COP.

The combined effect of T_a and intensity of solar radiation on the collector (absorber tube) to ambient temperature difference is shown in Figure 34. It puts in the perspective year-round performance of the system. It is well known that the collector efficiency is dictated by the collector tube loss, which scales with ($T_{at} - T_a$). In general, low ambient temperature (T_a) and low solar insolation (I_T) correspond to winter operation, and similarly high values of T_a and I_T correspond to summer operation. As seen in the Figure 34, for a given solar insolation, as the variation of ($T_{at} - T_a$) increases, the collector performance deteriorates since the heat loss from the collector significantly increases, in turn impacts the overall performance of the DX-SAHP system. Similarly, for any given ambient temperature, as solar insolation increases, the variation in ($T_{at} - T_a$) increases. Though it results in a marginal increase in heat losses, given in the evaporator/collector temperature (T_{at}) reflects an increase in the average fluid (CO_2) temperature. This raise in fluid temperature would translate into a higher coefficient of performance of the heat pump. This

is because, for a given condensing temperature, a heat pump be more efficient when the evaporator temperature is raised.

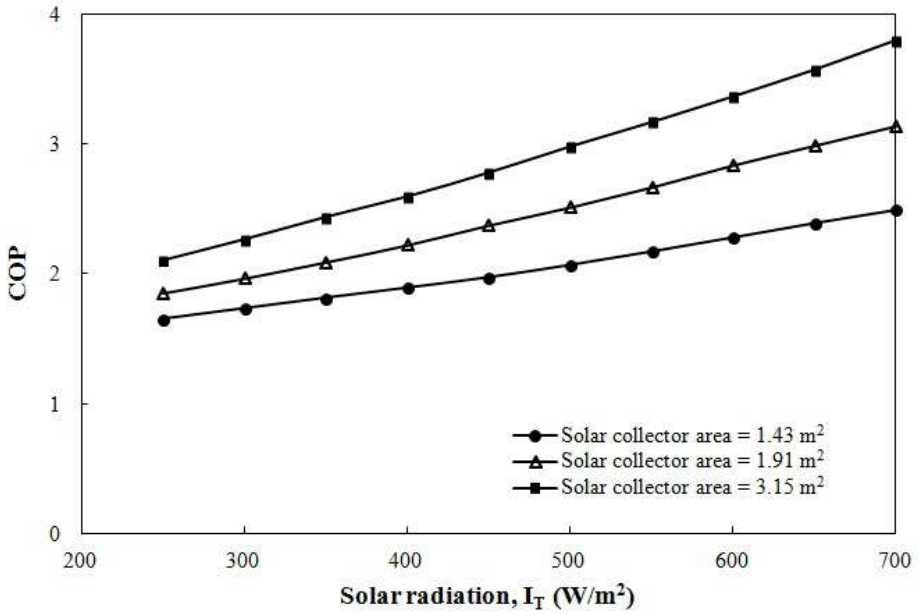

Figure 33: Effect of solar radiation for different collector area on COP values

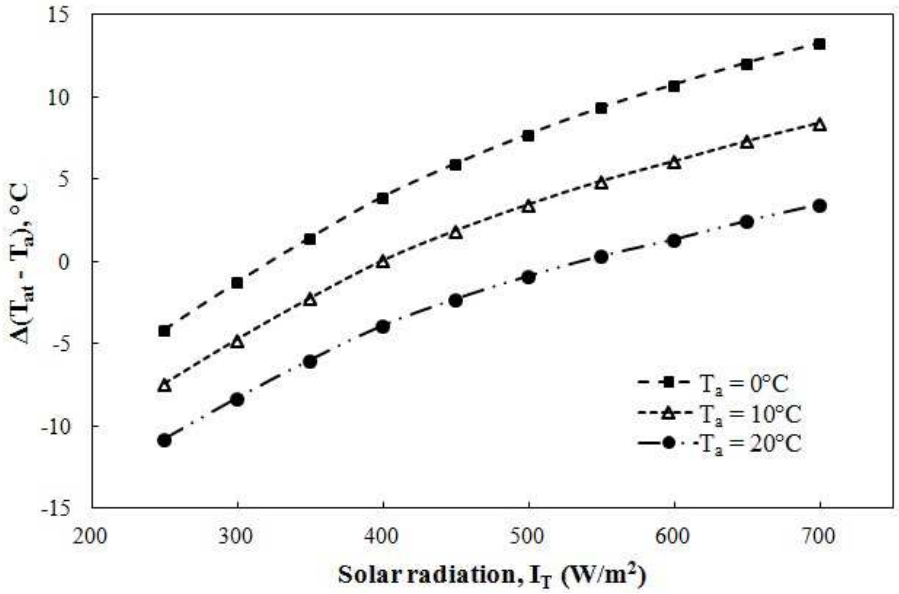

Figure 34: Variation of differences of mean fluid temperature over ambient temperature as a function of I_T and T_a

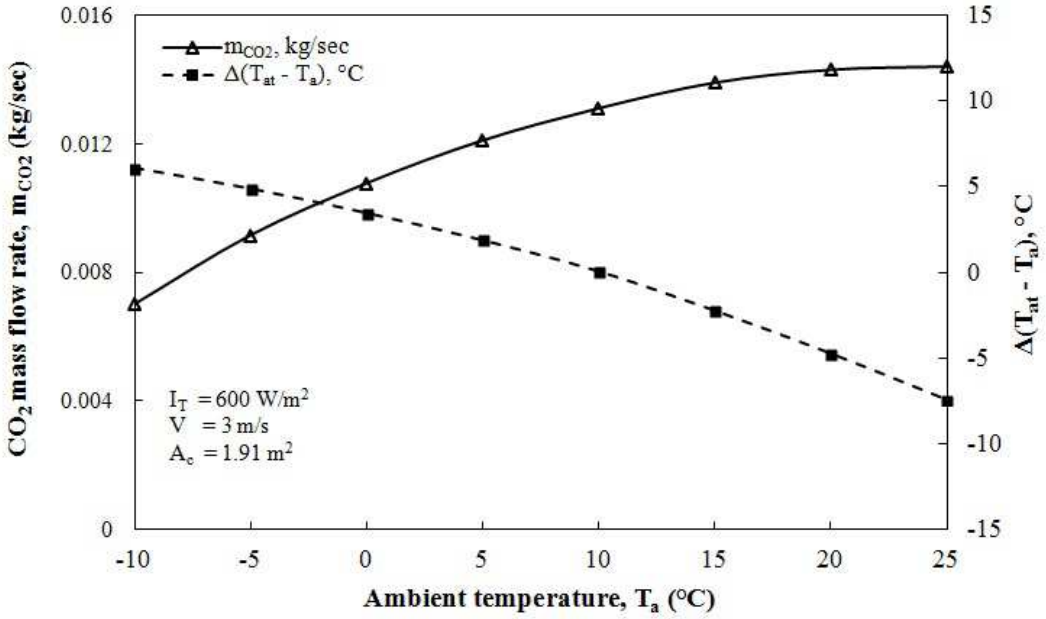

Figure 35: Variation of CO_2 mass flow rate as a function of T_a

The variation of the mass flow rate in the collector and the rise in collector temperature over the T_a, are shown in Figure 35. As shown with an increase in the value of T_a from -10° – 25°C, the fluid flow rate in the collector increases approximately by a factor of 2. For a given solar intensity, and mass flow rate in the collector, results in drop in collector temperature below ambient temperature. Hence, an apparently matched collector/compressor operation at low ambient temperature becomes a mismatched operation at higher ambient temperature.

6.2.3. Effect of Ambient Temperature and Wind Speed

To determine the effect of ambient temperature and wind speed on the collector efficiency and system COP, the ambient temperature was varied in steps of 5 degrees from -10°C to 20°C, and in steps of 1 m/s from 1 – 5 m/s, respectively. Figure 36 shows that higher ambient temperatures have positive influences on the thermal performance of

the system. This is because, higher ambient temperature reflects less heat losses from the collector, for the given operating range, affecting higher collector efficiency. Also, the required compressor work is reduced, thereby aiding higher COP.

Wind speed also plays a pertinent role in the system performance. As one would expect, an increase in the wind speed would enhance the heat transfer between the solar collector and the surroundings. Under the conditions when the absorber tube temperature (T_{at}) is lower than the ambient temperature (T_a), an increase in the wind speed increases forced convection currents between the surrounding and absorber tube, resulting in higher rates of heat transfer. However, based on this study with the given operating conditions, the effect of wind speed is not predominant compared to other operating parameters. Figure 37 shows the effect of wind speed on the system's COP.

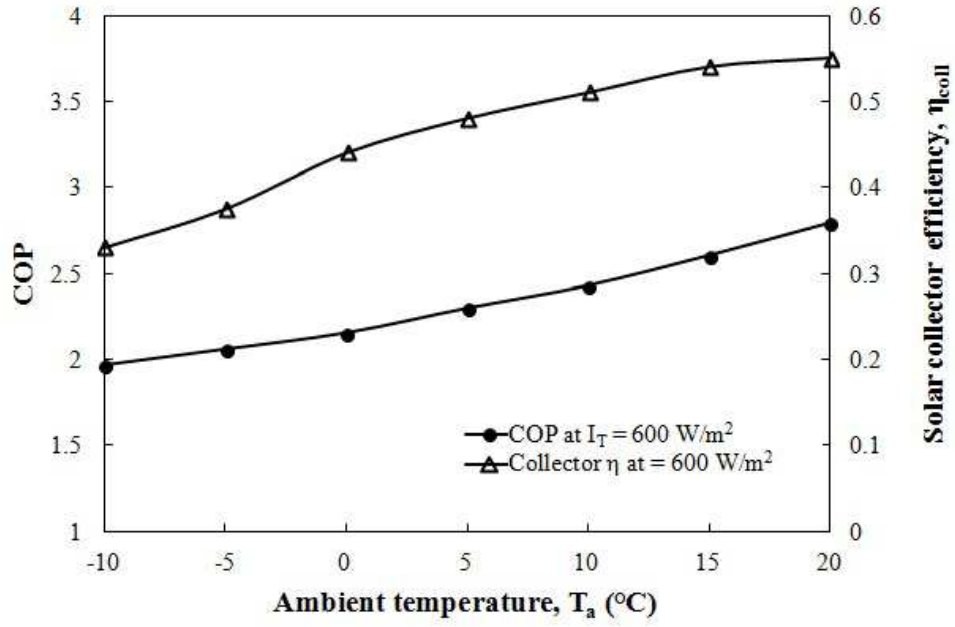

Figure 36: Effect of ambient temperature (T_a) on the system performance in terms of COP and solar collector efficiency

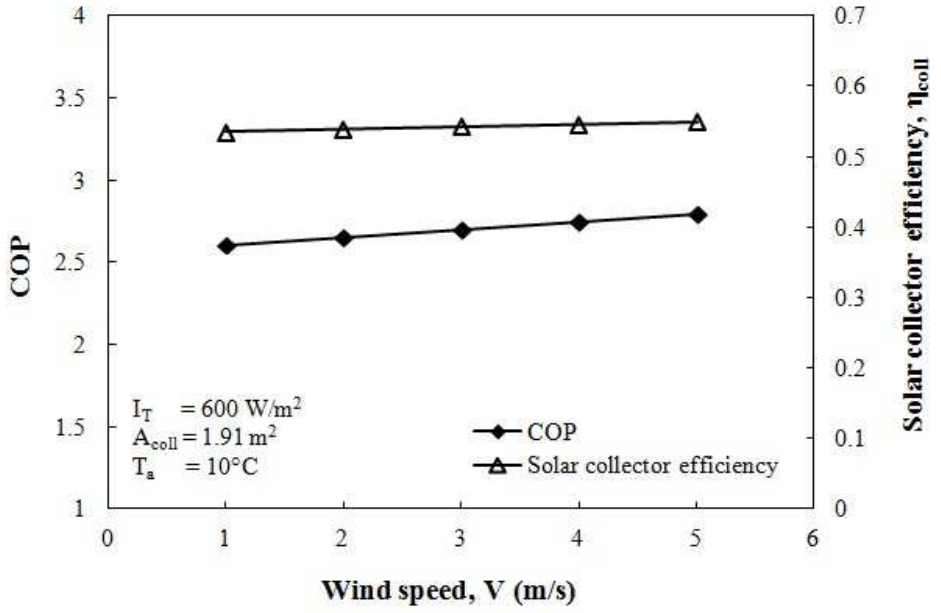

Figure 37: Effect of wind speed (*V*) on the system performance in terms of COP and solar collector efficiency

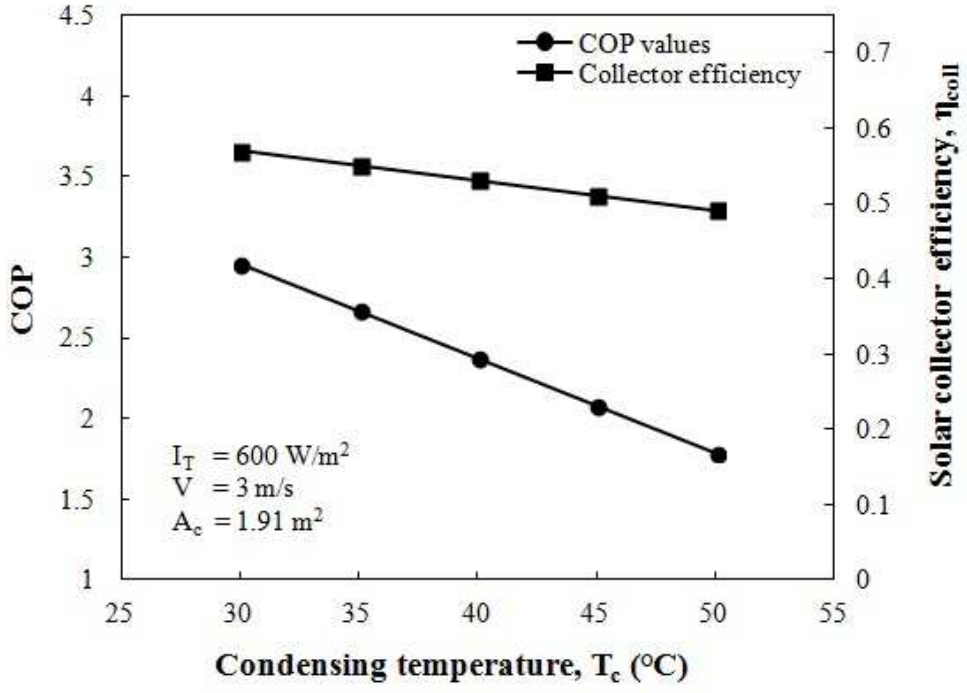

Figure 38: Effect of condensing temperature on system COP and collector efficiency

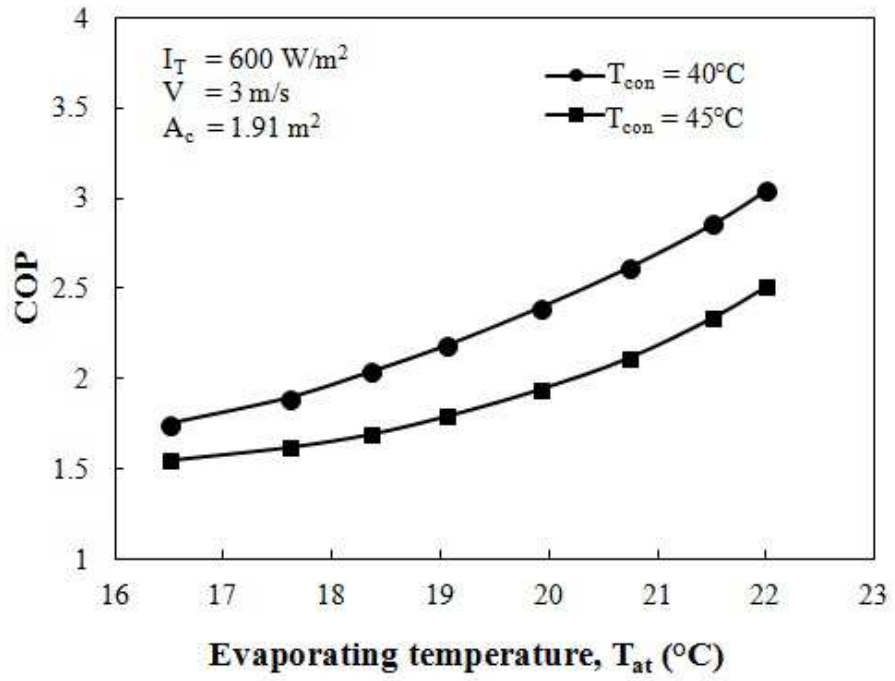

Figure 39: Effect of evaporating temperature on system COP at different condensing temperatures

6.2.4. Effect of Condensing and Evaporating Temperature

Condensing temperature (T_{con}) is also an important operating parameter that influences the system performance. For the given base-case Figure 38 illustrates the effect of T_{con} on COP and collector efficiency and it could be seen that with an increase in T_{con}, though there is a sharp reduction in COP value, the collector efficiency reduces only marginally. Higher condenser temperature interprets that the collector absorber tube temperature is higher which aids higher heat losses from the collector system. Hence, the COP of the heat pump cycle is dictated both by the T_{con} and T_{at}. A substantial rise in the condensing temperature along with a marginal increase in collector temperature leads to a considerable drop in the COP. Also, it could be apparent from Figure 38 that, at low condensing temperature, both COP and collector efficiencies are relatively higher. This

observation suggests that the proposed heat pump cycle is more suitable for low temperature applications like domestic water heating. Similar to the condensing temperature, the evaporating temperature also plays a role on the overall system performance. Figure 39 shows that an increase in evaporating temperature improves the COP of the system positively. It should also be noted from Figure 38 and 39 that both condensing temperature and evaporating temperature have an inverse relationship on the COP of the system. Hence, for a given collector area of 1.91 m^2, it is better to operate the system with a storage water temperature (condensing temperature) within the range of 40° – 45°C. Higher condensing temperature results in lower COP values, because of the fact that higher compression ratio (indicates the need for work input) is required to aid higher condensing temperature.

6.2.5. Combined Effect of Solar Collector Area and Storage Volume

Other than the condensing temperature, also a proper combination of solar collector area as well as storage tank sizing is necessary to determine the reliability of the proposed system design. Figure 40 and 41 illustrate the combined effects of solar collector area and storage tank volume on its performance. It is evident from the trend that, initially an increase in storage volume effects a rapid rise in both COP and collector efficiency. However, for the storage tank volume beyond 150 liters, the performance parameters (COP and η_{coll}) do not improve much. On the other hand, an increase in solar collector area for chosen tank volume effects the system COP positively, though having a negative impact on the collector efficiency. This phenomenon could be attributed to two main reasons: (i) for a given solar collector area, increasing tank volume lowers the condensing temperature which eventually results only a marginal decrease in the solar collector/evaporator

temperature. This paves a way for a relatively lesser amount of compressor work, in turn boosting the COP; (ii) For a given storage tank volume, an increase in solar collector area aids a rise in the fluid temperature of the evaporator, which results in an increase in COP, affecting a lower collector efficiency due to heat losses. Based on the numerical results, for the proposed DX-SAHP system, 100 – 150 L/m^2 turns out to be the optimum storage tank size.

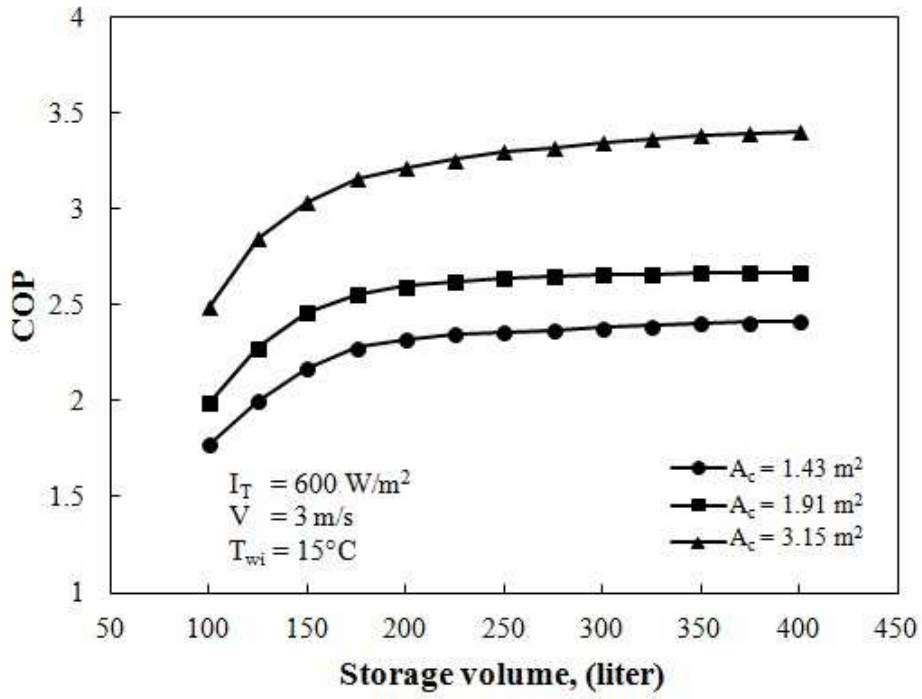

Figure 40: Combined effect of solar collector area and storage volume on COP

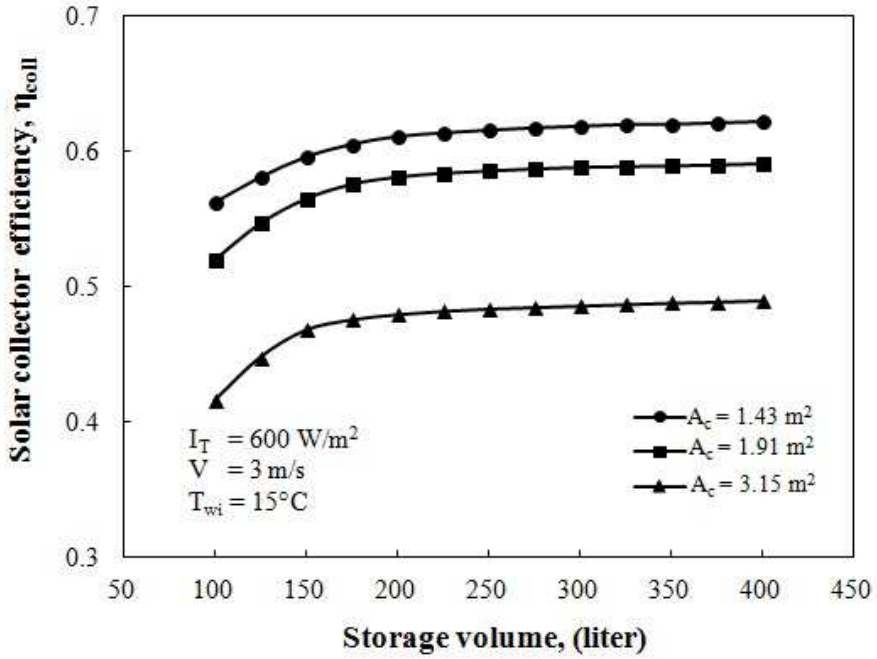

Figure 41: Combined effect of solar collector area and storage tank volume on collector efficiency

6.2.6. Effect of Solar Collector Area and Condenser Coil Length

This section of the study analyzes the influence of solar collector area on COP by varying condenser coil length. For solar collector area of 1.43, 1.91 and 3.15 m^2, the simulation was performed to optimize an appropriate range of condenser coil length (Figure 42). Simulation results show that system COP is significantly impacted by condenser coil length. For each solar collector area, there is an optimum condenser coil length for obtaining the best COP. As the solar collector area increases, the optimal condenser coil length also increases. However, as the condenser length increases for a given solar collector area, COP value increases sharply before reaching the optimum value and decreases marginally after the optimum point. It implies that an undersized coil length have more negative impact to the performance than the oversized length.

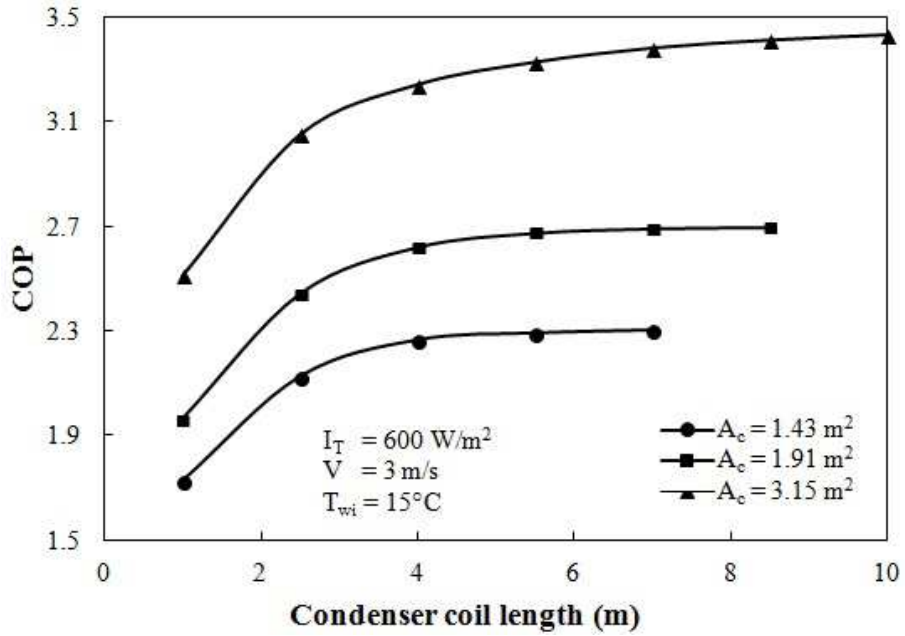

Figure 42: Effect of condenser coil length on the system performance

6.2.7. Seasonal Performance Variation

Apart from the above parametric study in specific to seasonal variables, computer simulation was also carried out to learn about the year-round performance in terms of COP as well as the storage tank water temperature of the system. Accordingly, the monthly averaged global solar radiation and T_a pertaining to the North Dakota region were used as the input, obtained from a local weather network data [89]. It should be pointed out that, the simulation was performed only for radiation values above 250 W/m^2. This is to ensure that the collector temperature (T_{at}) does not fall below the ambient temperature (T_a), which might drastically affect the system COP. Monthly averaged COP and solar collector efficiency of the proposed system is shown in Figure 43. It is evident from the calculated results that COP of the system during winter months (about 3.0 – 3.2) is generally higher than the COP during fall and spring period (about 2.0 – 2.5). This is because, the

difference between the condensation and evaporation temperature during winter months is particularly lower (Figure 44). Lower temperature difference reflects less work requirement in the compressor which impacts an enhancement in the COP. The system COP can be improved by lowering the compressor speed in relatively warmer seasons. The monthly averaged collector efficiency variation (45 – 62%) as shown in Figure 43 also confirms that the proposed system's collector efficiency is relatively higher compared to the conventional water driven solar flat-plate collector (about 40%). Monthly averaged year-round temperature variation of solar collector, condenser and storage tank water are shown in Figure 44. It is evident from the results that the difference between collector and condenser temperature stays higher during summer period (Jun – Aug) than that of winter months. Higher compressor work is needed when the difference between condenser and evaporator temperature remain higher and thus negatively impacts on COP value.

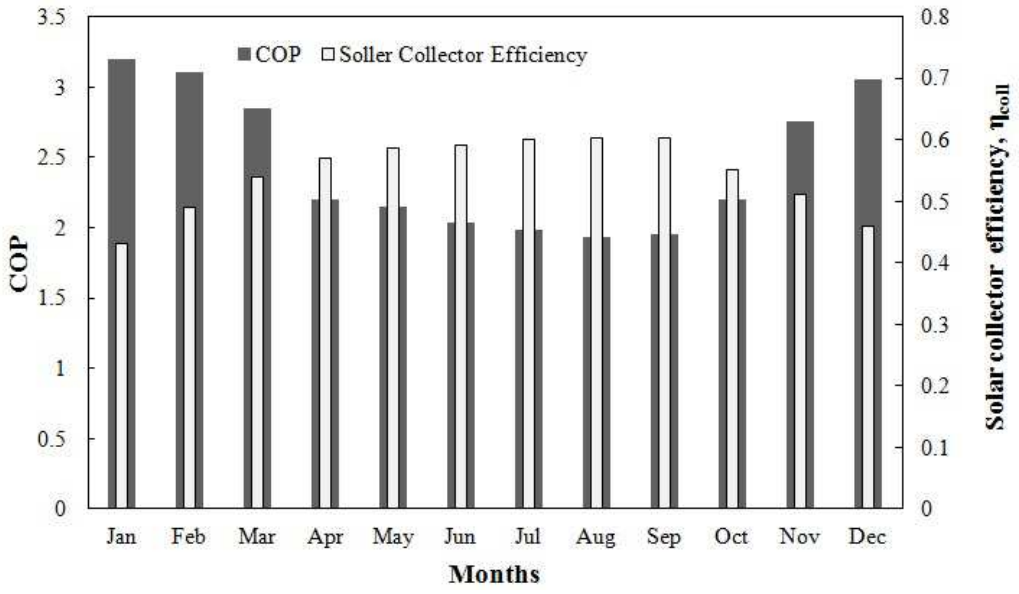

Figure 43: Variation of monthly averaged COP and solar collector efficiency

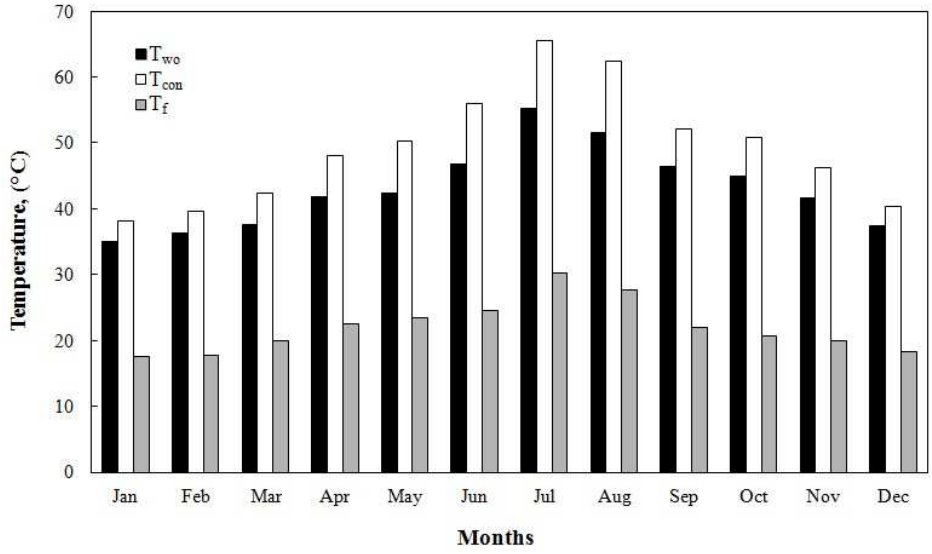

Figure 44: Variation of monthly averaged temperature profile for T_{wo}, T_{con}, and T_{at}

7. CONCLUSIONS AND FUTURE RESEARCH

The focus of the present study was to investigate the performance of the direct-expansion solar assisted heat pump (DX-SAHP) system using a CO_2 transcritical cycle for the water heating application. The theoretical analysis was used to develop a numerical simulation model assuming a quasi-steady state operation of the system. Experiments were also conducted to verify the simulation results under the meteorological conditions of North Dakota. The simulation and experimental results showed a reasonable agreement between them and hence, the model can be a good demonstration of the actual system.

Using the developed numerical model, the study examined the influences of several design and operating parameters on the overall performance of the DX-SAHP water heating system. The summarized design and operating characteristics identified by the simulation model can be described as follows:

- The simulation model has shown that the thermal performance of the discussed system is greatly influenced by solar collector area, global solar radiation, ambient temperature, compressor speed, storage volume, and evaporating and condensing temperatures. Results revealed that solar radiation and ambient temperature have a significant impact on the DX-SAHP system's thermal performance, although wind speed has shown to have negligible effect.
- To ensure improved system performance, it is pertinent to choose an appropriate compressor speed which highly depends on the collector evaporative load. It was observed that average COP value increases by 57% when compressor speed

decreases from 1500 to 900 rpm, given that all other operating parameters remain at their standard values.

- With a given compressor power, the higher collector area leads to an improved COP value and hence lowers the system operating cost by decreasing electrical power input. However, the higher collector area leads to a higher evaporating temperature and lower solar collector efficiency.
- Simulated results showed that it is possible to achieve about 62% solar collector efficiency for an evacuated tube U-pipe solar collector, which is much higher than the conventional glass evacuated tube solar collector efficiency, using water as the working fluid (40 – 45%) [81].
- For a constant water volume in the tank, an increase in evaporator or solar collector area increases the overall COP, although it has a negative influence on the collector efficiency. An optimum relation between the storage volume and solar collector area is found to be 100 – 150 liters/m^2.
- With an increase in condense temperature, the system performance (both COP and collector efficiency) decreases, which indicate that the said system is suitable for low load heat applications. However, evaporating temperature has a positive influence on the system COP. Therefore, condensing and evaporating temperature have an inverse relationship on the overall system performance.
- As the length of the condenser coil increases, the heat rejection capacity of the condenser also increases and eventually COP value increases up to a certain length of condenser coil. Therefore, an optimum length of condenser coil exists for different solar collector areas.

- A year-round thermal performance study on the proposed heat pump system revealed that the overall system performance was much more pronounced in winter months in terms of COP value when compared to rest of the months.

In terms of installation expenditures and energy cost over the total life of the system, solar water heating technology has proven to be cost efficient for several domestic and industrial applications. Residential solar water heating is a promising age old technology, which has been evolved and developed both in range and quality as a successful packaged market-product. Although the high initial cost of the evacuated tube U-pipe solar collector makes the proposed DXSAHP water heating system expensive, the low cost and environmentally benign CO_2, has great potential to be used in other integrated solar thermal applications as well.

7.1. FUTURE RESEARCH

The study comprises alternative natural refrigerant carbon dioxide as a working fluid in a DX-SAHP water heating system in which evacuated tube U-pipe solar collector is utilized as an evaporator. More in-depth analysis needs to be carried out in order to improve the feasibility of such a system. Therefore, future potential studies include:

- Theoretical analysis indicates that certain design modifications can be beneficial for obtaining higher heat energy output. In particular, the stratified storage tank maintains the thermal stratification to deliver more heat, which is superior in design over conventional non-stratified or mixed storage water tanks. Therefore, incorporating the stratified tank analysis model into the DX-SAHP system may enhance the heating effect significantly and thus improve the overall system COP.

- Technical feasibility of such a DX-SAHP water heating system should be verified by carrying out extensive experimentation. In this way simulation results can be validated using experimental results. Experimentation is also useful to identify the real time design issues of such a system, which is difficult to encompass in simulation.
- One of the widely acknowledged benefits of the SWH systems is in the potential of energy savings. Therefore, the economic evaluation and the life cycle analysis are necessary assessments to determine the feasibility of such systems. Economic evaluation factors that affect the SWH systems, used to find the specific energy efficient approaches depending on the size and particular energy demands, are also discussed in the review section.
- This study investigated only on heating application. A combined electrical power and heat generation approach using supercritical carbon dioxide can be more innovative and efficient means of solar energy utilization. Several studies reveal that this combined cycle can achieve higher electrical and solar thermal conversion efficiency. Therefore, more thorough theoretical analysis of such combined systems should be carried out to realize the potentiality.
- Design modifications for the studied DX-SAHP system can incorporate multi-mode operations, which may offer winter space heating, summer air conditioning, and year-round hot water supply. Although the DX-SAHP system complicates this multi-mode operation, but more study needs to be conducted to understand its potential.

REFERENCES

[1] O. Langniss and D. Ince, Solar water heating: a viable industry in developing countries. Refocus May-June 2004; 5(3): 18-21.

[2] Renewable Energy 2010: Key Facts and Figures for Decision Makers. Global status report. [Online] <http://www.ren21.net/Portals/0/documents/Resources/110929_GSR2011_FINAL.pdf>

[3] REN21 Renewables 2011 Global Status Report. [Online] <http://www.ren21.net>

[4] The Kyoto Protocol to the United Nations Framework Convention on Climate Change, 1997. [Online] <http://untreaty.un.org/cod/avl/ha/kpccc/kpccc.html>

[5] G. Lorentzen. “Trans-critical vapour compression cycle device.” (1990) Patent WO/07683.

[6] R744.com (November 26, 2009). "EcoCute shipments exceed 2 million landmark." [Online] <http://www.r744.com/articles/2009-11-26-eco-cute-shipments-exceed-2-million-landmark.php>

[7] USGS Northern Prairie Wildlife Research Center. [Online] < http://www.npwrc.usgs.gov/resource/habitat/climate/sunshine.htm>

[8] National weather service: North Dakota weather forecasts. [Online] <http://www.rssweather.com/climate/North%20Dakota/Fargo/>

[9] The Encyclopedia of Earth. [Online] <http://www.eoearth.org/article/De_Saussure,_Horace_B%C3%A9n%C3%A9dict>

[10] K. Butti and J. Perlin, A golden thread, Marion Boyars Publishers Ltd., London, UK (1981).

[11] B. D. Chiaro, Solar water heating, how California can reduce its dependency on natural gas; Environment California Research and Policy Center, April 2007. [Online] <http://www.environmentcalifornia.org/uploads/at/56/at563bKwmfrtJI6fKl9U_w/Solar-Water-Heating.pdf>

[12] K. Butti and J. Perlin, Early solar water heaters, A Golden Thread, Van Nostrand Reinhold Company, New York (1979), p. 117-127.

[13] S. A. Kalogirou, Solar energy engineering: processes and systems, Elsevier, London (2009).

[14] The Equitable Building Heat Pump System. A National Historic Mechanical Engineering Landmark. Dedicated May 8, 1980 in Portland, Oregon. [Online Access date: January 25, 2008] <http://www.bookrags.com/research/heat-pump-woi/>

[15] The unitary heat pump industry – 25 years of progress. [Online Access date: September 19, 2007] <http://adsabs.harvard.edu/abs/1977ASHRA.19.15P>

[16] X. Zhang, A. Plattern and L. Shen, Green property development practice in China: costs and barriers, Building and Environment 2011; 46(11): 2153-2160.

[17] S. A. Kalogirou, Solar thermal collectors and applications, Progress in Engineering and Combustion Science 2004; 30(3): 231-295.

[18] S. Kalogirou, Solar water heating in Cyprus: current status of technology and problems, Renewable Energy 1997; 10(1): 107-112.

[19] R. Uhlemann and N. K. Bansal, Side-by-side comparison of a pressurized and a nonpressurized solar water heating thermosyphon system. Solar Energy 1985; 34(4-5): 317-328.

[20] A. A. Mohamad, Integrated solar collector-storage tank system with thermal diode. Solar Energy 1997; 61(3): 211-218.

[21] Z. Li, C. Chen, H. Luo, Y. Zhang and Y. Xue, All-glass vacuum tube collector heat transfer model used in forced-circulation solar water heating system. Solar Energy 2010; 84(8): 1413-1421.

[22] Y. H. Kuang, K. Sumathy and R. Z. Wang, Study on a direct-expansion solar-assisted heat pump water heating system. International Journal of Energy Research 2003; 27(5): 531-548.

[23] J. A. Duffie, and W. A. Beckman, Solar Engineering of Thermal Processes, 1980 (John Wiley, New York); pp. 487-488.

[24] Z. Li, C. Chen, H. Luo, Y. Zhang and Y. Xue, All-glass vacuum tube collector heat transfer model used in forced-circulation solar water heating system. Solar Energy 2010; 84(8): 1413-21.

[25] A. Walker, F. Mahjouri and R. Stiteler, Evacuated-tube heat-pipe solar collectors applied to recirculation loop in a federal building: SSA Philadelphia. ASME 2004 International Solar Energy Conference (ISEC2004) Paper no. ISEC2004-65132; 217-222.

[26] Sonntag, R.E., C. Borgnakke, G.J. Van Wylen. "Fundamentals of Thermodynamics, 6th ed." John Wiley & Sons Inc; Hoboken, NJ (2003).

[27] T.L. Freeman, J.W. Mitchell, T.E. Audit, Performance of combined solar - heat pump systems. Solar Energy 1979; 22(2): 125-35.

[28] J.W. Macarthur, Theoretical analysis of the dynamic interactions of vapor compression heat pumps. Energy Conversion and Management 1984; 24(1): 49-66.

[29] J.A. Duffie, W.A. Beckman, Solar Engineering of Thermal Processes. Second edition, Willey, New York, 1991.

[30] K. Kaygusuz, N. Gultekin, T. Ayhan, Solar-assisted heat pump and energy storage for domestic heating in Turkey. Energy Conversion and Management 1993; 34(5): 335-46.

[31] P. Axaopoulos, P. Panagakis, S. Kyritsis, Experimental comparison of a solar-assisted heat pump vs. a conventional thermosyphon solar system. International Journal of Energy Research 1998; 22(13): 1107-20.

[32] S.K. Chaturvedi, M. Abazeri, Transient simulation of a capacity-modulated, direct-expansion, solar-assisted heat pump. Solar Energy 1987; 39(5): 421-28.

[33] S.K. Chaturvedi, D.T. Chen, A. Kheireddine, Thermal performance of a variable capacity direct expansion solar-assisted heat pump. Energy Conversion and Management 1998; 39(3-4): 181-91.

[34] M.N.A. Hawlader, S.K. Chou, M.Z. Ullah, The performance of a solar assisted heat pump water heating system. Applied Thermal Engineering 2001; 21(10): 1049-65.

[35] B.J. Huang, J.P. Chyng, Performance characteristics of integral type solar-assisted heat pump. Solar Energy 2001; 71(6): 403-14.

[36] G.L. Morrison, Simulation of packaged solar heat-pump water heaters. Solar Energy 1994; 53(3): 249-57.

[37] S.K. Chaturvedi and J.Y. Shen, Thermal performance of a direct expansion solar-assisted heat pump. Solar Energy 1984; 33(2): 155-62.

[38] S. K. Chaturvedi, D. T. Chen and A. Kheireddine, Thermal performance of a variable capacity direct expansion solar-assisted heat pump. Energy Conversion Management 1998; 39(3-4): 181-91.

[39] M. N. A. Hawlader, S. K. Chou, K. A. Jahangeer, S. M. A. Rahman and K. W. E. Lau, Solar-assisted heat-pump dryer and water heater. Applied Energy 2003; 74(1-2): 185-93.

[40] J. P. Chyng, C. P. Lee and B. J. Huang, Performance analysis of a solar-assisted heat pump water heater. Solar Energy 2003; 74(1): 33-44.

[41] Y. H. Kuang, K. Sumathy and R. Z. Wang, Study on a direct-expansion solar-assisted heat pump water heating system. International Journal of Energy Research 2003; 27(5): 531-48.

[42] Y. W. Li, R. Z. Wang, J. Y. Wu and Y. X. Xu, Experimental performance analysis on a direct-expansion solar-assisted heat pump water heater. Applied Thermal Engineering 2007; 27(17-18): 2858-68.

[43] A. Hepbasli, Exergetic modeling and assessment of solar assisted domestic hot water tank integrated ground-source heat pump systems for residences. Energy and Building 2007; 39(12): 1211-17.

[44] B. J. Huang, J. P. Lee and J. P. Chyng, Heat-pipe enhanced solar-assisted heat pump water heater. Solar Energy 2005; 78(3): 375-81.

[45] X. Guoying, Z. Xiaosong and D. Shiming, A simulation study on the operating performance of a solar-air source heat pump water heater. Applied Thermal Engineering 2006; 26(11-12): 1257-65.

[46] A. Pearson, Carbon dioxide - new uses for an old refrigerant. International Journal of Refrigeration 2005; 28: 1140-48.

[47] G. Lorentzen, and J. Pettersen, A new, efficient and environmentally benign system for car air-conditioning. International Journal of Refrigeration 1993; 16: 4-12.

[48] J. Pettersen, An efficient new automobile air conditioning system based on carbon dioxide vapor compression. ASHRAE Transactions 1994; 100: 657-65.

[49] M.H. Kim, J. Pettersen, C.W. Bullard, Fundamental process and system design issues in CO_2 vapor compression systems. Progress in Energy Combustion Science 2004; 30(2): 119-74.

[50] P. Neksa, CO_2 heat pump systems. International Journal of Refrigeration 2002; 25(4): 421-27.

[51] U.S. Secretary of Commerce. (2008). Thermophysical Properties of Fluid Systems. [Online] <http://webbook.nist.gov/chemistry/fluid>

[52] E.W. Lemmon, M.L. Huber, M.O. McLinden, NIST Standard Reference Database 23, Reference Fluid Thermodynamic and Transport Properties (REFPROP), Version 8.0. National Institute of Standards and Technology (2007).

[53] H.K. Oh, C.H. Son, New correlation to predict the heat transfer coefficient in-tube cooling of supercritical CO_2 in horizontal tubes. Experimental Thermal and Fluid Science 2010; 34: 1230-41.

[54] J. Pettersen, Flow vaporization of CO_2 in microchannel tubes. PhD Thesis, Norwegian University of Science and Technology, Norway (2002).

[55] J. Pettersen, A. Hafner, and G. Skaugen, Development of compact heat exchangers for CO2 air-conditioning systems. International Journal of Refrigeration 1998; 21: 180-93.

[56] B.T. Austin, Numerical simulation of a direct expansion geothermal heat pump using carbon dioxide in a transcritical cycle. M.Sc. Thesis, North Dakota State University, Fargo, ND, USA (2011).

[57] T.M. Oritz, D. Li, E.A. Groll, Evaluation of the performance potential of CO_2 as a refrigerant in air-to-air air conditioners and heat pumps: Systems modeling and analysis, ARTI 2003; Final report.

[58] T. Tamura, Y. Yakumaru, F. Nishiwaki, Experimental study on automotive cooling and heating air conditioning system using CO_2 as a refrigerant. International Journal of Refrigeration 2005; 28(8): 1302–07.

[59] S.G. Kim, Y.J. Kim, G. Lee, M.S. Kim, The performance of a transcritical CO_2 cycle with an internal heat exchanger for hot water heating. International Journal of Refrigeration 2005; 28(7): 1064-72.

[60] P. Neksa, H. Rekstad, G.R. Zakeri, P.A. Schiefloe, CO_2-heat pump water heater: characteristics, system design and experimental results. International Journal of Refrigeration 1998; 21(3): 172-79.

[61] P. Laipradit, J. Tiansuwan, T. Kiatsiriroat, L. Aye, Theoretical performance analysis of heat pump water heaters using carbon dioxide as refrigerant. International Journal of Refrigeration 2008; 32(4): 356-66.

[62] L. Cecchinato, M. Corradi, E. Fornasieri, L. Zamboni, Carbon dioxide as refrigerant for tap water heat pumps: A comparison with the traditional solution. International Journal of Refrigeration 2005; 28(8): 1250-58.

[63] J. Stene, Residential CO_2 heat pump system for combined space heating and hot water heating. International Journal of Refrigeration 2005; 28(8): 1259-65.

[64] M.R. Richter, S.M. Song, J.M. Yin, M.H. Kim, C.W. Bullard, P.S. Hrnjak, Experimental results of transcritical CO_2 heat pump for residential application. Energy 2003; 28(10): 1005-19.

[65] D. Voivontas, G. Tsiligiridis and D. Assimacopoulos, Solar potential for water heating explored by GIS. Solar Energy 1998; 62(6): 419-27.

[66] J. J. Mutch, Residential water heating: fuel conservation, economics and public policy. 1974 RAND Report, R 1498.

[67] B. Chandrasekar and T.C. Kandpal, Techno-economic evaluation of domestic solar water heating systems in India. Renewable Energy 2004; 29(3): 319-32.

[68] I. R. Pillai and R. Banerjee, Methodology for estimation of potential for solar water heating in a target area. Solar Energy 2007; 81(2): 162-72.

[69] T. C. Pan, J. J. Kao, and C. P. Wong, Effective solar radiation based benefit and cost analyses for solar water heater development in Taiwan. Renewable and Sustainable Energy Reviews 2012; 16(4): 1874-82.

[70] W. A. Beckman, S. A. Klein and J. A. Duffie, Solar Heating Design by the f-chart Method. 1977 Wiley Interscience, New York.

[71] R. S. Misra. Techno-economic optimization of thermosyphonic solar hybrid water heating systems. Energy Conversion and Management 1994; 35(3): 205-17.

[72] M.D. Antoni, O. Saro, Massive Solar-Thermal Collectors: A critical literature review. Renewable and Sustainable Energy Reviews 2012; 16(6): 3666-79.

[73] D. Mills, Advances in solar thermal electricity technology. Solar Energy 2004; 76(1-3): 19-31.

[74] Y. Kim, T. Seo, Thermal performances comparisons of the glass evacuated tube solar collectors with shapes of absorber tube. Renewable Energy 2007; 32(5): 772-95.

[75] L. Ma, Z. Lu, J. Zhang, R. Liang, Thermal performance analysis of the glass evacuated tube solar collector with U-tube. Building and Environment 2010; 45(9): 1959-67.

[76] X.R. Zhang, H. Yamaguchi, D. Uneno, K. Fujima, M. Enomoto, N. Sawada, Analysis of a novel solar energy-powered Rankine cycle for combined power and heat generation using supercritical carbon dioxide. Renewable Energy 2006; 31(12): 1839-54.

[77] X.R. Zhang, H. Yamaguchi, K. Fujima, M. Enomoto, N. Sawada, Study of solar energy powered transcritical cycle using supercritical carbon dioxide. International Journal of Energy Research 2006; 30(14): 1117-29.

[78] H. Yamaguchi, X.R. Zhang, K. Fujima, M. Enomoto, N. Sawada, Solar energy powered Rankine cycle using supercritical CO_2. Applied Thermal Engineering 2006; 26(17-18): 2345-54.

[79] H. Yamaguchi, N. Sawada, H. Suzuki, H. Ueda, X.R. Zhang, Preliminary study on a solar water heater using supercritical carbon dioxide as working fluid. Journal of Solar Energy Engineering 2010; 132(011010): 1-6.

[80] X.R. Zhang, H. Yamaguchi, Forced convection heat transfer of supercritical CO_2 in a horizontal circular tube. Journal of Supercritical Fluids 2007; 41(3): 412-20.

[81] X.R. Zhang, H. Yamaguchi, An experimental study on evacuated tube solar collector using supercritical CO_2. Applied Thermal Engineering 2008; 28(10): 1225-33.

[82] O. Baker, Simultaneous flow of oil and gas. Oil Gas Journal 1954; 53: 185-90.

[83] L.S. Tong, Boiling heat transfer and two-phase flow, John Wiley and Sons, Inc., New York, 1965.

[84] S.K. Chaturvedi, Y.F. Chiang, A.S. Roberts, Analysis of two-phase flow solar collectors with application to heat pumps. Journal of Solar Energy Engineering 1982; 104(4): 358-65.

[85] G.B. Wallis, One-dimensional two-phase flow, McGraw-Hill Book Company, New York, 1969.

[86] Q. Tian, Thermal performance of the U-type evacuated glass tubular solar collector. Building Energy and Environment 2007; 26(3): 51-4.

[87] B.S. Petukhov, Heat transfer and friction in turbulent pipe flow with variable physical properties. Advances in Heat Transfer 1970; 6: 503-64.

[88] R.B. Farrington, C.E. Bingham, Testing and analysis of load-side immersed heat exchangers for solar domestic hot water systems, Technical Report (SERI/TR-254-3094). Solar Energy Research Inst., Golden, CO (USA).

[89] North Dakota State Climate Office. North Dakota Annual Average Temperature. [Accessed online:] <http://www.ndsu.edu/ndsco/temp/monthly/2010.html>.

[90] F.M. White, Viscous Fluid Flow, McGraw-Hill Company, New York, 1974.

[91] Global solar trade. [Accessed online:] <http://www.alibaba.com/showroom/evacuated-tube-solar-collector.html>.

APPENDIX: PROGRAM CODE

A.1. MATLAB Functions

A.1.1. Heat Pump Model

Function: Main_heat_pump.m

```
% global model for thermodynamic analysis.

clc
P2=zeros(3,1);
T2=zeros(3,1);
%err_h=zeros(3,1);
T3=zeros(3,1);
h3=zeros(3,1);

%Input parameters
%-------Condenser parameters
      T_water_i=280.15;
      m_water=.035;
         viscosity=refpropm('V','T',T_water_i,'P',101.325,'WATER');
         Water_min_Re=m_water/(pi()*(.03^2-.008^2)/4)*(.03-.008)/viscosity;
%-------Solar Collector parameters-----------------
   I=500;
   S=0.8*I;
   T_air=283.2;

   V=3.5;
   ha=5.7+3.8*V;
   minallow=5;
   Tsup=5;

   T1=T_air-minallow;
   T_p=T_air+10;
P1=refpropm('P','T',(T1-Tsup),'Q',1,'CO2');

P2(1)=12000;
P2(2)=11000;

%iteration 1
[T2 m Wc]=compressor(T1,P1,P2(1));
[P4 T4 h4 x4]=solar_collector(T_air,T1,T_p,P1,m,S,I,ha);
[T3 P3 h3 Twout]=Condenser_1(T2,P2(1),m,T_water_i,m_water);
err_h(1)=h3-h4

%iteration 2
[T2 m Wc]=compressor(T1,P1,P2(2));
[P4 T4 h4 x4]=solar_collector(T_air,T1,T_p,P1,m,S,I,ha);
[T3 P3 h3 Twout]=Condenser_1(T2,P2(1),m,T_water_i,m_water);
err_h(2)=h3-h4
```

```
i=2;
while abs(err_h(i))>.1
   i=i+1;

   P2(i)=P2(i-1)-(err_h(i-1)*((P2(i-1)-P2(i-2))/(err_h(i-1)-err_h(i-2))))

   [T2 m Wc]=compressor(T1,P1,P2(i));
   [P4 T4 h4 x4]=solar_collector(T_air,T1,T_p,P1,m,S,I,ha);
   [T3 P3 h3 Twout]=Condenser_1(T2,P2(i),m,T_water_i,m_water);
   err_h(i)=h3-h4;
   if i>100
      break;
   end
end

P_2=P2(i);
P2_1=P2(i);

%output
h1=refpropm('H','T',T1,'P',P1,'CO2');
h2=refpropm('H','T',T2,'P',P_2,'CO2');
h3=refpropm('H','T',T3,'P',P3,'CO2');
h4=h3;
CO2_mass_flow_rate=m;
Water_out_temperature=Twout;
Compressor_work=Wc;
COP=m*(h2-h3)/Wc;
Heat_output=m*(h2-h3);
Heat_absorbed=m*(h1-h4);
C_pf=refpropm('C','T',(T1-Tsup),'P',P1,'CO2');

Sol_eff=Heatabsorbed/(12*I*2*pi()*0.0229*3.6)

format short e
Output=[P1;P2_1;P3;P4;x4;T1;T2;T3;T4; CO2_mass_flow_rate; Water_out_temperature;
Compressor_work;COP;Heat_output;Heat_absorbed]
format short


% Nomenclature
% err            J/kg    Δh across thermostatic expansion valve
% P1             kPa     comp inlet pr
% P2             kPa     comp outlet Pr
% P3             kPa     Condenser outlet pr
% P4             kPa     Solar Collector inlet pr
% T_water_i      K       Water inlet temp
% T1             K       comp inlet temp
% T2             K       comp outlet temp
% T3             K       Cond outlet temp
% T4             K       Solar collector inlet temp
% Tsup           K       degree of superheat at evap outlet
% Twout          K       Water outlet temp
% h3             J/kg    condenser outlet enthalpy
% h4             J/kg    solar collector inlet enthalpy
```

```
% i                       iteration number
% m             kg/s      CO2 mass flow rate
% m_water       kg/s      water mass flow rate
% minallow      K         min temp difference
% viscosity     Pa*s      water viscosity
% Water_min_Re             minimum water Reynolds #
% Wc            W         Comp power
% x4                       Solar collector inlet quality
% Sol_eff       %         Solar collector efficiency
```

A.1.2. Solar Collector Model

Function: solar_collector.m

```
function [P4 T4 h4 x4]=solar_collector(T_air,T1,T_p,P1,m_tot,S,I,ha)
n1=12; %number of tubes
m=m_tot/n1;
sigma = 5.6704*10^-8;  %Stefen-Boltzmann Const

%Evaporator dimensions
gl_abs=0.018;
gl_tr=0.907;
coat_abs=0.927;
Emsvty_g=0.083;
E_p=0.08;
E_0=0.06;
r0=0.0229;
rp=0.0179;
di=0.006;
L=3.4;  % U-tube length
dx=0.1;
N=L/dx;
A_r=2*pi()*r0*dx;
qi=I*A_r;

h_g_a=12.7;
h_p_g_c=0.2796;
U_e=0.1687;

G=m/((pi()/4)*di^2);
k_tube=400;
delta=0.0006;

w=0.0326*pi();
C_b=30;
B=35;    %contact angle
%-------------Finding U_L-----------------------------
T0=zeros(3,1);
T0_1=zeros(3,1);
err_T0=zeros(3,1);

%1st Iteration
T0(1)=T_air+1;
h_p_g_r=(sigma*E_p)*(T_p^2+T0(1)^2)*(T_p+T0(1))/(1+(E_p*2*rp)*(1-E_p)/(E_0*2*r0));
U_t=1/((1/h_g_a)+(1/(h_p_g_r+h_p_g_c)));
T0_1(1)=T_p-(U_t*(T_p-T_air))/(h_p_g_r+h_p_g_c);
err_T0(1)=T0(1)-T0_1(1);

%2nd Iteration
T0(2)= T_air+10;
h_p_g_r=(sigma*E_p)*(T_p^2+T0(2)^2)*(T_p+T0(2))/(1+(E_p*2*rp)*(1-E_p)/(E_0*2*r0));
U_t=1/((1/h_g_a)+(1/(h_p_g_r+h_p_g_c)));
T0_1(2)=T_p-(U_t*(T_p-T_air))/(h_p_g_r+h_p_g_c);
err_T0(2)=T0(2)-T0_1(2);
```

```
i=2;
while abs (err_T0(i))>0.01
   i=i+1;
   T0(i)=T0(i-1)-err_T0(i-1)*(T0(i-1)-T0(i-2))/(err_T0(i-1)-err_T0(i-2));
   h_p_g_r=(sigma*E_p)*(T_p^2+T0(i)^2)*(T_p+T0(i))/(1+(E_p*2*rp)*(1-E_p)/(E_0*2*r0));
   U_t=1/((1/h_g_a)+(1/(h_p_g_r+h_p_g_c)));
   T0_1(i)=T_p-(U_t*(T_p-T_air))/(h_p_g_r+h_p_g_c);
   err_T0(i)=T0(i)-T0_1(i);
   T0=T0_1(i);

end
T0=T0_1(i);
U_L=U_t+U_e;
% T_p=T_p_1(i)
   m_sc=(U_L/(delta*k_tube*(1+U_L/C_b)))^0.5;
   F=(tanh(m_sc*(w-di)/2))/(m_sc*(w-di)/2);

T=zeros(N+1,1);     %nodal temp array
P=zeros(N+1,1);     %nodal pr array
Q_u=zeros(N,1);     %segment heat transfer
x=zeros(N+1,1);     %nodal quality
h=zeros(N+1,1);     %nodal enthalpy
alpha=zeros(N+1,1);
%HTC_tot=zeros(N,1);

P(1)=P1;
T(1)=T1;
n=1;
h(1)=refpropm('H','T',T(1),'P',P(1),'CO2');
hv=refpropm('H','T',T(1),'Q',1,'CO2');
Reynolds_min=10000000;

%_____________________single-phase (vapor) flow in the sol coll_____
while h(n)>=hv && n<=N
   [u den k cp]=refpropm('VDLC','T',T(n),'P',P(n),'CO2');
   Re=G*di/u;                          %Re relation
      if Reynolds_min>Re
         Reynolds_min=Re;
      end
   Pr=u*cp/k;                          %Pr relation
%Pr drop
   fp=.0791*Re^-.25;                   %pr friction factor (Blasius)
   del_P=2*fp*dx*G^2*.001/(den*di);    %pr change (Darcy Weisbach)
   P(n+1)=P(n)+del_P;                  %segment inlet pr

%heat transfer
   f=(.79*log(Re)-1.64)^-2;            %friction factor (Petukhov's formula)
   Nu=(f/8)*(Re-1000)*Pr/(1.07+12.7*(f/8)^.5*(Pr^(2/3)-1));    %Nu correlation of Gnielinski
   alpha(n)=Nu*k/di;                   % 1-phase CO2 heat transfer coefficient

   F_prime=abs((1/U_L)/(w*((1+U_L/C_b)/(U_L*(di+(w-di)*F))+(1/C_b)+(1/(pi()*di*alpha(n))))));
   T(n+1)=(dx/(2*m*cp))*((gl_abs*r0*qi)+(gl_tr*gl_abs*qi*rp)+(gl_tr^2*coat_abs*rp*qi)-(r0*ha*(T0-
T_air))-(r0*sigma*Emsvty_g*(T0^4-T_air^4))+((2*m*cp*T(n))/dx));
%     TT=T(n+1)
```

```
    Q_u(n)=dx*w*F_prime*(S-U_L*(T(n+1)-T_air));

    h(n+1)=h(n)-Q_u(n)/m;
    n=n+1;
    hv=refpropm('H','T',T(n),'Q',1,'CO2');

end

hl=refpropm('H','T',T(n),'Q',0,'CO2');
x(n)=(h(n)-hl)/(hv-hl);


%__two-phase flow-boiling at solar collector_____________________________
 while h(n)<hv && n<=N && h(n)>hl
    [uv pv]=refpropm('VD','P',P(n),'Q',1,'CO2');              %CO2 vapor properties at inlet pr
    [ul pl kl cpl sften]=refpropm('VDLCI','P',P(n),'Q',0,'CO2');   %CO2 liq properties at inlet pr
    Re_lo=G*di/ul;
          if Reynolds_min>Re_lo
             Reynolds_min=Re_lo;
          end
    Prl=ul*cpl/kl;                    %Pr # at sat liq condition
    Xtt=((1-x(n))/x(n))^.9*(pv/pl)^.5*(ul/uv)^.1; %Lockhart-Martinelli factor;


%_______2-phase pressure drop____
    f_lo=.0791*Re_lo^-.25;     % Fanning friction factor
    phi_squared=(1+(pl/pv-1)*x(n))/(1+(ul/uv-1)*x(n))^.25;  %two-phase multiplier
    del_P=2*dx*f_lo*G^2*phi_squared*.001/(di*pl);
    P(n+1)=P(n)+del_P;

    [T(n+1)]=refpropm('T','P',P(n+1),'Q',1,'CO2');  %Temp at next node

%_____________2phase heat transfer coefficient____
    bd=.0146*B*(2*sften/(9.81*(pl-pv)))^.5;
    Fp=2.37*(.29+1/Xtt)^.85;
    htfus=hv-hl;
    coef_l=.023*kl/di*(Re_lo*(1-x(n)))^.8*Prl^.4;

    %first iteration
    qguess(1)=100000 ;
    Boil=qguess(1)/(G*htfus);
    if Xtt<1
       NN=4048*Xtt^1.22*Boil^1.13;
    else
       NN=2-.1*(Xtt)^.28*Boil-.33;
    end
    coef_sa=207*kl/bd*(qguess(1)*bd/(kl*T(n)))^.745*(pv/pl)^.581*Prl^.533;
    alpha_1(1)=NN*coef_sa+Fp*coef_l;
    F_prime=abs((1/U_L)/(w*((1+U_L/C_b)/(U_L*(di+(w-di)*F))+(1/C_b)+(1/(pi()*di*alpha_1(1))))));
    Q_u(1)=dx*w*F_prime*(S-U_L*(T(n+1)-T_air));

    err(1)=qguess(1)-Q_u(1);

    %second iteration
    qguess(2)=qguess(1)-100;
```

```
   Boil=qguess(2)/(G*htfus);
   if Xtt<1
      NN=4048*Xtt^1.22*Boil^1.13;
   else
      NN=2-.1*(Xtt)^.28*Boil-.33;
   end
   coef_sa=207*kl/bd*(qguess(2)*bd/(kl*T(n)))^.745*(pv/pl)^.581*Prl^.533;
   alpha_1(2)=NN*coef_sa+Fp*coef_l;
   F_prime=abs((1/U_L)/(w*((1+U_L/C_b)/(U_L*(di+(w-di)*F))+(1/C_b)+(1/(pi()*di*alpha_1(2))))));
   Q_u(2)=dx*w*F_prime*(S-U_L*(T(n+1)-T_air));

   err(2)=qguess(2)-Q_u(2);

   j=2;

while abs(err(j))>.001
      j=j+1;
      qguess(j)=qguess(j-1)-err(j-1)*(qguess(j-1)-qguess(j-2))/(err(j-1)-err(j-2));
      Boil=qguess(j)/(G*htfus);
      if Xtt<1
         NN=4048*Xtt^1.22*Boil^1.13;
      else
         NN=2-.1*(Xtt)^.28*Boil-.33;
      end
      coef_sa=207*kl/bd*(qguess(j)*bd/(kl*T(n)))^.745*(pv/pl)^.581*Prl^.533;
      alpha_1(j)=NN*coef_sa+Fp*coef_l;
      F_prime=abs((1/U_L)/(w*((1+U_L/C_b)/(U_L*(di+(w-di)*F))+(1/C_b)+(1/(pi()*di*alpha_1(j))))));
      Q_u(j)=dx*w*F_prime*(S-U_L*(T(n+1)-T_air));

      err(j)=qguess(j)-Q_u(j);
   end

   alpha(n)=alpha_1(j);

   F_prime=abs((1/U_L)/(w*((1+U_L/C_b)/(U_L*(di+(w-di)*F))+(1/C_b)+(1/(pi()*di*alpha(n))))));
   T(n+1)=(dx/(2*m*cp))*((gl_abs*r0*qi)+(gl_tr*gl_abs*qi*rp)+(gl_tr^2*coat_abs*rp*qi)-(r0*ha*(T0-
T_air))-(r0*sigma*Emsvty_g*(T0^4-T_air^4))+((2*m*cp*T(n))/dx));
%    TT=T(n+1)
   Q_u(n)=dx*w*F_prime*(S-U_L*(T(n+1)-T_air));

   h(n+1)=h(n)-Q_u(n)/m;

   hv=refpropm('H','P',P(n+1),'Q',1,'CO2');
   hl=refpropm('H','P',P(n+1),'Q',0,'CO2');
   n=n+1;
   x(n)=(h(n)-hl)/(hv-hl);

 end

x4=x(n);

%-----------------------subcooled CO2-------------------------------
while n<=N && h(n)<=hl
   [u den k cp]=refpropm('VDLC','T',T(n),'P',P(n),'CO2');
   %heat transfer
```

```
   Re=G*di/u;                    %Re equation
      if Reynolds_min>Re
         Reynolds_min=Re;
      end
   Pr=u*cp/k;                    %Pr
   Nu=.023*Re^.8*Pr^.4;   %Dittus-Boelter correlation
   alpha(n)=Nu*k/di;

   F_prime=abs((1/U_L)/(w*((1+U_L/C_b)/(U_L*(di+(w-di)*F))+(1/C_b)+(1/(pi()*di*alpha(n))))));
   T(n+1)=(dx/(2*m*cp))*((gl_abs*r0*qi)+(gl_tr*gl_abs*qi*rp)+(gl_tr^2*coat_abs*rp*qi)-(r0*ha*(T0-
T_air))-(r0*sigma*Emsvty_g*(T0^4-T_air^4))+((2*m*cp*T(n))/dx));
%     TT=T(n+1)
   Q_u(n)=dx*w*F_prime*(S-U_L*(T(n+1)-T_air));

   h(n+1)=h(n)-Q_u(n)/m;
   P(n+1)=P(n);
   n=n+1;

end

T4=T(n);
P4=P(n);
h4=h(n);
end


%Nomenclature
% A_r            m^2          carbon dioxide-side area
% alpha          W/m^2*K      carbon dioxide conv heat transfer coef
% coef_sa        W/m^2*K      Nucleate pool boiling ht coef of Stephan & Abdelsalam
% cp             J/kg*K       sp heat of carbon dioxide
% cpl            J/kg*K       sp heat of carbon dioxide (liq)
% del_P          kPa          pr drop
% den            kg/m^3       density
% di             m            inner dia of tube
% do             m            outer dia of tube
% f_lo                        liq only friction factor
% fp                          friction factor
% Fp                          heat transfer enhancement factor
% G              kg/m^2*s     mass flux
% h4             J/kg         Evap inlet enthalpy
% hl             J/kg         sat liq enthalpy
% ha             J/kg         air conv ht transfer coef
% HTC_tot        W/m^2*K      total ht trans coef
% hv             J/kg         sat vapor enthalpy
% k              W/m*K        therm cond carbon dioxide
% kl             W/m*K        therm cond carbon dioxide (liquid)
% ktube          W/mK         thermal cond of tube
% L              m            circuit length
% dx             m            fragment length
% m              kg/s         carbon dioxide mass flow rate in each tube
% m_tot          kg/s         total carbon dioxide mass flow rate
% n                           iteration number
% NN                          Nucleate boiling factor
% Nu                          Nusselt number
```

```
% phi_squared                two phase multiplier
% pl              kg/m^3     density (liquid)
% Pr                         Prandtl number
% pv              kg/m^3     density (vapor)
% Q               W          local heat transfer rate
% Q_u             W          useful heat energy
% Re                         Reynolds number
% S               W/m^2      global solar radiation intensity
% T1              K          compressor inlet temp
% T_air           K          ambient temp
% T_p             K          solar collector plate temp
% T4              K          Solar Collector inlet temp
% u               Pa*s       viscosity
% ul              Pa*s       viscosity (liquid)
% uv              Pa*s       viscosity (vapor)
% x                          quality
% x4                         Solar Collector inlet quality
% Xtt                        Lockhart-Martinelli factor
```

A.1.3. Compressor Model

Function: compressor.m

```
function [T2 m Wc]=compressor(T1,P1,P2)

%Input Parameters
N=50;
Vs=.00001972;

%___ Oritz, Li and Groll efficiency relations
n_v=0.9207-0.0756*(P2/P1)+0.0018*(P2/P1)^2; %volm eff
n_tot=-0.26+0.7952*(P2/P1)-0.2803*(P2/P1)^2+0.0414*(P2/P1)^3-0.0022*(P2/P1)^4;    %total eff:
isentropic*mech
n_m=0.9083-0.0884*(P2/P1)+0.0051*(P2/P1)^2;%mech eff of compr

[h1 s1 rho1]=refpropm('HSD','T',T1,'P',P1,'CO2'); %properties at comp inlet
s2s=s1;                         %ideal discharge entropy
h2s=refpropm('H','P',P2,'S',s2s,'CO2');  %ideal discharge enthalpy
m=n_v*rho1*Vs*N;                    %mass flow rate
Wc=m*(h2s-h1)/n_tot;             %power input required by comp
Loss=(1-n_m)*Wc;
h2=h1+(Wc-Loss)/m;              %real discharge enthalpy[J/kg]
T2=refpropm('T','P',P2,'H',h2,'CO2');    %discharge temp [K]
end

% Nomenclature
% T1            K               inlet temp
% P1            kPa             inlet pr
% n_v                           volumetric eff
% n_tot                         total eff
% n_m                           mechanical eff
% h1            J/kg            inlet enthalpy
% s1            J/kgK           inlet entropy
% rho1          kg/m^3          inlet carbon dioxide density
% s2s           J/kgK           discharge isentropic compression entropy
% h2s           J/kg            discharge isentropic compression enthalpy
% Loss          w               Losses of comp
% N             rpm             compressor speed
% Vs            m^3             swept volume
% P2            kPa             discharge pr
% T2            K               discharge temp
% m             kg/s            mass flow rate of carbon dioxide
% Wc            W               comp power
% h2            J/kg            actual outlet enthalpy
```

A.1.4. Condenser Model: Part 1

Function: Condenser_1.m

```
function [T3 P3 h3 T_water minRe]=Condenser_1(T2,P2,m,T_water_i,m_water)

% arrays
T_wi=zeros(3,1);
T_wo=zeros(3,1);
err=zeros(3,1);

%water outlet temp
T_wo(1)=T2-2;
T_wo(2)=T2-4;

SOLVE=Condenser_2(T2,P2,m,m_water);

[T_wi(1) T3 P3 h3 minRe]=SOLVE(T_wo(1));
   err(1)=T_water_i-T_wi(1);  %1st iteration water inlet
[T_wi(2) T3 P3 h3 minRe]=SOLVE(T_wo(2));
   err(2)=T_water_i-T_wi(2);   %2nd iteration water inlet
   j=2;
   while abs(err(j))>.001
      j=j+1;
   T_wo(j)=T_wo(j-1)-err(j-1)*(T_wo(j-1)-T_wo(j-2))/(err(j-1)-err(j-2));
      [T_wi(j) T3 P3 h3 minRe]=SOLVE(T_wo(j));
         err(j)=T_water_i-T_wi(j);  %j-th iteration water inlet
   end
T_water=T_wo(j);
end

%Nomenclature
% T_water       K              water outlet temp
% minRe                        min carbon dioxide Re number
% T_wi          K              water inlet temp
% T_wo          K              water outlet temp
% err                          error
```

A.1.5. Condenser Model: Part 2

Function: Condenser_2.m

```
function SOLVE=Condenser_2(T2,P2,m,m_w)
SOLVE=@shooting;
   function [T_w_calc T3 P3 h3 min_reynolds]=shooting(Two)

%Condenser dimensions
L=15;
l=.1;      % segment length [m]
N=L/l;
di=.005;
do=.007;
D=.016;
ktube=400;

%parameters
A_r=pi()*di*l;              %refrigerant segment area
A_w=pi()*do*l;              %H20 segment area
Dh_w=D-do;                  %hydraulic diam
G_w=m_w/(pi()*(D^2-do^2)/4);  %mass vel of H20
G=m/(pi()/4*di^2);          %mass vel of refrigerant

%define initial values
T=zeros(N+1,1);   %temp gradient values
T_w=zeros(N+1,1);
P=zeros(N+1,1);   %pr gradient values
Q=zeros(N,1);     %HT for each condenser element
h=zeros(N+1,1);
HTC_r=zeros(N+1,1);

T(1)=T2;          %refrigerant inlet temp
T_w(1)=Two;       %assume H2O outlet temp
Outletguess=Two;
min_reynolds=10000000;   %a starting assumption
P(1)=P2;
DIF_cal=20;

for n=1:N

  if T_w(n)<274, break, end

%----H2O-Side----
   [Cp_w visc_w cond_w]=refpropm('CVL','T',T_w(n),'P',101.325,'WATER');
   Re_w=G_w*Dh_w/visc_w;          %Re_water
   Pr_w=visc_w*Cp_w/cond_w ;      %Pr_water

   % H2O-side HT coeff
   ffw=(0.79*log(Re_w)-1.64)^-2;
   Nu_w=((ffw/8)*(Re_w-1000)*Pr_w)/(1.07+12.7*(ffw/8)^.5*(Pr_w^(2/3)-1));
   CF=.86*(do/D)^(-.16);
   HTC_w=CF*Nu_w*cond_w/Dh_w;
```

```
    [HTC_r(n) Twall]=cond_coil(T(n),T_w(n),P(n),di,do,l,ktube,G,HTC_w,DIF_cal);

    DIF_cal=T(n)-Twall;
    UA=(1/(A_r*HTC_r(n))+1/(A_w*HTC_w)+log(do/di)/(2*pi()*l*ktube))^-1;
    [Cp_rb]=refpropm('C','T',T(n),'P',P(n),'CO2');
    Cr=m*Cp_rb;
    Cw=m_w*Cp_w;
    Cmin=min(Cr,Cw);
    Cmax=max(Cr,Cw);
    C=Cmin/Cmax;
    NTU=UA/Cmin;
    eff=(1-exp(-NTU*(1-C)))/(1-C*exp(-NTU*(1-C)));
    T_w(n+1)=(eff*Cmin*T(n)/Cw-T_w(n))/(eff*Cmin/Cw-1);
    Q(n)=eff*Cmin*(T(n)-T_w(n+1));
    T(n+1)=T(n)-Q(n)/Cr;

%refrigerant Pr drop
    [dens visc]=refpropm('DV','T',T(n),'P',P(n),'CO2');
    Re=G*di/visc;                %Re number refrigerant at bulk temp
                if min_reynolds>Re
                   min_reynolds=Re;
                end
        if Re>=20000
           ee=.184*Re^-.2;  %Darcy friction factor using Blasius
        elseif Re<=20000 && Re>=2300
           ee=.316*Re^-.25;   %Darcy friction factor using Blasius
        else
           disp 'Laminar CO2 flow.'
           ee=64/Re;
        end
    del_P=.001*ee*G^2*l/(2*dens*di);     %Pr drop:  Darcy-Wesibach
    P(n+1)=P(n)-del_P;

end

if T_w(n)<274
        T_w_calc=(N+1-n)*((T_w(1)-T_w(n))/n); %H2O inlet calculation
        %output assignments
        P3=P(n);
        T3=T(n);
        h3=h(n);
 else

%Results
    T_w_calc=T_w(N+1);
    P3=P(N+1);
    T3=T(N+1);
    h3=refpropm('H','T',T3,'P',P3,'CO2');
    end
end
end
```

%Nomenclature

% cond_w	kg/m^3	H_2O thermal conductivity
% del_P	kPa	CO_2 pr drop
% dens	kg/m^3	refrigerant density at bulk temp
% Cmax	kJ/s*K	max rate of heat capacity
% Cmin	kJ/s*K	min rate of heat capacity
% Dh_w	m	H_2O side hydraulic dia
% ee		refrigerant friction factor
% eff		HE effectiveness
% ffw		H_2O side friction factor
% G_w	kg/s*m^2	H_2O mass flux
% G_w	kg/s*m^2	refrigerant mass flux
% HTC_r	W/m^2*K	local refrigerant HT coeff
% HTC_w	W/m^2*K	local H_2O HT coeff
% h	kJ/kg	refrigerant local enthalpy
% h3	kJ/kg	refrigerant outlet enthalpy
% ktube	W/m*K	thermal conductivity of tube
% L	m	condenser length
% l	m	segment length
% min_reynolds		min refrigerant Re number
% N		No of elements of segment
% Nu_w		H_2O Nu
% P	kPa	local refrigerant pr
% Q	W	local rate of HT
% Re_w		H_2O side Re
% Cp_rb	kJ/kg*K	refrigerant sp heat at bulk temp
% Cp_w	kJ/kg*K	H_2O specific heat
% T	K	local refrigerant temp
% T_w	K	local H_2O temp
% T_w_calc	K	H_2O inlet temp
% Twall	K	refrigerant tube coil temp
% T_water	K	H_2O outlet temp
% Two	K	H_2O outlet temp
% UA	W/K	overall heat conductance
% visc	Pa*s	refrigerant viscosity at bulk temp
% visc_w	Pa*s	H_2O viscosity

A.1.6. Condenser Model: Part 3

Function: cond_coil.m

```
function [HTC wall_temp]=cond_coil(T_rb,T_water,P,di,do,l,k,G,HTC_w,DIF_cal)


   %Bulk properties-------
   [rho_rb Cp_rb visc_rb K_rb]= refpropm('DCVL','T',T_rb,'P',P,'CO2');
   Re_rb=G*di/visc_rb;              %Re number CO2 at bulk temp
   Pr_rb=visc_rb*Cp_rb/K_rb;      %Pr number CO2 at bulk temp
   f_b=(0.79*log(Re_rb)-1.64)^-2;
   Nu_b=((f_b/8)*(Re_rb-1000)*Pr_rb)/(1.07+12.7*(f_b/8)^.5*(Pr_rb^(2/3)-1));

   %coil temp initial estimations
   T_rw(1)=T_rb-.5;              %1st estimation
   T_rw(2)=(T_rb+T_water)/2;       %2nd estimation

   %Calculate heat transfer coef using 1st estimation
   [rho_rw Cp_rw visc_rw K_rw]=refpropm('DCVL','T',T_rw(1),'P',P,'CO2');
   Re_rw=G*di/visc_rw;              %Re number CO2 at coil temp
   Pr_rw=visc_rw*Cp_rw/K_rw;      %Pr number CO2 at coil temp
   f_w=(0.79*log(Re_rw)-1.64)^-2;
   Nu_w=((f_w/8)*(Re_rw-1000)*Pr_rw)/(1.07+12.7*(f_w/8)^.5*(Pr_rw^(2/3)-1));

   Nu=((Nu_b+Nu_w)/2)*K_rw/K_rb; %overall CO2 Nu(correlation of Pitla et al)
   HTC_r=Nu*K_rb/di;            %CO2 ht trans coeff
   UA=(1/(pi()*l*di*HTC_r)+1/(pi()*l*do*HTC_w)+log(do/di)/(2*pi()*l*k))^-1;
   Qc=UA*(T_rb-T_water);
   Twall=T_rb-Qc/(pi()*di*l*HTC_r);
   err(1)=Twall-T_rw(1); %err between actual and calculated coil temp

   %Calculate heat transfer coef using 2nd estimation
   [rho_rw Cp_rw visc_rw K_rw]=refpropm('DCVL','T',T_rw(2),'P',P,'CO2');
   Re_rw=G*di/visc_rw;
   Pr_rw=visc_rw*Cp_rw/K_rw;
   f_w=(0.79*log(Re_rw)-1.64)^-2;
   Nu_w=((f_w/8)*(Re_rw-1000)*Pr_rw)/(1.07+12.7*(f_w/8)^.5*(Pr_rw^(2/3)-1));

   Nu=((Nu_b+Nu_w)/2)*K_rw/K_rb;
   HTC_r=Nu*K_rb/di;                  %CO2 ht trans coeff
   UA=(1/(pi()*l*di*HTC_r)+1/(pi()*l*do*HTC_w)+log(do/di)/(2*pi()*l*k))^-1;
   Qc=UA*(T_rb-T_water);
   Twall=T_rb-Qc/(pi()*di*l*HTC_r);
   err(2)=Twall-T_rw(2);  %error between actual and calculated coil temp

   n=2;
   while abs(err(n))>.001 && n<=25
      n=n+1;
      %next estimation of coil temp
      T_rw(n)=T_rw(n-1)-(err(n-1)*(T_rw(n-1)-T_rw(n-2)))/(err(n-1)-err(n-2));

      if T_rw(n)<T_water    % correction if updated coil temp is too low
```

```
        TooLow=T_rw(n)
        T_rw(n)=T_rw(1)
    end

    if n>25          % final value selected if too many iterations
        T_rw(n)=T_rb-DIF_cal;
        Bulk=T_rb
        estimate=T_rw(n)
    end
    %Calculate heat transfer coef using current coil temp
    [rho_rw Cp_rw visc_rw K_rw]=refpropm('DCVL','T',T_rw(n),'P',P,'CO2');
    Re_rw=G*di/visc_rw;          %Re number CO2 at coil temp
    Pr_rw=visc_rw*Cp_rw/K_rw;    %Pr number CO2 at coil temp
    f_w=(0.79*log(Re_rw)-1.64)^-2;
    Nu_w=((f_w/8)*(Re_rw-1000)*Pr_rw)/(1.07+12.7*(f_w/8)^.5*(Pr_rw^(2/3)-1));

    Nu=((Nu_b+Nu_w)/2)*K_rw/K_rb;
    HTC_r=Nu*K_rb/di;                %CO2 ht trans coeff
    UA=(1/(pi()*l*di*HTC_r)+1/(pi()*l*do*HTC_w)+log(do/di)/(2*pi()*l*k))^-1;
    Qc=UA*(T_rb-T_water);
    Twall=T_rb-Qc/(pi()*di*l*HTC_r);
    err(n)=Twall-T_rw(n);
  end
HTC=HTC_r;
wall_temp=T_rw(n);
end


%Nomenclature
% Cp_rb         kJ/kg*K         carbon dioxide spec. heat @ bulk temp
% Cp_rw         kJ/kg*K         carbon dioxide spec. heat @ coil temp
% rho_rb        kg/m^3          carbon dioxide density @ bulk temp
% rho_rw        kg/m^3          carbon dioxide density @ coil temp
% K_rb          W/m*K           carbon dioxide K @ bulk temp
% K_rw          W/m*K           carbon dioxide K @ coil temp
% di            m               inner-tube inner-dia
% DIF_cal       K               temp diff between coil and bulk
% do            m               inner-tube outer-dia
% Nu                            carbon dioxide Avg Nu
% Nu_b                          carbon dioxide Nu @ bulk temp
% Nu_w                          carbon dioxide Nu @ coil temp
% Pr_rb                         carbon dioxide Pr number @ bulk temp
% Pr_rw                         carbon dioxide Pr number @ coil temp
% Re_rb                         carbon dioxide Re number @ bulk temp
% Re_rw                         carbon dioxide Re number @ coil temp
% HTC_r         W/m^2*K         carbon dioxide heat transfer coeff
% HTC_w         W/m^2*K         water heat transfer coefficient
% f_b                           carbon dioxide friction factor @ bulk
% f_w                           carbon dioxide friction factor @coil temp
% G             kg/s*m^2        carbon dioxide mass flux
% HTC           W/m^2*K         final carbon dioxide ht trans coeff
% k             W/m*K           tube coil thermal conductivity
% l             m               length of segment
% P             kPa             carbon dioxide Pr
```

```
% Qc          W       overall heat transfer rate
% T_rb        K       carbon dioxide bulk temp
% T_rw        K       calculated carbon dioxide coil temperature
% Twall       K       calculated carbon dioxide -side coil temp
% T_water     K       water temperature
% UA          W/K     overall heat conductance
% visc_rb     Pa*s    carbon dioxide visc @ bulk temp
% visc_rw     Pa*s    carbon dioxide visc @ coil temp
% wall_temp   K       final carbon dioxide coil temp
```

LIST OF PUBLICATIONS

1. M. Raisul Islam, K. Sumathy and Samee Ullah Khan, "Solar Water Heating Systems and their Market Trends," *Renewable and Sustainable Energy Reviews*, 17 (2013): 1-25.

2. M. Raisul Islam, K. Sumathy and Samee Ullah Khan, "Performance Study on Solar Assisted Heat Pump Water Heater using CO_2 in a Transcritical Cycle," *Int. Conference on Renewable Energy and Power Quality (ICREPQ12)*, CD-Rom Proceedings, pp 1-5, Santiago de Compostela, Spain, March 28-30, 2012.

3. M. Raisul Islam and K. Sumathy, "Carbon Dioxide driven Solar-assisted Heat Pump Water Heating System: A Theoretical Analysis", *International Research Journal of Environmental Sciences*. 2014 edition (In Press; Manuscript ID: ISCA-IRJEvS-2013-204).

4. R.Shukla, K.Sumathy and M. Raisul Islam, "An Experimental Study on a Density Driven Solar Water Heating System Using Supercritical CO_2 as Working Fluid", *International Journal of Environment and Resource,* 2014 edition (Accepted).